

Modelling the effects of excavation pits on fringing reefs

Master thesis

Sebastiaan Klaver



The cover shows a satellite photograph of the Southernmost island of Kwajalein Atoll, Marshall Islands, a remote country that consists of low-lying atolls with high population densities and limited resources such as construction materials. Among other factors, these limited resources contribute to the country's proneness to coastal hazards, such as flooding, sensitivity to coastal erosion and salinization of freshwater lenses. The photograph shows the island's coral fringing reef structure, which acts as a natural breakwater and protects the island (note the breaking waves on the east and southeast reef crests). At the so-called reef flats on the intertidal areas at ocean-side, as well as in the inner lagoon of the atoll, rocky sediments have been removed from the reef flat by means of excavating. Clearly, human interventions such as reef excavating have a significant impact on the structure of the reef's coastal system.

Source: https://coralreefs.wr.usgs.gov/images/kwajalein_wv2.jpg

Modelling the effects of excavation pits on fringing reefs

a Master thesis by

Sebastian Klaver

in partial fulfillment of the requirements for the degree of

Master of Science
in Civil Engineering

at the Delft University of Technology (TU Delft)

&

Master of Science
in Hydraulic Engineering & Water Resources Management

at the National University of Singapore (NUS)

to be defended publicly on Monday January 22nd, 2018 at 08:30 AM (UTC+01:00),
in Lecture Hall E of the faculty of Civil Engineering & Geosciences of the TU Delft.

Student numbers:	4093305 (TU Delft)	E0012872 (NUS)
Project duration:	May 1 st , 2017	January 22 nd , 2018
Chair committee:	Prof. dr. ir. S.G.J. Aarninkhof	TU Delft
Committee members:	Dr. ir. A. Giardino	Deltares
	Ir. C.M. Nederhoff	Deltares
	Dr. A.J.F. van der Spek	Deltares, TU Delft
	Dr. M.E.S. Tissier	TU Delft
	Dr. J. Yuan	NUS

An electronic version of this thesis is available at <http://repository.tudelft.nl/>.

Preface

This is the final report of the thesis research that I conducted at Deltares, as a conclusion of the double degree program in Hydraulic Engineering & Water Resources Management at the National University of Singapore and Delft University of Technology. Over the course of performing the research and writing this thesis, I've developed old and new skills and learned a great deal about reefs and academic research.

This achievement wouldn't have been possible without the support of my family and friends, for which I'm very grateful.

Also, the involvement of all the members of the thesis committee has been very valuable. Especially that of Kees and Alessio, whom I had daily contact with, have aided me in steering into the right direction and have helped me produce a final thesis that I can say I'm proud of.

Finally, I would like to thank Deltares and its employees and my fellow graduating students, who have provided me with an excellent working space and learning environment. And also Janet, Murray, and Mark, who have shared the dataset of their field experiments, and whose publications have served as a source of inspiration.

I'm satisfied with the process and outcome of this research and have enjoyed many memorable moments in the past months. This document represents the pinnacle of my career as a student in civil engineering and will bring this phase of my life into completion. I look forward to the road ahead and will look back on many years well spent studying the field that interests me most.

*Sebastiaan Klaver
Delft, January 2018*

Summary

Introduction

Small island developing states (SIDS), many of them in the Pacific and Indian Oceans, are among the most vulnerable to climate change (e.g. sea level rise) and to seasonal to inter-annual climate variability. These islands are prone to flooding due to swell waves and wind waves, coastal erosion and salinisation of the subsoil freshwater lenses, all of which have a significant impact on the local populations, nature and infrastructure. Many of these island states are characterised by their small size and dense population in low lying areas (several meters above sea level), such as atolls and fringing reefs. The small size and geographic isolation of SIDS makes them vulnerable to ecological and economic shocks, especially in the light of the increasing impacts of urbanization and above-mentioned climate change.

In order to combat these potential coastal hazards and produce economically feasible construction materials such as sand and aggregate, parts of the reef flat are excavated. The size of these excavations are not rarely exceeding that of football fields and significantly impact the structure and geometry of the reef and coastal system. Currently, still little is known about the impact of these pits and if these excavations can be considered a sustainable or climate-resilient engineering practice. At the time of writing, only two studies have been published that provide an initial insight into the potential hydrodynamic effects of this practice, though both studies only considered a single reef (Ford et al., 2013; Yao et al., 2016). Other aspects, such as the impact on ecology and morphology, have not been discussed.

Objectives

The scope of this thesis is limited to assessing the impact of excavation pits on reef hydrodynamics. This allows for a more complete and general understanding of the implications of this practice on hydrodynamics. This study provides insights into the effects of pits on a large variety of fringing reefs, related to hydrodynamics and wave runup, by using a depth-averaged one-dimensional (1D) and a depth-averaged two-dimensional (2DH) process-based wave-resolving hydrodynamic model (XBeach non-hydrostatic+, "XBnh+"). In this report, an introduction to the problem and objectives of the research are given, as well as a presentation of all relevant results and conclusions. The report functions as a detailed description of the process of this thesis research and its findings.

Firstly, in Chapter 1 an introduction to the problem is given. Furthermore, the research objectives, questions, and research approach are presented. This is followed by a literature review of relevant reef hydrodynamics (see Chapter 2.2). The objectives of this study are:

1. "To increase the understanding of the effects of reef excavating on fringing reef hydrodynamics."
2. "To assess the accuracy and validity of using XBnh+ for modelling fringing reefs with excavation pits."

Validation

Currently, there is only one dataset available that includes measurements of hydrodynamics of a fringing reef with excavation pit. These measurements were used to calibrate and validate the 1D XBnh+ model. Near-shore hydrodynamics were modelled with moderate accuracy and contain all relevant processes that were observed in previous field studies. However, an accurate calibration was not possible because of limitations of the dataset. Therefore, it is recommended to obtain more detailed near-shore measurements in order to fully calibrate and validate the model. The XBnh+ model is an improved version of the original XBeach non-hydrostatic model (XBnh), but includes an extra computational layer in the vertical. This is needed to model steep bathymetry gradients, such as fore reef slopes and excavation pits. The XB model has demonstrated its predictive skill regarding fringing reef hydrodynamics in previous research, and therefore provides sufficient confidence to be valid for this study as well (Gawehn et al., 2016; Pearson et al., 2017; Quataert et al., 2015; Van Dongeren et al., 2012). Based on this and the results of the validation study, it is assumed that the model

simulates the measured near-shore hydrodynamics sufficiently well and is able to capture relevant near-shore processes (see Chapter 3).

Model setup

Based on literature a parameter space was defined that includes the ranges of forcing parameters, reef geometry parameters and pit geometry parameters. The used 1D XBNH+ model gave insights on the most important and sensitive of these modelling parameters. Six of these were used in a multi-parameter sensitivity study: fore reef slope, reef submergence, reef flat width, beach slope, excavation pit width and cross-shore location of excavation. In total, 9375 different reefs with different excavation pits were modelled in order to assess the influence on hydrodynamics and runup during extreme events ($H_s = 5$ m), which cause most coastal inundations. (See Chapter 4.)

Infra-gravity

A generic effect of pits on fringing reefs is that it causes a decrease in infra-gravity (IG) wave height. At Majuro, Marshall Islands, it was observed that this is possibly the result of a disruption of the quasi-standing IG wave pattern that is present due to the spatial structure of the reef (Ford et al., 2013). Ford et al. (2013) found a high correlation between the decrease in IG wave energy and the decrease in wave energy around the 1/4 and 3/4 wavelength normal modes. The effect of the excavation pit is to decrease the resonant amplification around these frequencies. This was seen for the majority (95%) of all modelled reefs. The width of the excavation and cross-shore location have a strong influence on this mechanism, as wider pits cause a larger decrease in IG wave height, as well as pits located closer to the reef crest.

High frequency

Changes in variance in the HF band were also observed. These can partly be explained by a combination of decreased wave dissipation, which results in larger spectral peaks, and wave-wave (triad) interaction, causing less energy transfer from the (HF) peak to both super- and subharmonics. The efficiency of both these processes decreases with larger water depths. In the case of an excavation, the combined effect of these processes is to increase the variance in the spectral peak and to decrease the variance in the spectral (HF) tail. The model results show that there can be either an increase or decrease in HF energy due to the pit. Wider pits cause an increase in wave energy in the HF peak, but also a (slight) increase in wave energy in the HF tail. Pits located closer to the reef crest have an increased HF tail.

Wave runup

The general effect of excavation pits on wave runup is that they cause a decrease of 5% on average. An increase in runup was seen in 15% of all modelled reefs. The change in runup ranged from +10% to -20%. The increased runup was associated with larger spectral peak and IG wave height, and lower HF tail. The probability of a negative impact (increase) on runup is expected to decline in the case of sea level rise. The lowest probabilities of an increase in runup are found for: gentle beach slopes (~ 5%), large reef flat submergence (~ 8%), very gentle or very steep fore reef slopes (~ 12%), narrow reef flats (~ 7%), narrow excavation pits (~ 5%), and excavation pits located near the reef crest (~ 8%).

Two-dimensional effects

Additionally, excavation pits cause a decrease in mean water level shoreward of the pit. This resulted in circulation patterns around the excavation in the 2D XBNH+ model (see Chapter 5). These can result in coastal erosion and entrapment of sediments. Also, alongshore variation in wave height near the shore was modelled, causing a variation in runup across the coastline. The effect of an excavation on (HF) wave height and runup can extend significantly in alongshore direction to the coastline, around the same length as the pit.

Recommendations

Based on the modelling results that focused on wave runup, the following recommendation can be made regarding for reef excavating:

Excavation pits should be constructed relatively narrow (in cross-shore direction) and close to the reef crest (positioned further away from the beach), in order to reduce the probability of an adverse effect on wave runup and subsequent hazards.

Contents

Preface	iii
Summary	v
List of Figures	ix
List of Tables	xi
List of Definitions	xiii
List of Symbols	xv
1 Introduction	1
1.1 Problem description	1
1.2 Research objectives	3
1.2.1 Research questions	3
1.3 Research approach	3
2 Background	5
2.1 Reef coasts	5
2.1.1 Reef classification	5
2.1.2 Reef morphology.	7
2.2 Relevant reef hydrodynamics	8
2.2.1 Effects of climate change.	8
2.2.2 Ecological aspects	8
2.2.3 Hydrodynamic forcing.	8
2.2.4 Wave transformation on reefs	9
2.2.5 Runup & overtopping	13
2.2.6 Hydrodynamic effects of excavation pits	14
3 Validation of XBeach non-hydrostatic+	17
3.1 Introduction	17
3.2 Data analysis	18
3.2.1 Offshore wave data.	18
3.2.2 Nearshore wave data.	19
3.3 Methodology	21
3.4 Model setup.	21
3.5 Model calibration.	22
3.6 Model validation	24
3.7 Conclusion	28
4 1D modelling study	29
4.1 Introduction	29
4.2 Methodology	29
4.2.1 1D model & setup	29
4.2.2 Single-parameter sensitivity study	30
4.2.3 Multi-parameter sensitivity study	31
4.2.4 Wave height & mean water level estimation	32
4.2.5 Wave runup estimation	33
4.3 General 1D model results	34
4.3.1 General hydrodynamic effects of excavation pits.	34
4.3.2 General modelled hydrodynamic effects of excavation pits	36

4.4	Results multi-parameter sensitivity analysis	40
4.4.1	Effect on hydrodynamic processes	40
4.4.2	Effect on wave runup	45
4.5	Conclusion	53
5	2D modelling study	55
5.1	Introduction	55
5.2	Methodology & 2D Model setup.	55
5.3	2D Model results & discussion	55
5.3.1	Comparison of 1D and 2D output	55
5.3.2	Observed 2D effects	59
5.4	Conclusion	61
6	Discussion & limitations	63
6.1	Limitations of XBNh+	63
6.2	Model simplifications.	63
6.3	Model results	64
7	Conclusions	67
7.1	Modelling with XBeach non-hydrostatic+.	67
7.2	Effects of excavation pits on fringing reef hydrodynamics.	67
7.3	Effects of excavation pits on wave runup	68
8	Recommendations	71
8.1	Modelling with Xbeach non-hydrostatic+.	71
8.2	Reef excavation practices & designs.	71
8.3	Future research	71
	Bibliography	73
A	Validation	A-1
A.1	Comparison of XBeach modules	A-1
A.1.1	Introduction & background	A-1
A.1.2	Output analysis	A-3
A.2	Grid discretisation	A-6
A.3	Results calibration event	A-9
B	1D modelling	B-13
B.1	Water level & wave height estimation	B-13
B.2	Runup estimation.	B-18
B.3	Reef geometry simplification	B-24
B.4	Single-parameter sensitivity analysis	B-25
B.4.1	Influence of hydrodynamic forcing	B-25
B.4.2	Influence of reef geometry	B-26
B.4.3	Influence of pit geometry	B-29
C	2D modelling	C-31
C.1	Comparison of hydrodynamics in 2D & 1D, without pit	C-31

List of Figures

1.1	Bar graph with elevations of Small Island Development States (SIDS)	1
1.2	Satellite and aerial photos from Kwajalein Atoll, Republic of the Marshall Islands	2
1.3	Flow diagram of main components of MSc research	4
2.1	Schematisation of the three reef classifications of Darwin (1842)	6
2.2	Global distribution of warm water coral reefs	6
2.3	Conceptual 1D cross-shore schematization of a fringing reef with excavation pit	7
2.4	Breakpoint forcing mechanism on a fringing reef	11
2.5	Resonance mechanisms on fringing reefs and contributing factors	13
2.6	Schematic representation of runup according to Stockdon et al. (2006)	14
3.1	Satellite image of Majuro Atoll, with locations of the two used dataset	18
3.2	Time series of the CDIP offshore wave buoy	19
3.3	Satellite image of nearshore measuring site and bathymetry of the two measured transects	20
3.4	Measured wave transformations at Majuro Atoll	20
3.5	Model setup for validation study	22
3.6	Computed and measured water levels and wave heights during the validation event	25
3.7	Computed and measured variance density spectra during the validation event	26
3.8	Scatter plots of computed and measured wave heights during the validation event	27
4.1	Model setup used in the 1D study	30
4.2	Example of time series of runup gauge output	34
4.3	Effects of relevant reef flat processes on variance density spectrum	34
4.4	Schematic visualisation of an amplification curve for a damped system	36
4.5	Cross-shore transformation of hydrodynamics for a reef with and without excavation	37
4.6	Incoming and outgoing wave heights across a reef with and without excavation	38
4.7	Variance density spectra of incoming and outgoing wave signals at reef crest and beach-toe	39
4.8	Boxplots of variance spectra & change in variance, for all modelled reefs	41
4.9	ECDFs of changes in wave heights at the four natural frequencies of the original reef	42
4.10	Density scatter plot of changes in wave heights around $f_{n,0}$ and in the IG band	42
4.11	ECDFs of changes in $H_{s,f_{n,i}}$ at the beach-toe as a function of pit width and cross-shore location	43
4.12	ECDFs of change in wave height at the HF peak and HF tail, as a function of pit width	44
4.13	ECDF of change in wave height at the HF band, HF peak and HF tail	44
4.14	Density scatter plots of relation between wave heights in the HF peak and HF tail	45
4.15	Boxplots of computed runup for every modelled parameter in multi-parameter sensitivity study	46
4.16	PDF's of used input variables and ECDF and EPDF of total output (normalized runup)	47
4.17	Changes in mean variance density due to pit, for reefs with an increase and decrease in runup	48
4.18	ECDFs of normalized runup for each parameter included in multi-parameter sensitivity study	50
4.19	Percentage of reefs with an increase in runup due to pit, as function of six parameters	51
4.20	Percentage of reefs with an increase in runup due to pit, with high MSL	52
5.1	Comparison of wave heights and mean water levels of a 1D and 2D run	56
5.2	Comparison of variance density spectra at the beach-toe, for the 1D & 2D model	57
5.3	Runup as a function of n , a comparison between 1D and 2D model outputs	57
5.4	Comparison of normalized wave heights and mean water level for 1D & 2D	58
5.5	Spatial variation of wave height and mean water level & resulting currents	59
5.6	Long-shore variation in wave height, mean water level and runup	60
6.1	Density scatter plots of wave height and change in wave height at the beach-toe and swash	65

A.1	Comparison of the instantaneous water level, for XBSB, XBnh & XBnh+	A-3
A.2	Wave transformations of the full wave signal and mean water level, for XBSB, XBnh & XBnh+	A-4
A.3	Wave transformations of the incoming wave signal for XBSB, XBnh & XBnh+	A-4
A.4	Wave transformations of the outgoing wave signal for XBSB, XBnh & XBnh+	A-5
A.5	Normalized wave heights, swash, mean water level and mean shoreline for different grid sizes	A-6
A.6	Surface elevation time series and variance density spectra, for different grid sizes	A-7
A.7	HF wave transformation & pit wall steepness	A-7
A.8	Surface elevation time series and variance density spectra of water line, for different Δx	A-7
A.9	Variation in swash and normalized runup, for different Δx	A-8
A.10	Measured and computed water levels and wave heights during the mode calibration	A-9
A.11	Scatter plots measured and computed wave heights during the calibration event	A-10
A.12	Measured and computed variance density spectra during the calibration event	A-11
B.1	Relative errors in computation of hydrodynamics due to sampling	B-14
B.2	SCI & bias of wave heights and mean water level, due to sampling	B-15
B.3	Relative errors in computation of effect of pits on hydrodynamics due to sampling	B-16
B.4	SCI & bias of normalized (pit/no pit) wave heights and mean water level, due to sampling	B-17
B.5	ECDF of the peaks in a 24 hr runup gauge signal on a fringing reef with pit	B-18
B.6	Boxplots of absolute runup and normalized (pit/no pit) runup for different extreme quantiles	B-19
B.7	Correlation, bias & scatter for different $R_{1\%}$, compared to a baseline $R_{2\%}$	B-19
B.8	Correlation of changes in runup for different quantiles	B-19
B.9	SCI & bias of different runup values, due to sampling	B-20
B.10	Relative errors in runup computation due to sampling	B-21
B.11	Relative errors in normalized (pit/no pit) runup, due to sampling	B-22
B.12	SCI & bias of different (normalized, pit/no pit) runup values, due to sampling	B-23
B.13	Wave and water level transformation across the measured reef and a schematized case.	B-24
B.14	Wave (HF & IG) and mean water level transformation for different values of reef submergence	B-25
B.15	Variations in HF and IG wave heights at five locations of the reef, for different reef submergence	B-25
B.16	Normalized water levels and wave heights for different values of reef submergence	B-26
B.17	Normalized water levels and wave heights for different values of reef submergence (MSL).	B-27
B.18	Normalized water levels and wave heights for different values of fore reef slope.	B-27
B.19	Water levels and wave heights for different values of reef flat width.	B-28
B.20	Normalized runup levels and swash components for different values of beach slope.	B-29
B.21	Normalized water levels and wave heights for different values pit width.	B-29
B.22	Normalized water levels and wave heights for different values of cross-shore pit location.	B-30
B.23	Variation in mean water levels and wave heights for different values of pit wall slope	B-30
C.1	Comparison of wave heights and mean water levels of a 1D and 2D run without pit	C-32

List of Tables

3.1	Calibration parameters used in validation of XBNh+	24
3.2	Model skill scores for the validation event	24
4.1	Full parameters space used in 1D modelling	31
4.2	Parameter space used during the multi-parameter sensitivity study	32
4.3	Model skill in estimating wave height and mean water level (sampling errors)	33
4.4	Model skill in runup estimation	34

List of Definitions

1D	one-dimensional
2D	two-dimensional
2DH	two-dimensional in the horizontal plane
2DV	two-dimensional in the vertical plane
3D	three-dimensional
BLW	bound long wave
CDIP	Coastal Data Information Program
corr.	Pearson's correlation coefficient
ECDF	empirical cumulative distribution function
EPDF	empirical probability density function
HF	high-frequency band ($0.04 \text{ Hz} < f < 0.4 \text{ Hz}$)
HF peak	high-frequency peak band ($0.04 \text{ Hz} < f < 0.12 \text{ Hz}$)
HF tail	high-frequency tail band ($0.12 \text{ Hz} < f < 0.4 \text{ Hz}$)
IG	infra-gravity band ($f < 0.04 \text{ Hz}$)
JONSWAP	JOint North Sea WAve Project
LBW	long bound wave
MSL	mean offshore sea level
RB	relative bias
RMSE	root-mean-squared error
runup	maximum elevation of a wave on the beach slope: wave runup
SCI	scatter index
SIDS	Small Island Developing States
VLF	very low frequency band ($f < 0.004 \text{ Hz}$)
XB	XBeach
XBnh	XBeach non-hydrostatic module
XBnh+	XBeach non-hydrostatic+ module
XBSB	XBeach surfbeat module

List of Symbols

α_{beach}	beach slope	[-]
α_{pit}	excavation pit wall slope	[-]
α_{reef}	fore reef slope	[-]
γ	JONSWAP peak enhancement factor	[-]
Δx	grid size	[m]
ζ	surface elevation	[m]
η	surface elevation	[m]
$\bar{\eta}$	mean surface elevation	[m]
λ	wave length	[m]
σ	directional spreading of offshore waves	[rad]
σ_t	standard deviation of sample size t	[-]
$c_{f,crest}$	reef crest roughness	[-]
$c_{f,flat}$	reef flat roughness	[-]
$c_{f,pit}$	roughness pit bottom	[-]
$E_{t=24hr}$	expected value of a 24 hr sample	[-]
f	frequency	[Hz]
$f_{0,peak}$	peak frequency in the offshore variance density spectrum	[Hz]
f_1, f_2	first & second free wave components in wave-wave interaction (triads)	[Hz]
f_3	sub- or super-harmonic resulting from wave-wave interaction (triads)	[Hz]
$f_{n,i}$	i^{th} natural frequency	[Hz]
f_{split}	split frequency between HF peak and HF tail bands ($f_{split} = 0.12$ Hz)	[Hz]
g	gravitational acceleration	[ms ⁻²]
H	wave height (at waterline)	[m]
H_s	significant wave height (= $H_{1/3} = H_{m0}$)	[m]
$H_{s,0}$	significant offshore wave height	[m]
$H_{s,HF}$	significant high frequency ($f > 0.4$ Hz) wave height	[m]
$H_{s,IG}$	significant infra-gravity ($f < 0.04$ Hz) wave height	[m]
k	wave number	[m ⁻¹]
\vec{k}	wave number vector ($\vec{k} = (k_x + k_y)$)	[m ⁻¹]
l_{pit}	length of pit (in y-direction)	[m]
MSL	mean (offshore) sea level	[m]
m_0	zero th -order spectral moment	[m ²]
$R_{n\%}$	runup level at n^{th} -quantile	[m]
r	Pearson's correlation coefficient	[-]
S	variance density	[m ² s]
S_s	significant swash	[m]
$S_{s,HF}$	significant high frequency ($f > 0.4$ Hz) swash	[m]
$S_{s,IG}$	significant infra-gravity ($f < 0.04$ Hz) swash	[m]
s	JONSWAP spreading parameter	[rad ⁻²]
s_0	offshore wave steepness	[-]
T	simulation period	[s] or [hr]
T_f	filter period between subsequent waves in runup signal	[s]
T_p	peak wave period	[s]
T_{spinup}	spinup time used in simulations	[s]
W_{pit}	width excavation pit (in x-direction)	[m] (or [%] of reef width)
W_{reef}	reef flat width	[m]
x	cross-shore location	[m] (or [%] of reef width)
x_{pit}	cross-shore location excavation pit	[m]
y	long-shore location	[m]
z	bottom elevation	[MSL+m]
z_{pit}	excavation pit depth	[m]

Introduction

1.1. Problem description

Many small island developing states (SIDS), and in particular nations of the Pacific and Indian Oceans, are among the most vulnerable to climate change (e.g. sea level rise) and to seasonal to inter-annual climate variability. Many of them are characterized by their small size and dense population in low-lying areas (see Figure 1.1), such as atolls and fringing reefs. Flooding due to swell waves and extreme events, coastal erosion and salinization of the fresh water lenses are among some of the major hazards to those islands, resulting in large-scale damages to the local populations, nature and infrastructures on the islands. Some of these nations face the likely possibility of land loss due to coastal erosion and sea level rise resulting from climate change (UN-Habitat, 2015).

According to UN-Habitat (2015), urbanization will continue to create problems for Small Island Development States (SIDS) if it remains unaddressed. Though the urban context for SIDS is unique, there remains a priority of capitals leading to wild growth of informal settlements. The small size and geographic isolation of SIDS make them vulnerable to ecological and economic shocks, especially in light of the increasing impacts of urbanization and climate change.

Additionally, the limited financial means of those countries, in combination with a high degree of knowledge fragmentation among the organizations operating on the numerous islands, are highly limiting factors, preventing the use of sustainable and climate-resilient engineering practices.

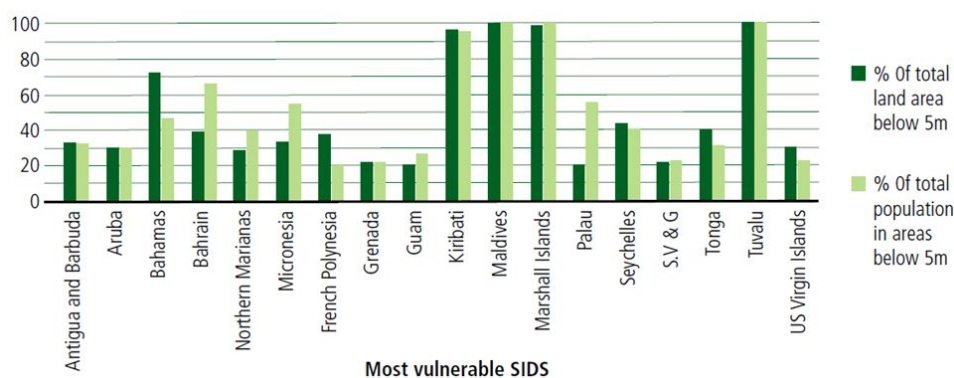


Figure 1.1: Percentage of populated and total land area below 5 m above mean sea level (MSL) of the most vulnerable SIDS according to UN-Habitat (2015). Especially Kiribati, Maldives, Marshall Islands and Tuvalu, all of which are reef islands or atolls, are characterized by extremely low elevations, remoteness in open oceans and a dense population.

In particular, the excavation of mining pits on fringing reefs is a common practice on atoll islands, due to the scarce availability of aggregate resources (see Figure 1.2 for an example). Mining pits are generally excavated in order to derive suitable material for coastal engineering projects or other constructions. Sea level rise and

possible changes in the intensity and frequency of extreme events will result in an increasing demand of suitable aggregate for coastal protection works, enhancing the current need of available material. There is an urgent need for new coastal engineering knowledge and tools to be applied in those environments in order to preserve resilience and allow them to survive sea level rise and climate change. One of the alternatives to reef mining is the importation of rocks and other armour units. However this approach may result in extremely high costs for coastal protection projects.



Figure 1.2: Satellite and aerial photos of Kwajalein Atoll, Republic of the Marshall Islands. The figure clearly shows the excavations that have been made in the reef flat on the ocean-side fringing reef. Dimensions of one of the excavations are shown in the aerial photo of the island, and correspond to an averagely sized reef excavation. Other general features of atolls, such as the high level of urbanization, low elevation and small size of the island are also visible. (source: www.alifemapped.com)

Little is known regarding the effects of these pits on the resilience of atolls. Therefore, new knowledge, new tools and a more integrated system approach are required in order to address these emerging challenges. Also the effects of these excavation pits, in terms of ecology, hydrodynamics and sediment dynamics, remains unclear and it is therefore unknown whether these excavation pits provide a sustainable solution to above-mentioned problems.

Clearly, the blasting of alive coral poses a threat to the existence and future of the present ecosystems. However, this is not as straightforward in the case of dead reefs. Increased turbidity could potentially harm the ecosystem and the pits could trap polluting materials that are being dumped from the islands (Banner, 1968). Contrastingly, the construction of pits could introduce new favourable habitat conditions due to the creation of ponds for aquatic life.

A number of recent studies (e.g. Ford et al., 2013; Yao et al., 2016) have looked into the hydrodynamic effects of mining pits on nearshore wave dynamics by means of measurements and numerical modelling. Nevertheless, these studies only focused on a limited number of wave input conditions and pit geometries. Moreover, the impacts and coastal management implications of these pits (e.g. on coastal flooding, erosion, fresh water salinization) have so far not been addressed.

Similarly, the effects of the excavation pits on the sediment dynamics have not been studied. The pits could act as a trap for sediments, thereby changing the sediment budgets of the system. Also, an alteration of the hydrodynamics could change the local erosion or accretion.

1.2. Research objectives

Based on a literature review and recommendations made in previous research, the main objectives of this research have been formulated as:

1. "To increase the understanding of the effects of reef excavating on fringing reef hydrodynamics."
2. "To assess the accuracy and validity of using XBnh+ for the modelling of fringing reefs with excavation pits."

The first objective aims to assess the relevant reef hydrodynamics by means of a literature review. From this, and also using previous research, relevant parameters related to reef geometry, pit geometry and offshore forcing, can be identified.

Following this, a substantiated assessment is made of the effects of pits on fringing reef hydrodynamics, using 1D and 2D XBnh+ models. Also, parameters that significantly influence the observed effects of pits are identified.

The final part of this objective aims to identify the possible impacts of reef excavations on wave runup on fringing reef beaches.

The second objective focuses on the validity of the use of XBnh+ for modelling fringing reefs with excavation pits. This will include the calibration of an XBnh+ model with previously made measurements by Ford et al. (2013). The validation will assess the accuracy of the model, the introduced numerical effects and the errors made, for example by spatial discretization and computation of wave heights and runup.

1.2.1. Research questions

In order to reach the objectives of this thesis, the following research questions have been formulated:

- "What are the effects of excavation pits on fringing reef hydrodynamics?"
- "What are the general implications of excavation pits with different dimensions and designs on wave runup on a range of fringing reef coasts during extreme conditions and for future sea level rise?"
- "What would be an optimal design for an excavation pit on a fringing reef, in order to reduce potential negative impact?"
- "What are the numerical errors that XBnh+ introduces during modelling of fringing reefs and excavation pits"
- "Can the XBnh+ model be used to model hydrodynamic processes of fringing reefs with an excavation pit?"

1.3. Research approach

In order to reach the objectives and answer the questions that have been formulated for this thesis, the research has been divided into five parts. This study starts with a literature study on fringing reefs and relevant hydrodynamics, which provides a scientific context for this thesis. This is followed by the validation of the XBnh+ model, followed by a 1D and later 2D study on the effects of excavation pits on fringing reef hydrodynamics and runup.

- **Literature study on fringing reefs and relevant hydrodynamic processes.**
The literature study is performed in order to provide a context for this thesis research and identify important processes of reef hydrodynamics, relevant parameters for numerical modelling and knowledge gaps in the current state of research. The literature study is summarized in Chapter 2.
- **Validation of XBnh+.**
The validation of the XBnh+ model consists of calibration of the model using nearshore wave measurements and bathymetric data provided by Ford et al. (2013) and offshore wave conditions obtained from a wave buoy. Firstly, these data are analysed, from which suitable wave events are obtained that are used in model calibration and subsequent validation. The calibration and validation provide information on the accuracy and applicability of XBnh+ for the modelling of fringing reefs with excavation pits.

Additionally, numerical errors and instabilities of the model and methods that were used to analyse the results were assessed. This chapter provides insights on the validity of the results of the conceptual studies and the accuracy of the used models. (see Chapter 3).

- **1D single parameter sensitivity study on the effects of excavations on reef hydrodynamics.**

A schematized fringing reef is used in the 1D parameter sensitivity study that will assess the impacts of excavation pits on fringing reefs. Besides assessing the impact of parameters on the effects of pits on fringing reefs, the parameter sensitivity study identifies the effect of parameters on reef hydrodynamics, the results of which can be with findings from previous studies. Previous studies on fringing reefs are used to define the parameter space. Model runs are set up in a way that covers the full range of the parameter space, therefore becoming a rough representation of a large percentage of reefs around the world. This sensitivity study is used to identify the parameters that have the largest impact on reef hydrodynamics and the effect of pits. This is found in Appendix B.4.

- **1D multi-parameter sensitivity study on effects of excavations on runup.**

The important parameters that are found in the first sensitivity study are used in a multi-parameter sensitivity study that models each possible combination of parameter values. The output of this large amount of model runs is used to find the general effect of excavation pits on the runup on fringing reefs. Storm wave heights are used during this study, and the effect of sea level rise is taken into account as well. For this study, the number of values for each parameter is reduced in order to lower time constraints. All 1D modelling is elaborated further in Chapter 4.

- **2D modelling study.**

This study focuses on the two-dimensional effects of excavation pits, such as alongshore variability in wave heights and runup, but also circulation patterns. The results of the 1D models are compared with the 2D models. Additionally, an assessment is made of the impacts on the 2D effects. This study is discussed in more detail in Chapter 5.

The approach of this thesis research is visualized in Figure 1.3.

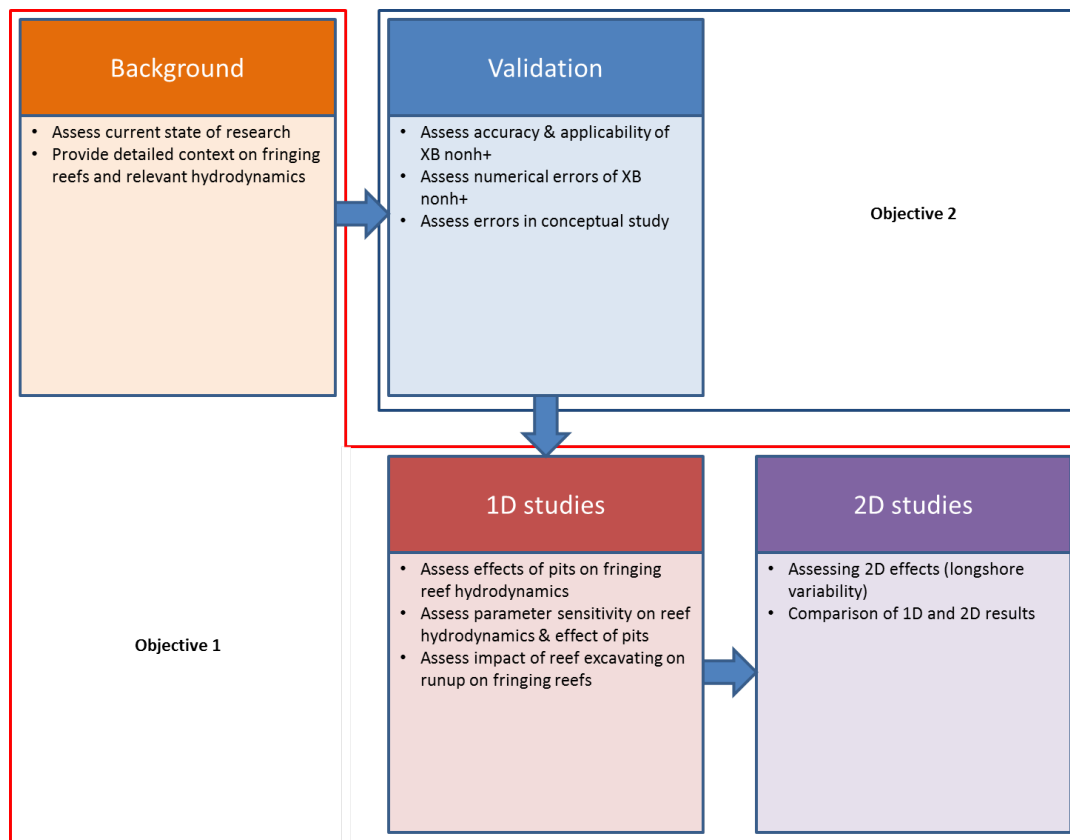


Figure 1.3: Flow diagram showing the four main components of the thesis research: background on fringing reefs and hydrodynamics, validation of XB nonh+, 1D modelling studies and a 2D modelling study.

2

Background

2.1. Reef coasts

A coastal reef functions as a protective barrier that, through interactions between the offshore hydrodynamic forcing (e.g., swell waves, wind, tides) and the specific morphology of the reef, determines the hydrodynamic processes (waves, currents and water levels) that occur in the near-shore zone (Pomeroy et al., 2012a). Recently, the value of coral reefs as nature-based flood defenses has been recognized (Ferrario et al., 2014; Narayan et al., 2016)

The physical presence of a reef shapes the nearshore transport pathways, controls the associated long-term morphological changes to a coastline, and helps to buffer coasts from extreme forcing events such as swell and tropical cyclones and tsunamis (Kunkel et al., 2006; Sanderson, 2000; Storlazzi et al., 2004).

Reefs host complex and valuable ecosystems that support abundant marine species and provide resources for fisheries, recreation and even building materials (Gawehn et al., 2016).

2.1.1. Reef classification

In general, a distinction is made between four types of reefs (see also Figure 2.1):

1. **Fringing reefs** grow near the coastline around islands and continents. They can be separated from the shore by narrow, shallow lagoons.
2. **Barrier reefs** also occur parallel to the coastline but they are separated by deeper, wider lagoons. This lagoon is usually defined by having a minimum width of 500 m and a minimum depth of 5 m. At their shallowest point, they can reach the water's surface forming a "barrier" to navigation. The Great Barrier Reef in Australia is the largest and most famous barrier reef in the world.
3. **Coral atolls** are rings of coral that create protected lagoons. Atolls usually form when islands surrounded by fringing reefs sink into the sea or the sea level rises around them (these islands are often the tops of underwater volcanoes). The fringing reefs continue to grow and eventually form spherical structures with a large and deep (~ 50 m) lagoon in the center. The reefs of these atolls that reach the surface become low lying islands.
4. **Patch reefs** are small, isolated reefs that grow up from the open bottom of the island platform or continental shelf. They usually occur between fringing reefs and barrier reefs. They vary greatly in size, and they rarely reach the surface of the water.

The first three types of reefs were described by Darwin (1842), and the fourth type of reef is more properly considered to have regular micro-scale reef features of all three of the macro-scale reef types that were first described. Figure 2.1 shows a visualization of the three main reef types. An island (mostly volcanic islands) with a fringing reef subsides into the ocean, while the reef continues to grow on the edges of the island. This way, a barrier reef can be formed. Further subsidence of the island can completely submerge the landmass, leaving behind only the reef itself; the atoll. The reefs of the individual islands on the atolls could also be categorized as fringing reefs.

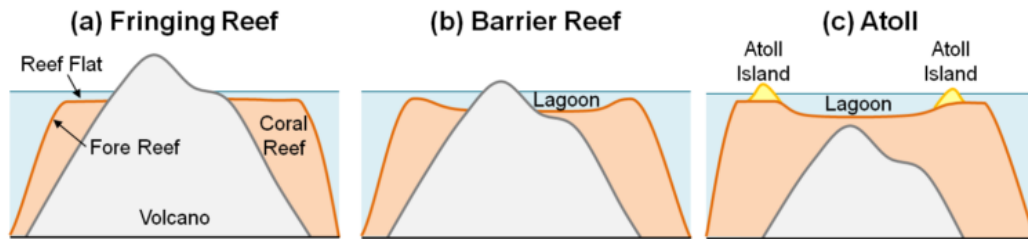


Figure 2.1: Schematized visualization of the cross-sections of the three main reef types first described by Darwin (1842). The figure shows a fringing reef (a), barrier reef (b) and coral atoll (c), and makes a distinction between coral reef structure (red) and subsoil (gray). The atoll islands are indicated in yellow, between which a lagoon forms due to land subsidence of (volcanic) islands. (Pearson, 2016)

As can be seen in figure 2.2, coral reefs are located mainly around tropical islands. These include all four types of reefs that were addressed in the previous section. Most of the small reef islands are found in the Southern Pacific area, as well as the Indian Ocean and the Caribbean.

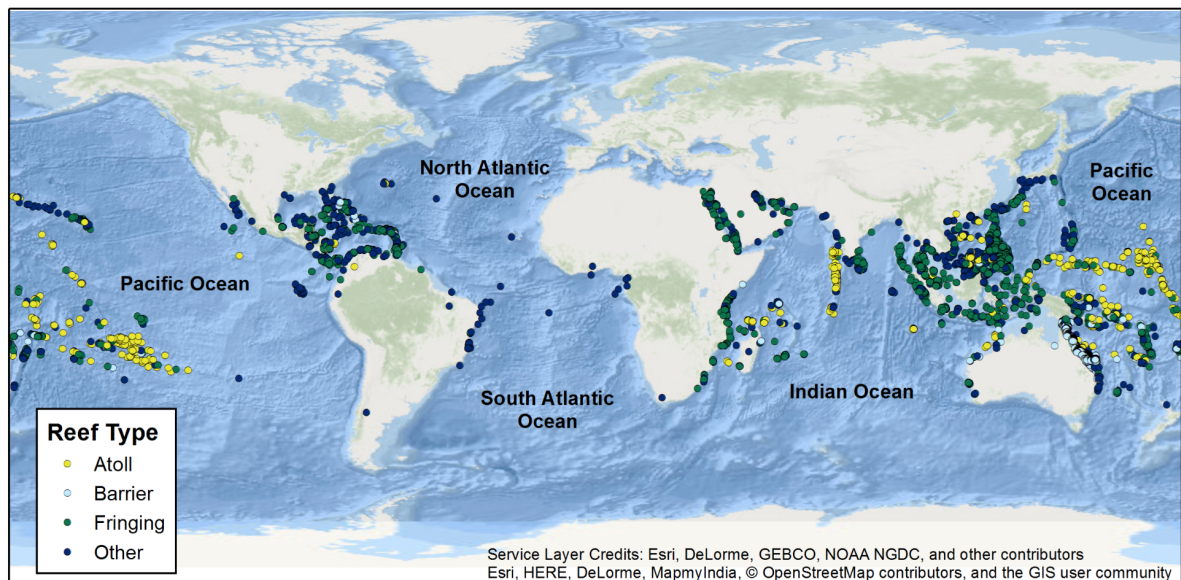


Figure 2.2: Global distribution of warm water coral reefs. A distinction is made between coral atolls (yellow), barrier reefs (cyan), fringing reefs (green) and other types such as path reefs (navy). Coral atolls are most abundant in the Pacific ocean in relatively remote areas. (Pearson, 2016)

2.1.2. Reef morphology

Unlike rocky shores, reefs are composed of living organisms, and hence have unique ecological dependencies. According to Baldock et al. (2014), changes to the health of the reef have impact on its morphology. Schematically, a fringing reef consists of a fore reef, a reef flat and a beach (see figure 2.3). Whereas a barrier reef also consists of a lagoon shore-ward of the reef crest, generally with a larger water depth compared to the fringing reef.

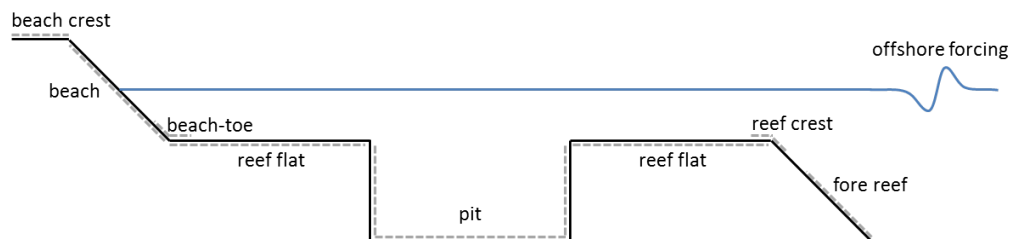


Figure 2.3: Schematization of cross-shore profile of a fringing reef, showing the definitions of parts of the reef as are used in this thesis. From deep ocean to nearshore these are: fore reef, reef crest, reef flat, excavation pit, beach-toe (or inner reef flat), beach and beach crest.

2.1.2.1 Fore reef

The fore reef steeply rises from the deep ocean up to the reef crest. The morphology of the fore reef depends on the sea level history, karstification and cementation, biological construction and erosion processes, and collapses or slides from major storms, tsunamis, and earthquakes (Hopley, 2011). The top of the fore reef which connects to the reef flat is referred to here as the reef crest.

2.1.2.2 Reef flat

The reef flat extends as a platform from the reef crest to the shoreline and is covered in coral, rubble, sand and algae (Hopley, 2011). Typical widths of reef flats range from 40 to 2000 m (Kolijn, 2014; Quataert, 2015). According to Brander et al. (2004), when the reef crest rises above the mean elevation of the reef flat, resulting in ponding at low tide, the reef resembles a barrier reef. Topographical variations of the reef have a large influence on the wave transformation across the reef flat (Brander et al., 2004).

2.1.2.3 Beach

The beach transitions the reef flat to the emerged part of the shore. Beach sediment is typically calciumcarbonate-based, originating from coral sources on the reef and transported ashore (Hopley, 2011). The slope of beaches strongly influences the runup (Stockdon et al., 2006). Additionally, beach percolation and porosity can also play a role in the attenuation of wave runup (Beetham et al., 2016; Kench et al., 2009). The highest points on atolls are typically ridges built by waves depositing sediment, which possibly protects the interior of islands from inundation (Smithers and Hoeke, 2014). Smithers and Hoeke (2014) also found that older parts of a village on Nukutoa was located on higher ground than newer expansions, which suggest that vulnerability to flooding will increase with increasing development.

2.1.2.4 Reef ecology & roughness

Roughness length scales of reefs can vary significantly over short distances, as well as the heterogeneous character of reef bathymetry, making reef roughness difficult to parameterize (Jaramillo and Pawlak, 2011). Coral forms large, complex canopies along the seabed which can greatly distort the spatial flow structure across them (Lowe and Falter, 2015). According to Monismith et al. (2015), high ecological roughness is associated with healthy coral organisms. The health of the coral has a strong influence on the hydrodynamic processes that act on the reef (Baldock et al., 2014). Reef mortality can increase the wave energy reaching the shoreline, by decreasing the hydrodynamic roughness (Sheppard et al., 2005).

2.1.2.5 Longshore variations

For fringing reefs, the particular geometry of the lagoon and/or channels (gasps) in the reef have been shown to play a major role in the momentum balances established across reef-lagoon systems and ultimately the magnitude of the wave-driven flows and related coastal flushing rates (Lowe et al., 2010) and potentially sediment dynamics. Longshore variations of the shoreline can amplify wave heights or setup (Lowe et al., 2010). Additionally, varying bathymetry can result in wave focusing due to refraction (Rogers et al., 2015). Besides refraction, also edge waves may decrease the infragravity (IG, 0.004-0.04 Hz) wave period (Beetham et al., 2016). Since low-frequency waves require a very specific combination of reef geometry and offshore hydrodynamic forcing to become resonant and cause flooding, the heterogeneous bathymetry of many reefs results in a decrease in coastal hazards (Roerber and Bricker, 2015). The shore-normal directed spur (ridge) and groove (trough) formations on the fore reef form in environments with high wave energy (Rogers et al., 2013).

2.2. Relevant reef hydrodynamics

2.2.1. Effects of climate change

Climate change will have negative impacts on the protective properties of coral reefs through sea level rise. Changing wave conditions, changing reef hydrodynamics such as increased dominance of low frequency resonance, degradation of reef properties such as roughness and increased mortality due to ocean acidification and changing water temperatures, resulting in coral bleaching or hydrodynamic stresses, can all result in more frequent extreme wave-driven coastal flooding and geomorphic change (Beetham et al., 2016; Cherriton et al., 2016; Grady et al., 2013; Hoegh-Guldberg et al., 2007; Merrifield et al., 2014; Péquignot et al., 2009; Quataert et al., 2015; Sheppard et al., 2005; Storlazzi et al., 2011). The destruction of reefs due to climate change is expected to vary spatially, temporally, by species and depends on the amount of human interventions (Pandolfi et al., 2011). Reef flat accretion rates (1-4 mm/yr) (due to coral growth) are an order of magnitude smaller than projected sea level rise (8-16 mm/yr) (Grinsted et al., 2010; Montaggioni, 2005). Sea level rise is projected to exceed year 2000 levels by up to 2 m by year 2100, according to estimates of Grinsted et al. (2010) and observations of Vermeer and Rahmstorf (2009) that include the effects of thermal expansion and ice melting .

2.2.2. Ecological aspects

Near-shore hydrodynamic processes (e.g. wave breaking) have been identified to be important to many ecological processes within reef environments such as: the control of the spatial distribution of dissolved and particulate nutrient uptake by reef organisms, ecological zonation and larval recruitment pathways (Atkinson and Falter, 2003; Dollar, 1982; Kraines et al., 2001; Roberts, 1997; Wyatt et al., 2010; Yahel et al., 1998; Zhang et al., 2011). Wave-induced forces have a detrimental effect by destroying delicate reef organisms. Therefore wave exposure is often used as a predictor of the community structure of coral reefs (Dollar, 1982; Dollar and Tribble, 1993; Grigg, 1998). Alternatively, there is an increasing evidence that water motion can benefit coral reef organisms by increasing the rate at which these organisms take up nutrients and hence their overall productivity. Many coral reefs are found in coastal regions with significant wave activity such that wave-induced shear stresses are exerted on the bed. These stresses can often be much larger than the stress attributed to the unidirectional current. This enhanced wave stress can increase the rate of nutrient uptake (Atkinson and Bilger, 1992; Baird and Atkinson, 1997; Falter et al., 2004; Thomas and Atkinson, 1997).

2.2.3. Hydrodynamic forcing

2.2.3.1 Water levels

According to Péquignot et al. (2011), wave energy on reefs is dependent on the reef submergence, with more energy reaching the shoreline at higher water levels, though wave-induced setup decreases with increasing depth. Local sea level change due to atmospheric pressure variations is inversely proportional to pressure, which occurs during tropical cyclones (Hoeke et al., 2013).

Tides

The tides influence the submergence depth of the reef, which in turn influences the significant wave height across the reef platform by increasing the wave height at high tide and vice versa at low tide (Brander et al., 2004). According to Becker et al. (2016), stationary conditions are required to generate modal behaviour at low frequencies, therefore the tide puts temporal constraints on the window during which extreme runup can occur. Up to 30 % of all reefs are tidally dominated (Lowe et al., 2015).

Regional & global sea level changes

For coral atolls, changes in water levels are important because they control the submerged reef flat depth, which affects the reef hydrodynamics, and because they reduce the elevation of the island above sea level. Accelerated global sea level rise and regional sea level fluctuations linked to the El Niño-Southern Oscillation (ENSO), atmospheric pressure changes, or other anomalies, such as Rossby Waves or equatorially trapped internal gravity waves, may greatly increase the severity of relatively minor wave events (Church et al., 2006; Hoeke et al., 2013; Wunsch and Gill, 1976).

2.2.3.2 Offshore waves

Extratropical regions tend to generate swell via large storms and infra-gravity (IG, $f < 0.04$ Hz) or even very low frequency (VLF, $f < 0.004$ Hz) waves are generated at greater distances (Pearson, 2016; Rawat et al., 2014). Swell is the result of directional and frequency dispersion, and is generally generated far away from the site of interest (Munk et al., 1963).

Locally generated sea

Locally wind-generated sea waves are characterized by a broader spectrum and higher frequencies, which results in higher steepness and lower groupiness (Pearson, 2016). Additionally, waves generated on wide reef flats will be limited to local water depth (Nelson, 1997).

Infragravity & very low frequency Waves

Offshore IG waves are influenced by complex interactions between shoreward-propagating bound long waves (BLW) and seaward-directed IG waves generated by the breakpoint mechanism (Pomeroy et al., 2012b). Non-linear interactions between HF wave components with slightly different frequencies create bound long waves (BLW) (Herbers et al., 1994). Narrower spectra (with higher groupiness), that result from remotely generated swell is a stronger source of BLW compared to locally-generated waves. This explains why BLW are strongest in high energy swell conditions (Herbers et al., 1995; Van Dongeren et al., 2003).

Gawehn et al. (2016) differentiates between VLF and IG waves because resonance at the fundamental mode is typically associated with timescales of several minutes, which is in the VLF range (Lugo-Fernández et al., 1998). Péquignet et al. (2009) demonstrated that resonance at the fundamental mode significantly increased the amount of VLF energy reaching the shoreline during storm conditions at Ipan Reef in Guam. These motions possibly contributed to the inundation of parts of the island. Laboratory experiments conducted by Nakaza and Hino (1991) revealed that increased amplitude modulation of incoming short wave groups increased the amplitude of resonating waves.

2.2.4. Wave transformation on reefs

As waves approach an island from offshore, they rapidly shoal and then break along the upper slope of the fore reef and reef crest, dissipating energy in the process. Further wave propagation is characterized by continued energy loss due to breaking and frictional dissipation across the reef flat. The dominant frequencies become lower due to the breaking of shorter, steeper waves. Important characteristics of wave transformation across reefs are wave height reduction and spectral evolution from HF dominance offshore to multimodal spectra at mid-reef, followed by low-frequency dominance at the shoreline (Pearson, 2016).

2.2.4.1 Wave height reduction

The wave height at the shoreline is inversely proportional to reef flat width (Péquignet et al., 2011). Across the reef flat, the large majority of the wave energy is dissipated (78-97 %) when it reaches the shoreline (Beetham et al., 2016; Brander et al., 2004; Péquignet et al., 2011). There is a strong linear relationship between wave height and reef submergence (Brander et al., 2004).

2.2.4.2 Bimodal spectra

In the zone of wave breaking, the energy in the high frequency (HF, $f = 0.04 - 0.4$ Hz) band is also transferred to higher and lower wave frequencies (LF) (Gerritsen, 1980), causing wave spectra to become bimodal (Young, 1989). This is also because HF and low frequency (IG and VLF) wave components have different spatial trends in growth and decay (Pomeroy et al., 2015). Spatial variation in wave energy is frequency dependent, and decreases across the reef flat, but IG wave energy peaks on mid-reef flat and VLF energy peaks at inner reef flat (Cheriton et al., 2016).

2.2.4.3 Low frequency dominance

Across the reef flat, which acts as a low-pass filter, IG waves play an increasingly important role, and ultimately become dominant, in contrast with the reef crest, where HF waves are dominant (Lowe et al., 2005; Pomeroy et al., 2012a; Van Dongeren et al., 2012). According to Young (1989), IG wave energy over the reef flat increases with increasing water depth and increases further towards the shoreline (Nwogu and Demirbilek, 2010). The HF wave height shoals and then decreases rapidly at the reef crest, followed by gradual dissipation across the reef flat, while IG wave height also shoals and then rapidly decreases at the crest, but consequently grows higher as the IG waves propagate across the reef flat, allowing IG waves to dominate closer to shore, which can lead to extreme water levels during storm events (Blacka et al., 2015; Pomeroy et al., 2012a, 2015).

2.2.4.4 Shoaling

Waves approaching the reef will begin to shoal due to a decrease in depth across the fore reef slope. Shoaling occurs fast due to the rapidly varying bathymetry. As a result waves steepen and generate bound higher harmonics, due to an increase in non-linearity. Steeper fore reefs can (partly) reflect waves in offshore direction (Young, 1989). In the case of a barrier reef, where the water depth increases after the reef crest, higher harmonics are freed, which results in the broadening of the spectrum (Young, 1989). Shoaling continues up to the point of breaking, or if the water depth increases.

2.2.4.5 Wave breaking

Swell wave breaking on fore reef slopes differ significantly to mild-slope beaches (Massel and Gourlay, 2000; Sheremet et al., 2011). As waves break on a reef they produce an increase in the mean water surface elevation, creating a pressure gradient (radiation stress) that drives reef circulation (Longuet-Higgins and Stewart, 1964). Wave breaking along the fore reefs results in an increase of the mean water level on the reef flat due to wave-induced setup (Becker et al., 2014; Gerritsen, 1980; Vetter et al., 2010) and generates IG waves over the reef flat (Péquignet et al., 2014, 2009; Pomeroy et al., 2012a; Symonds et al., 1982). These processes, which can lead to large wave runup and flooding of the shore, are controlled by morphological parameters such as reef dimensions, topography, and roughness, as well as hydrodynamic forcing parameters such as offshore wave and tidal conditions (Quataert et al., 2015). Wave breaking on reefs is depth limited, but due to the steep bathymetry of the fore reef the breaker ratio is found to be significantly higher ($\gamma = 0.8 - 1.13$) than for typical coasts (Blacka et al., 2015; Vetter et al., 2010). This contrasts the breaker ratio of the reef flat, which is significantly lower ($\gamma = 0.12 - 0.22$) (Vetter et al., 2010). Yao et al. (2012) found that the steepness of the fore reef determines the width of the surf-zone. After initially propagating as a bore on the reef flat, the wave will return to an oscillatory form after sufficient energy is lost, for which friction is dominant (Nelson, 1996; Young, 1989).

2.2.4.6 Low frequency generation

IG wave energy on the reef flat is the result of two processes. First due to shoaling bound long waves (BLW), second due to surf zone generated waves as a result of breakpoint forcing. The importance of breakpoint forcing is thought to significantly increase as the relative slope at the breakpoint increases. This implies that a transition exists between these two generation regimes based on the slope (Baldock, 2012; Battjes, 2004; Masselink, 1995).

Bound long waves

IG waves in the form of (coupled) forced long waves that are generated by nonlinear interactions between incident (primary) HF waves traveling from deep water to nearshore. Due to the continuous forcing of these waves by the shoaling primary HF waves, the coupled IG waves are amplified over the sloping seabed in the nearshore zone up to the zone of initial breaking and possibly within the surf zone (Foda and Mei, 1981; List, 1992; Longuet-Higgins and Stewart, 1964; Masselink, 1995). These bound long waves (BLW) are thought to be "released" as free waves during short period wave breaking in the surf zone (Pomeroy et al., 2012a). The BLW dissipate in the surf zone, along with HF wave breaking, and contribute minimally to the IG wave energy shoreward of the crest, and could give way to breakpoint generation of LF waves (Péquignet et al., 2014; Pomeroy et al., 2012b).

Breakpoint forcing

The dominant source of IG energy on reefs is due to breakpoint forcing (see figure 2.4), (Pomeroy et al., 2012a). Free (standing) IG waves are generated within the surf zone on a sloping beach, both shoreward and seaward directed, by the time-varying oscillation (excursion) of the HF wave breakpoint (Symonds et al., 1982). The amplitude of these free IG waves is dependent on the mean breakpoint location, group frequency and fore reef slope and is insensitive to incident wave height. The upper and lower incident wave heights determine the maximum cross-shore excursion of the breakpoint. While the frequency of these fluctuations depends on the wave group length. The efficiency of the IG wave generation by breakpoint forcing is influenced by the groupiness of the incident wave spectrum, and shows to be strongest if the breakpoint excursion is small compared to the standing wavelength (Baldock et al., 2000; Pearson, 2016). This suggests that steeper fore reefs and narrow spectra prove to be more efficient at IG wave generation. VLF waves on the reef originate from a dynamic setup generated by breaking HF waves at the reef crest, and is much more efficient at generating VLF waves than BLW forcing (Péquignet et al., 2014, 2009). Similarly, shoreline IG waves are found to be consistent with breakpoint forcing (Merrifield et al., 2014). The breakpoint forcing efficiency is reduced by increased reef flat submergence, mainly due to the decrease in depth-limited breaking of HF waves, which also results in a decrease in wave-induced setup (Pomeroy et al., 2012b).

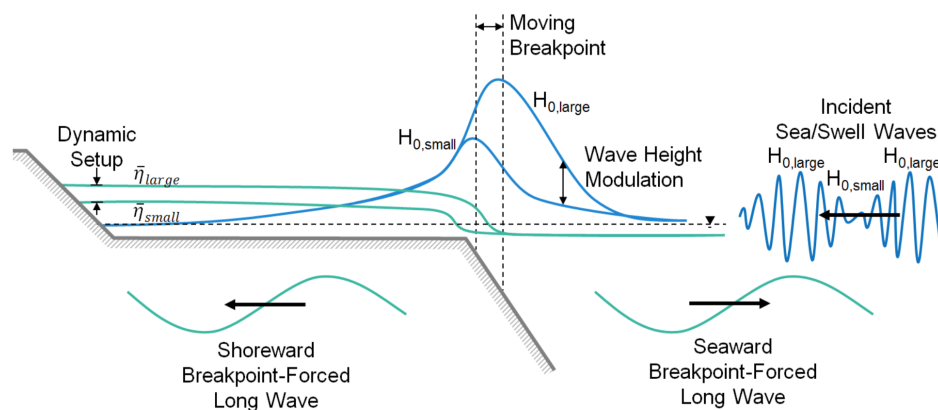


Figure 2.4: A schematization of the breakpoint forcing mechanism. Due to changes in wave height on wave group scale, the breakpoint moves in cross-shore direction, resulting in an oscillating mean water level on the reef flat in the frequency range of IG waves. (Pearson, 2016).

2.2.4.7 Frictional dissipation

After breaking, which is the dominant dissipation mechanism along the fore reef and reef crest, HF waves will further attenuate due to bottom friction dissipation on the reef flat (Lowe et al., 2005; Monismith et al., 2015; Pearson, 2016). This is attributed to the rough surface generated by the reef organisms, which makes the reef highly efficient at dissipating energy by bottom friction (Lowe et al., 2005). However, reef porosity has a limited influence on the frictional dissipation (Young, 1989). Bottom friction dissipation on the reef flat also dampens LF waves, but to a lesser extent than the HF waves (Pomeroy et al., 2012a). This attenuation is controlled by wave shape, local hydrodynamic roughness, water depth, and the width of the reef flat (Péquignet et al., 2009; Pomeroy et al., 2012b). At smaller depths, this results in progressive-dissipative LF waves dominating the observed spectra (Cheriton et al., 2016; Hardy and Young, 1996; Pomeroy et al., 2012a). However, at larger water depths, LF waves can reflect back from the shoreline, increasing the possibility of standing and even resonating LF oscillations. Rates of bottom friction dissipation can be substantial (due to the large biogenic roughness of coral reefs) and often dominates over the reef flat once wave breaking becomes minimal (Lowe et al., 2005).

This is in contrast to some assumptions made about dissipation on other coral reefs (Massel and Gourlay, 2000; Vetter et al., 2010; Young, 1989), where wave breaking is assumed to dominate and bottom friction makes a smaller contribution. Little frictional dissipation can result in an increase of IG wave height across the reef flat, also in offshore direction due to reflected waves (Cheriton et al., 2016).

Hydrodynamic controls on frictional dissipation

Dissipation due to friction varies with reef flat submergence depth, and influences the IG wave height (Pomeroy et al., 2012a). The variations in the rate of IG wave generation play a minor role here, as the frictional dissipation is a function of the water depth over the reef flat (Van Dongeren et al., 2012). Also, the importance of frictional dissipation decreases on the fore reef with increasing wave height (Lowe et al., 2005).

2.2.4.8 Non-linear wave processes

Triad wave-wave interactions on the reef flat are important for the transfer of energy to both IG and HF bands (Nwogu and Demirbilek, 2010). Superharmonic wave components (at multiples of the peak frequency) are formed during the shoaling process (Filipot and Cheung, 2012). The energy that is transferred to these higher frequencies by triad interactions is dissipated from the system (Sheremet et al., 2011). Wave period on the reef flat is tidally modulated since HF waves are filtered out at low tide (Beetham et al., 2016). Moreover, the impact of seiches on a coastline may be further increased by an irregular wave shape: time-lapse photographs taken during the approach of a typhoon in 1987 at Okinawa showed a wave bore, comparable to a tsunami (Nakaza and Hino, 1991). This is consistent with laboratory observations by Nwogu and Demirbilek (2010) and is caused by the nonlinear effects of advection and bottom friction that deform resonantly generated VLF waves into bore-like surges (Nakaza and Hino, 1991).

Due to the high propagation speed, the inertial forces at the front of such bores have the potential to transport boulders far inland (Kennedy et al., 2016) or cause severe damage to buildings (Pistrika and Jonkman, 2010).

2.2.4.9 Reflection

Little wave reflection occurs at a reef, because a vast majority of the wave energy is dissipated or transmitted into the lagoon (Seelig, 1983). According to Péquignet et al. (2009), an increase in wave steepness decreases the amount of reflection. Therefore, LF waves are more reflective than HF waves (Yao et al., 2012). Reflection increases for fore reefs with a slope steeper than 1/4 (Yao et al., 2012). Mild beach slopes ($< 1/20$) lead to low reflection, and beach slopes of 1/6 are fully reflective for IG and VLF waves (Cheriton et al., 2016; Pomeroy et al., 2012a).

2.2.4.10 Resonance

Once free IG waves propagate out of a surf zone toward shore, they can then reflect seaward at the shoreline (leading to a standing wave pattern in the cross-shore direction) or are trapped as alongshore-propagating edge waves (Huntley et al., 1981; Munk and Sargent, 1948; Suhayda, 1974). This can occur when the width of the reef flat is 1/4 of a given wavelength (Péquignet et al., 2009). IG waves make an important contribution to the overall water motion within reef-lagoon systems (Brander et al., 2004; Hardy and Young, 1996; Lugo-Fernández et al., 1998). The amplitude of IG waves can be significantly enhanced during periods of resonance, when the time scale of the offshore forcing matches the resonant mode of the reef geometry (Nakaza and Hino, 1991; Nwogu and Demirbilek, 2010; Péquignet et al., 2009). An increase of water level on a reef can increase the resonant frequencies, potentially allowing a wider range of wave conditions to excite reef resonant modes (Péquignet et al., 2009). Standing waves can be resonantly excited by wave groups with a forcing period that corresponds to one of the natural reef-frequencies or eigenmodes (Lugo-Fernández et al., 1998; Nwogu and Demirbilek, 2010; Péquignet et al., 2009; Pomeroy et al., 2012b). VLF waves are important drivers of flooding of low-lying coral reef islands. In particular, VLF wave resonance is known to drive large wave runup and subsequent overwash, and could be of importance when evaluating coastal flooding hazards (Gawehn et al., 2016). VLF motions are categorized by Gawehn et al. (2016) into four different classes: resonant, (non-resonant) standing, progressive-growing and progressive-dissipative waves. Reef flats are typically too dissipative to accommodate LF resonance at higher modes, i.e., flats are either too wide and/or the water too shallow; therefore, resonance is mostly observed for the longest fundamental mode. This mode has a water level node near the reef crest and an anti-node at the shoreline, meaning that a quarter wavelength matches the width of the reef flat (Lugo-Fernández et al., 1998).

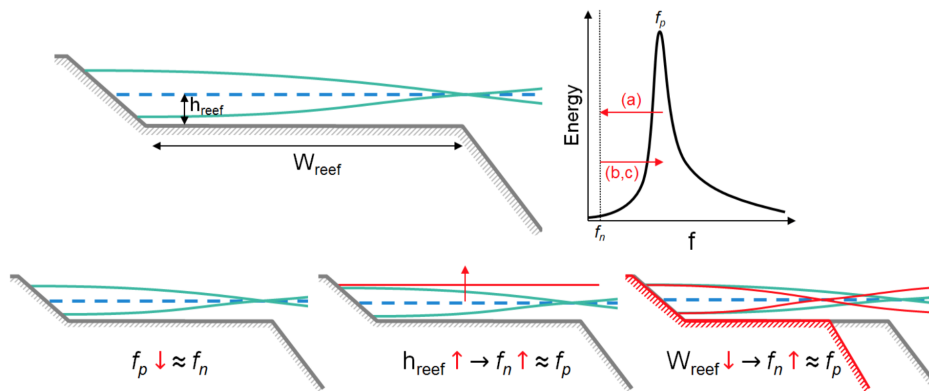


Figure 2.5: Schematic presentation of factors influencing resonance on a fringing reef, including a decrease of the forcing frequency, an increase of water depth over the reef flat and a decrease of the reef width (Pearson, 2016).

Morphologic controls on resonance

Three main parameters can change the initiation of resonance: reef width, offshore wave forcing frequency and reef submergence. Wider reefs experience larger resonance amplification and require lower frequency forcing to become resonant, but are also characterized by having relatively more frictional dissipation (Pomeroy et al., 2012b). Resonant amplification is affected by the bottom friction, while the resonant frequency is not (Pomeroy et al., 2012b).

Hydrodynamic controls on resonance

Resonance is more likely to occur during a large storm or swell event, which are characterized by significant LF wave energy, or when an increase in submergence depth reduces the natural frequency to match the forcing (Pearson, 2016; Péquignot et al., 2009; Pomeroy et al., 2012b). Sea level rise will therefore increase the probability of IG resonance (Van Dongeren et al., 2012). Also, ocean acidification and increasing seawater temperatures threaten the coral health, and could reduce the damping of resonant conditions due to a possible decrease in hydrodynamic roughness (Quataert et al., 2015).

2.2.5. Runup & overtopping

2.2.5.1 Wave runup

Stockdon et al. (2006) decompose wave runup into three main components: wave-induced setup (η), IG swash (S_{IG}) and HF swash (S_{HF}) (see Figure 2.6).

Wave setup

On reefs, HF waves start to break in a narrow surf zone close to the reef crest. This results in wave-induced setup in the order of 0.5 m to 2 m, much larger than for sandy beaches (Gourlay, 1996a; Longuet-Higgins and Stewart, 1964; Vetter et al., 2010). Setup is a function of the incoming wave height and period, is tidally dependent, and increases with decreasing offshore tidal water levels (Becker et al., 2014; Gerritsen, 1980; Gourlay, 1996b; Nwogu and Demirbilek, 2010; Quataert et al., 2015; Seelig, 1983; Vetter et al., 2010). Bosserelle et al. (2015) found that wave setup is of high importance to extreme water levels. Spatial variation of setup depends on surf zone width, which in turn depends on fore reef slope (Yao et al., 2012). The magnitude of the setup is depended on the incident wave height (Vetter et al., 2010).

Swash

Even though setup decreases with increased reef flat submergence, an increase in IG wave contributions to runup can compensate for this (Nwogu and Demirbilek, 2010). Although IG swash dominates, HF swash still plays an important role in reef hydrodynamics and runup (Gawehn et al., 2016). IG swash increases with increasing frequency spread and decreases with increasing directional spread, according to Guza and Feddersen (2012). Swash is defined here as the vertical motions of the shoreline. A distinction is made between HF and IG swash components. For gentle beach slopes, IG swash becomes dominant as HF motions dampen out. For steeper slopes, HF swash becomes increasingly important.

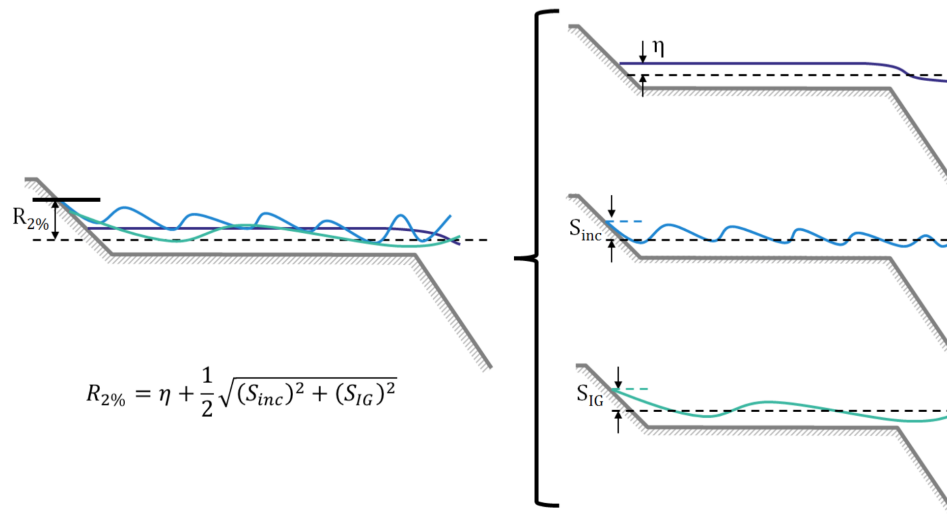


Figure 2.6: Schematic presentation of the three components of runup: wave-induced setup, high-frequency swash and infra-gravity swash (Pearson, 2016).

Tidal modulation

Tidal fluctuations influence the relative contributions of swash and setup to the total runup (Becker et al., 2014; Beetham et al., 2016; Cheriton et al., 2016; Pomeroy et al., 2015; Vetter et al., 2010). Sea level rise is expected to reduce the wave setup, but this might be compensated by increased HF and IG wave energy across the reef flat (Becker et al., 2014; Péquignot et al., 2009). This can result in an exponential increase in the importance of waves to flooding, compared to sea level rise alone (Merrifield et al., 2014).

2.2.5.2 Overtopping & inundation

Overtopping of sea water on an atoll due to wave action, tsunamis, or tropical storms forms a layer of salt or brackish water on top of the freshwater lens inside the porous substrate. This layer moves down into the soil and mixes with the freshwater inside the aquifer (Terry and Chui, 2012). Extreme water levels at the beach-toe act as a proxy for runup, which can estimate the amounts of overtopping (Merrifield et al., 2014). Gunasekara et al. (2014) and Shimozono et al. (2015) have found a clear relationship between reef width, wave period and flooding.

2.2.6. Hydrodynamic effects of excavation pits

The effects of excavation pits on fringing reefs have not been studied in detail, with respect to hydrodynamics and sediment dynamics. Recently, two subsequent studies have been performed for a case at Majuro Atoll, the Marshall Islands (Ford et al., 2013; Yao et al., 2016), in order to assess the implications of the hydrodynamics of excavation pits on fringing reefs.

2.2.6.1 Observed effects of an excavation pit on a fringing reef

From the measurements that have been performed over a 41 day period it has been observed by Ford et al. (2013) that the net decrease in total wave energy for a cross-section with pit is due to a slight increase in HF energy, and a decrease in IG energy. Due to the increase in water depth over the pit and removal of rough surface, there are lower rates of HF wave attenuation. Findings have suggested that the size of the excavated area has a significant impact on HF wave transformations across the reef.

The finding that the IG wave energy decreases in the presence of the pit suggests that the excavation pit disrupts the quasi-standing wave structure that IG waves tend to display on fringing reefs (Ford et al., 2013).

There are three key issues with reef flat excavation from a morphodynamic perspective of view: excavation can lead to the disruption of carbonate sediment production through the removal of reef flat, the habitat of many key sediment producers. Secondly, in areas of high sediment transport, excavation pits may act as traps by capturing cross-reef and alongshore movement of sediment (Xue, 2001). Finally, the geomorphic alteration of the reef flat can modify hydrodynamic processes, resulting in the morphodynamic readjustment

of the shoreline and potentially increasing vulnerability to inundation hazards.

Ford et al. (2013) recommend avoiding excavating on the outer sections of the reef flat, since these are the most significant features with respect to dissipating wave energy. It also suggests that for the observed conditions the construction of coastal protection does not require additional strengthening to account for increased wave energy at the shoreline.

However, one of the key concerns of reef flat excavation is the potential to drive erosion both proximally and throughout the coastal system. The shorelines landward of excavation pits around Majuro are typically armoured, reducing the likelihood of site-specific erosion. However, the possibility that shorelines farther along sediment transport pathways will be starved of material, is a management issue that would need further examination.

The conclusions that follow from Ford et al. (2013) are that reef flat excavation exerts a certain degree of control on reef flat wave processes. The shoreline adjacent to the excavation pit receives smaller wave heights (8%) than a nearby shoreline adjacent to an unmodified reef. The most profound impact of the pit is the disruption of IG wave energy.

2.2.6.2 Modelled wave processes over a fringing reef with an excavation pit

Following Ford et al. (2013), Yao et al. (2016) have performed a numerical study based on one-dimensional weakly dispersive, highly non-linear Boussinesq equations. The model simulations were compared to the field observations made at Majuro Atoll from Ford et al. (2013).

According to Yao et al. (2016), the presence of a pit on the modeled reef reduces IG wave height and increases HF wave heights, for certain daily wave conditions, which is consistent with Ford et al. (2013). An empirical orthogonal function (EOF) analysis suggests that the reduction in IG wave heights is due to a modification of the 1/4 and 3/4 wave length IG wave standing modes across the reef flat, caused by the presence of the pit (Yao et al., 2016). For the modeled reef of Yao et al. (2016), an excavation pit disrupts the modal IG energy excited by breakpoint forcing, while transmitting HF energy. The distance of the location of the pit to the shoreline influences both the IG and the HF wave heights at the shoreline, as they increase for a pit located closer to shore (Yao et al., 2016). Pit width also has an effect on the shoreline wave heights. A wider pit increases the total wave height at the shoreline, while increasing HF wave heights and decreasing IG wave heights (Yao et al., 2016).

2.2.6.3 Ecological effects of excavating in fringing reefs

The effects of live coral mining on the ecology has been studied in Mafia Island, Tanzania, where it has been concluded that the amount of alive coral is significantly lower near excavation sites, as well as the fish abundance and diversity. Also, the loss of shoreline and mangrove forest is believed to be a result of coral mining that leads to the loss of natural breakwaters (Dulby et al., 2016). These observations have also been made in the Maldives (Brown and Dunne, 1988).

3

Validation of XBeach non-hydrostatic+

3.1. Introduction

The objective of the validation is to setup a model that can accurately reproduce all relevant hydrodynamic processes that are present on fringing reef coasts with excavation pits. In order to achieve this, a one-dimensional XBeach non-hydrostatic+ (XBnh+) model is used to reproduce the published observations from Ford et al. (2013). XBnh+ has been selected from three different XBeach modules. The main body of this report does not focus on the analysis of the models' results and the selection procedure. A brief description on why XBnh+ has been used in this study is explained here, and is further elaborated on in Appendix A.1. XBnh+ is preferred because it contains an extra (hydrostatic) computational layer in z-direction, which theoretically allows for more accurate modelling of hydrodynamic processes in the presence of steep bathymetry and large depth gradients (such as fore reef slopes and vertical walls of excavation pits). The analysis included in Appendix A.1 demonstrates the advantages of modelling with XBnh+.

Offshore wave data from the Coastal Data Information Program (CDIP) of the SCRIPPS Institute of Oceanography, as well as nearshore wave data from Ford et al. (2013) have been used in this study. The measuring campaign that produced the dataset nearshore has been specifically produced in order to study the effects of excavation pits (Ford et al., 2013). As of December 2017, this is the sole dataset that focuses on reef hydrodynamics, which includes the effect of excavation pits, which has been used in publications and the only dataset that was available for this research (Ford et al., 2013; Yao et al., 2016).

Firstly, the available data on hydrodynamics of reef excavating is presented and analysed (Section 3.2). The available data on waves consist of measured surface elevation time series at a reef flat including two cross-shore transects (one with and one without excavation pit) in Majuro Atoll, the Marshall Islands. Offshore wave data were obtained from a nearby wave buoy located in deep water. From these data, wave events are selected that are used in the calibration and ultimately the validation of the XBnh+ model. This section also deals with the limitations of the available data sets.

Secondly, the model setup is discussed, including the chosen calibration parameters (Section 3.4). The model setup is based on the previous data analysis and model calibration (included in Appendix A.3). The bathymetry and location of point outputs that were compared with measurements are obtained from Ford et al. (2013). The following section (3.3) deals with the methods that are used in the computation of variance density spectra and wave heights, as well as assessing the models accuracy and skill.

The results of the validation event are presented by comparing measured and computed water levels, wave heights and variance density spectra (see Section 3.6). For the wave heights and variance density spectra, the model's skill has been assessed.

Following the results of the validation event, the limitations and possible improvements of the validation study are discussed. Finally, some conclusions are made on the modelling of fringing reefs with excavation pits with XBnh+ (Section 3.7).

3.2. Data analysis

Wave measurements were collected at two locations in the coastal system of Majuro Atoll. The Coastal Data Information Program (CDIP) of the SCRIPPS Institute of Oceanography publishes data online from an offshore wave buoy, located to the South East of Majuro Atoll, see Figure 3.1.

Approximately 5 km to the west of the CDIP buoy, observations were collected by Ford et al. (2013) in the period between June 4th and July 16th in 2011, who measured pressure variations on different locations along two transects of the reef flat, including one transect with excavation pit. The pressure signal time series were transformed into water depth time series and have been made available for this thesis by dr. Janet Becker. Bathymetry and location and elevation of the sensors were obtained from Ford et al. (2013).

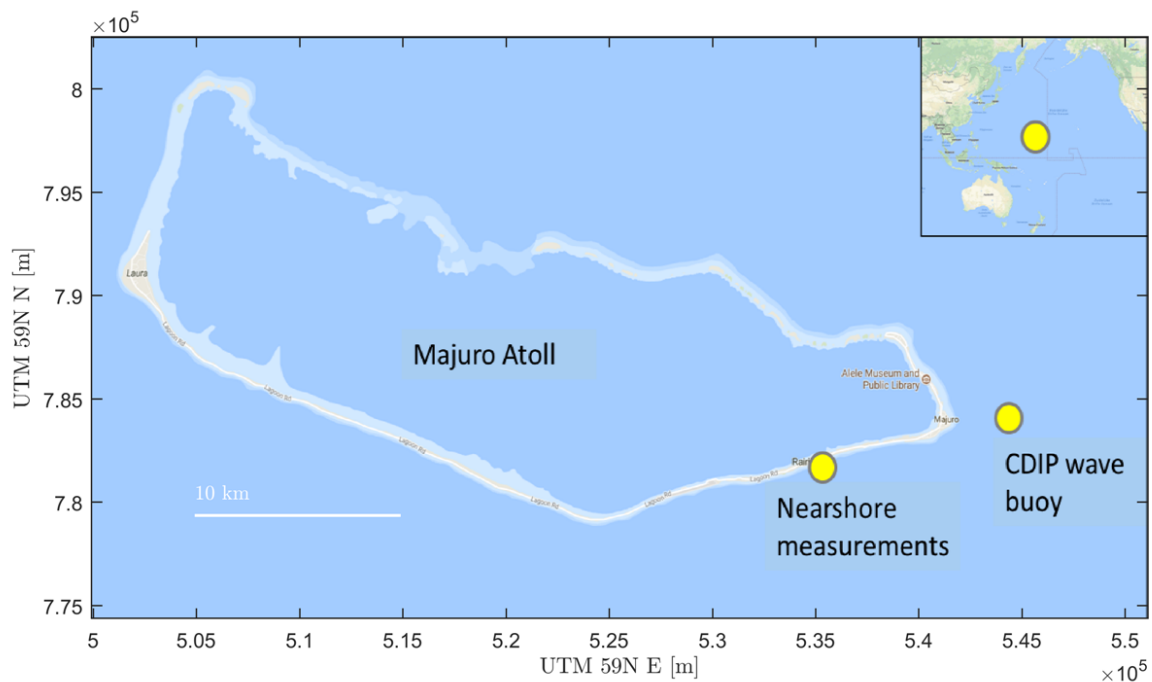


Figure 3.1: Majuro Atoll & Arno Atoll, the Republic of the Marshall Island and the locations of the two data sources. This includes the offshore wave buoy at the East side of the atoll, located in a water depth of approximately 500 m, as well as the measurements recorded by pressure sensors on the ocean-side reef flat of the southern part of the atoll.

3.2.1. Offshore wave data

The CDIP wave buoy provides parametric wave data such as significant wave height, peak period and peak direction, as well as a 9-band energy and directional spectrum. Due to the different location of the wave buoy compared to the measurements performed by Ford et al. (2013), waves that come from a different direction than the south have not been considered suitable for this study. The main reason for this is that using wave conditions from a wave event that is not a predominantly northward direction will include wave conditions that were most likely not present at the near-shore site due to near-shore hydrodynamic processes, such as refraction and diffraction of waves around the atoll. This increases the uncertainty of the forced wave conditions on the model boundary. Figure 3.2 shows the time series of the significant wave height, peak period, peak direction, as well as an estimate of the astronomical tide, for the duration of the measurement campaign in 2011. Red dots indicate events that are characterized by a mainly southern peak direction.

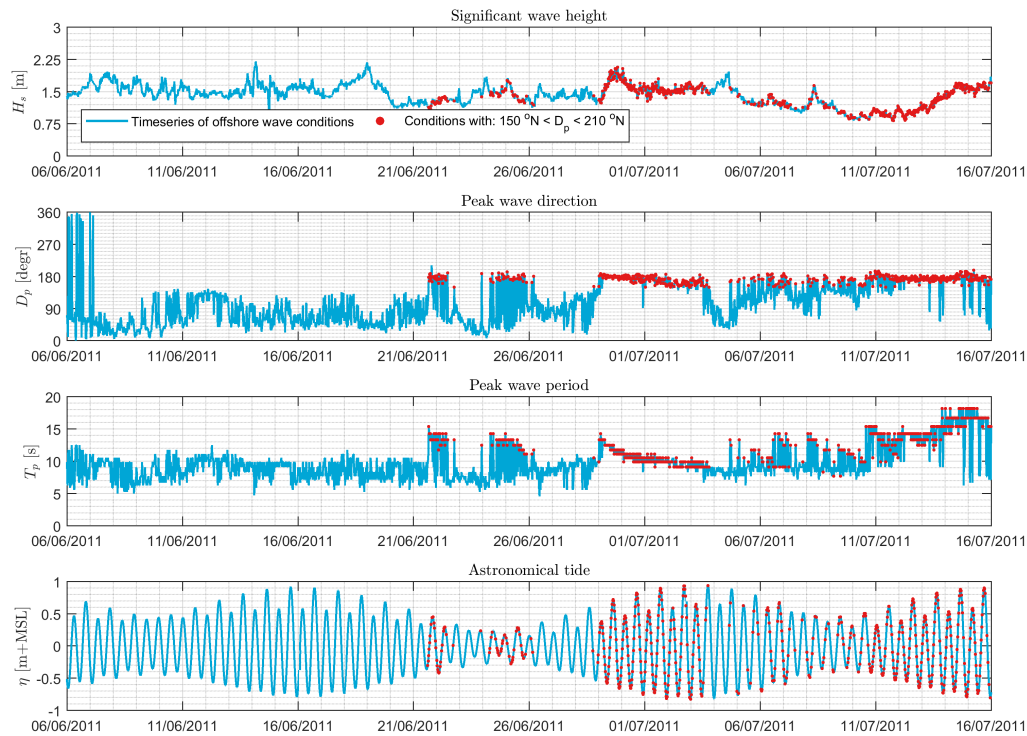


Figure 3.2: Time series of the CDIP wave data (buoy 163, source: <https://cdip.ucsd.edu/>), which include significant wave height, peak direction and peak period. The bottom pane shows an estimate of the astronomical tide. Red dots indicate wave events that are characterized by having a mainly southern peak direction, which are therefore most suitable to be used as boundary conditions during calibration or validation.

3.2.2. Nearshore wave data

The nearshore wave data consist of time series of water depths, measured by four pressure sensors on the reef flat on the southern coast of Majuro Atoll, located approximately 5 km to the west of the CDIP wave buoy. Two deployments of the sensors have been performed in the period between June 4th and July 16th in 2011. The first deployment measured pressure variations of the four sensors (referred to here as sensors 1, 2, 3 & 4) along a cross-shore transect including an excavation pit. The second deployment measured pressure variations of four sensors along two transects, the same as during the first deployment (sensors 1 & 3), and a second transect located approximately 50 m alongshore to the west, which does not have an excavation pit (sensors 5 & 6), see Figure 3.3. Data on the bathymetry of the two transects have been obtained from Ford et al. (2013) and is illustrated in Figure 3.3, including the cross-shore locations and elevations of the pressure sensors, with reference to a MSL.

The sensors located closer to shore emerge during low tide (mainly sensors 1 and 5). During the second deployment, a small inundation event occurred on the 29th of June, which can be used to calibrate the XBNh+ model for extreme events.

The transformation of waves over the reef during the first deployment is visualized in Figure 3.4. HF wave heights over the excavation pit decrease due to an increase in water depth. The IG wave height increases gradually in shore-ward direction, which is consistent with regular fringing reefs.

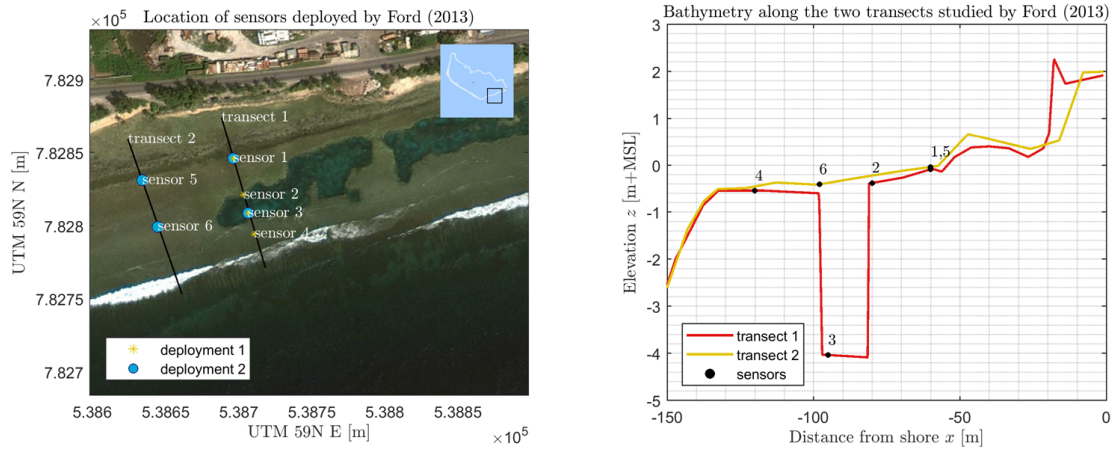


Figure 3.3: Satellite image obtained from Google Earth, showing the location of the two transects and locations of the pressure sensors (left), and the bathymetry measured along each transect as well including the sensor locations and elevation (right) (Ford et al., 2013).

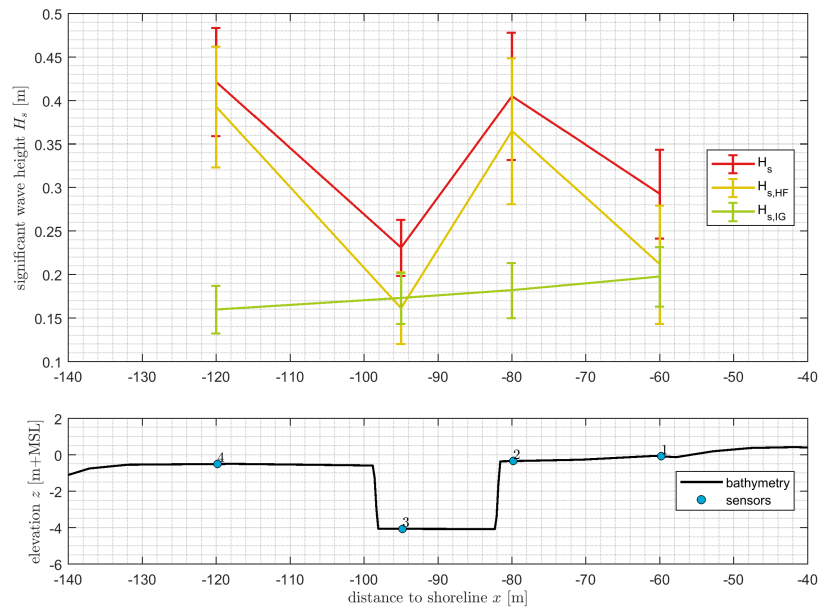


Figure 3.4: Transformation of significant wave heights (total ($f < 0.4$ Hz), IG ($f < 0.04$ Hz) and HF ($0.04 \text{ Hz} < f < 0.4$ Hz)) across transect 1 (during deployment 1). The figure clearly shows the gradual increase in IG wave heights. Total and HF wave heights are decreased by the pit and increase again at sensor 2. The error bars show the 95% interval.

3.3. Methodology

In order to assess the applicability of the XBnh+ model and its accuracy, the following method was used. Firstly, a 1D XBnh+ model was set up using the available data on bathymetry and roughness values found in other fringing reefs, see Section 3.4.

From the wave data, two events were selected, one to calibrate the model settings while forcing a moderate wave event, and the second to validate the model setup while forcing extreme wave conditions at the boundary.

The final accuracy of the model was assessed with the validation event, using the scatter index (SCI) and the relative bias (RB) to quantify the model's skill. The SCI is given by:

$$SCI = \frac{\sqrt{(c - m)^2}}{\max(\sqrt{m^2}, |\bar{m}|)} \quad (3.1)$$

Where c is the computed value and m is the measured value. The (RB) is given by:

$$RB = \frac{(c - m)}{\max(\sqrt{m^2}, |\bar{m}|)} \quad (3.2)$$

The outputs of the model were evaluated at different locations on the reef, corresponding to the locations of the pressure sensors used by Ford et al. (2013). The model output was compared with the measurements regarding:

- wave heights (total, HF and IG frequency bands)
- water levels
- variance density spectra

Variance density spectra were estimated with a fast Fourier transform (FFT) of the time series of the measured and computed surface level elevations. These spectra were used to estimate the wave heights, using the zeroth-order moment:

$$H_s = 4 \cdot \sqrt{m_0} \quad (3.3)$$

The wave heights were calculated at intervals of 30 minutes, similar to the intervals of the recorded offshore wave conditions.

3.4. Model setup

XBnh+ is used instead of XBeach surf-beat (XBSB), see Appendix A.1 for a detailed argumentation. For non-hydrostatic XBeach calculations, depth-averaged flow due to waves and currents are computed using the non-linear shallow water equations, including a non-hydrostatic pressure. For the XBnh+ model, a second computational layer is added which uses hydrostatic pressure. This results in better solutions of the advection-diffusion equation, leading to increased model skill for steep bathymetry, e.g. fore reef slopes and/or excavation pits in fringing reef coasts. All wave components are resolved in XBnh+. The main advantages of the non-hydrostatic mode are that the incident-band (short wave) runup and overwashing are included. Wave breaking is implemented by disabling the non-hydrostatic pressure term when waves exceed a certain steepness, after which the bore-like breaking implicit in the momentum-conserving shallow water equations takes over. Wave breaking stops when a minimal wave steepness is computed, and non-hydrostatic conditions return.

The model was setup using the bathymetric data from Ford et al. (2013), in order to create a computational grid with a minimum grid spacing of $\Delta x = 0.25$ m across the reef flat and a maximum grid spacing of $\Delta x = 4$ m on the fore reef slope which extends in offshore direction. A minimum grid spacing of $\Delta x = 0.25$ m was chosen as this provided sufficiently accurate and stable results of the model. More argumentation on the chosen grid spacing can be found in Appendix A.2. (See Figure 3.5 for a visualization of the model setup).

Roughness values have currently been set to $c_{f,crest} = 0.4$ and $c_{f,flat} = 0.01$, based on Quataert (2015).

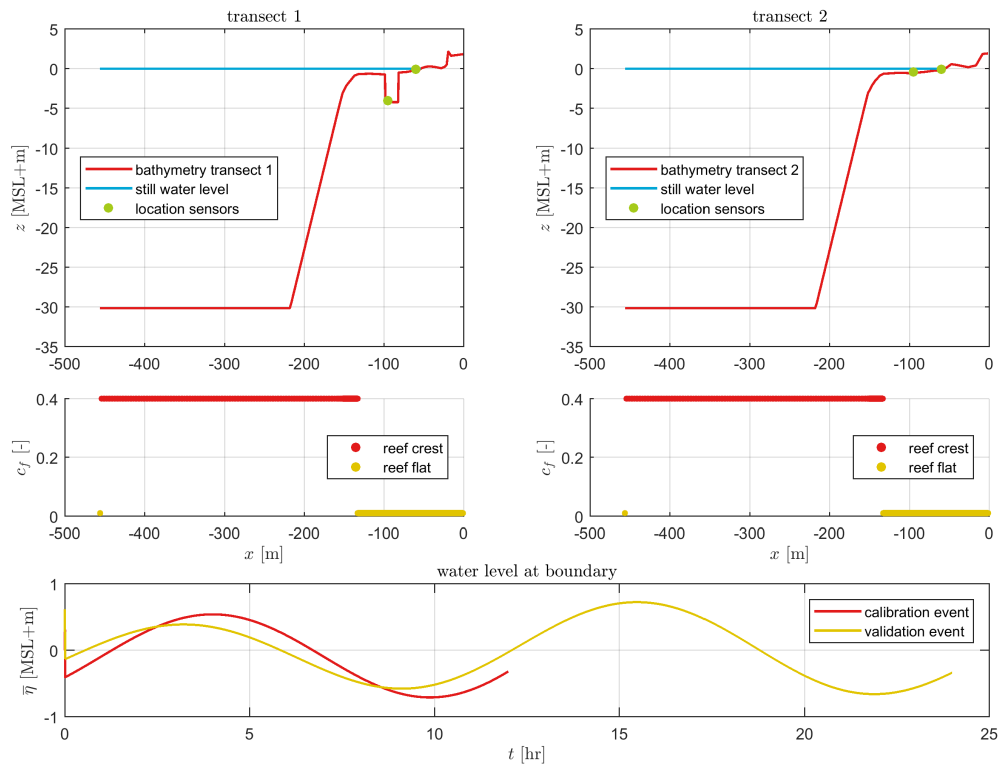


Figure 3.5: Model setup for validation study. Top two plots show the bathymetry of the two studied transects, including the still water level (SWL) and the locations of the point outputs, which match those of the pressure sensors. In offshore direction, the fore reef slope is cut off at a depth of $z = 30$ m. This is to ensure intermediate water depth at the boundary, which is required by the model. To compensate for the fact that the offshore wave buoy is located at deep water ($z \approx 540$ m), the maximum depth is extended in offshore direction. The two subplots below show the roughness values used along the two transects for the reef crest and the reef flat (including excavation). The bottom plot shows the time series of the mean water level at the boundary during the calibration and validation events.

3.5. Model calibration

Based on the offshore wave data provided by the CDIP wave buoy, the morning of the 14th of July in 2011 (00:00 AM to 12:00 PM) was assumed to have suitable conditions to use as boundary conditions for the modeling of a moderate swell event (see Figure 3.2). This moderate wave event was used to calibrate the model. No suitable wave conditions (e.g. predominantly from a south direction) were recorded during the first deployment, which could have provided insight on four locations on the reef in a single transect. However, an event from the second deployment gave the opportunity to compare both transects. The original variance density spectrum observed by the wave buoy was forced on the boundary at a depth of 30 m. Significant wave heights in this period varied from 1.3 to 1.7 m, peak periods varied from 13 to 19 seconds and the peak direction was mainly from the south ($225^{\circ} N > D_p > 135^{\circ} N$).

Tidal elevations were estimated from astronomical tide at the specific location at Majuro Atoll, thus excluding any unknown effects of large-scale water level variations (e.g. air pressure or El Niño Southern Oscillation events). The tidal signal was forced on the reference level published by Ford et al. (2013).

Uncertainties in dataset

Due to limitations of the dataset, there were a number of unknown parameters. The missing variables in the dataset are:

- Measured offshore water level (MSL);

- Accurate offshore spectrum;
- Reference level of bottom profile and sensor(s) with respect to MSL;
- Cross-shore bottom profile and slope, seaward of reef crest.

The influence of each of these parameters was modelled and it was found that all have a significant impact on the reef hydrodynamics compared to conventional calibration parameters, such as roughness values or wave breaking parameters. Previous studies from Pearson (2016) and Roelvink et al. (2015) have shown that these parameters are important for the calibration of models of a fringing reef. However, compared to the unknown parameters, these showed negligible impact on computed hydrodynamics. Therefore, previously defined values for reef crest and reef flat roughness by Quataert (2015) were used in this validation study as well as default values for wave steepness parameters that define the wave breaking criteria used in the XBnh+ model.

There were no recordings of a mean sea level in the dataset of the near-shore pressure sensors, which all include a significant wave-induced setup in the order of decimeters. The bathymetry published in Ford et al. (2013) has a zero-level reference set at the mean elevation of sensors 4 or 6, thus disregarding mean water setup. As reef submergence plays a significant role in reef hydrodynamics, so does the forced MSL for this model. Due to this, the offshore water level was used as a calibration parameter in order to obtain more accurate results. The offshore mean water level was set at -0.12 m, with respect to the published zero-level reference (Ford et al., 2013). This water level at the boundary resulted in the most accurate simulation of wave heights at the innermost sensors.

An accurate offshore wave spectrum was missing due to the location of the used wave buoy, which also recorded waves approaching from direction blocked by land at the near-shore site. Also, processes such as refraction and diffraction were not accounted for. The same holds for locally generated waves by wind, which increases energy in the HF band. The offshore wave spectrum was not used as a calibration parameter, because the data of the wave buoy provide a best guess in this case. Changing this would increase model uncertainties.

The reference level of the bathymetry and sensors with respect to MSL was missing in the dataset, as mentioned above, and was obtained from digitizing published figures from Ford et al. (2013). This resulted in a difference between the measured mean water levels and computed water levels. The elevations of the sensors were not all determined with the same equipment. Additionally, the bathymetry of the excavation was not measured in detail due to large local depth variations. This can explain the inconsistencies in mean water levels of the modelling results compared to the measurements.

The cross-shore bottom profile seaward of the reef crest was not measured accurately. Instead an inferred bathymetry was added to the published figures (Ford et al., 2013). However, the fore reef slope plays a large role in the generation of IG waves and the mean setup on the reef flat. Changes in reef slope also shift peak frequencies.

These four unknowns parameters have a significant impact on computed hydrodynamics. Because of this, the conventional calibration parameters could not be used to calibrate the model. Instead, these four parameters were used for calibration. However, this resulted in less realistic and credible results, as these four unknowns represent physical parameters (e.g. bathymetry, water level) and not numerical (e.g. hydrodynamic roughness). In order to limit the resulting uncertainties, only the offshore water level was varied and used as a parameter to fit the simulated data on the measurements.

The results of the modelling of the calibration event are shown in Appendix A.3. The final modelling parameters that were used in this study are taken from literature (see Table 3.1). These parameters could not be used to calibrate the model in a conventional approach, because the impact of these parameters was near-negligible compared to the unknown factors stated above. The bottom profile of the fore reef slope was obtained from an "inferred" bathymetry that was published by Ford et al. (2013), which resulted in relatively accurate simulation of wave heights. All results from the calibration are presented in Appendix A.3.

Parameter	Value	Unit	Source
Reef crest roughness: $c_{f,crest}$	0.4	[-]	Quataert (2015)
Reef flat roughness: $c_{f,flat}$	0.01	[-]	Quataert (2015)
Maximum wave steepness until breaking ¹ : $maxbrsteep$	0.6	[-]	Roelvink et al. (2015)
Wave reform steepness ² : $reformsteep$	0.25	[-]	Roelvink et al. (2015)
Offshore water level (with respect to reference level: $z_b = 0$)	-0.12	[m]	Ford et al. (2013)
Offshore wave spectrum			CDIP wave buoy
Cross-shore bathymetry and elevations of sensors			Ford et al. (2013)

Table 3.1: Final parameter values and sources that were used during modelling. 1: maximum wave steepness in XBNh+, before wave breaking occurs. Wave breaking is computed in XBNh+ using a hydrostatic pressure distribution under breaking bores. 2: The breaking process in XBNh+ stops when the breaking wave reaches a steepness of reformsteep.

3.6. Model validation

The 29th of June was characterized by a small overwash event at the measuring site (Ford et al., 2013). This event was used to validate the model setup for XBNh+ during extreme conditions.

Figure 3.6 shows the computed water levels and wave heights for the validation wave event on the 29th of June 2011. The model is able to match the observations fairly well for wave heights, but overestimates the wave heights on the excavation, as pointed out by Ford et al. (2013). This is because it is likely that linear wave theory does not provide a valid method to transform wave pressure variation signals in excavation pits, due to the steep change in bathymetry. Because of this, measured surface elevations in the pit and therefore wave heights were expected to be underestimated by the pressure sensors (Ford et al., 2013). Computed water levels are assumed to be inconsistent with the measurements due to the limited accuracy of the measurements of the sensors elevations.

The model is able to compute the wave heights reasonably accurate (see Figure 3.8). Figure 3.7 shows the computed and measured variance density spectra during high and low water at each of the sensors. The model has a shift of the HF and IG peaks to lower frequencies, compared to the measurements. This could be related to inaccurate bathymetry shoreward of the reef crest, since fore reef slope has a large influence on IG wave generation on the reef flat. The shift of the HF peak could be related to inaccurate offshore forcing that was used in the model. The wave spectrum from the CDIP wave buoy was used directly in the model. This neglects the fact that the wave buoy is able to capture waves from more directions due to its exposure to the East side of Majuro Atoll.

For the validation event, total wave heights are overestimated at the beach-toe, but not as much as HF waves (see Table 3.2). HF waves show even less accurate results at mid-reef. IG energy is modelled accurately at the beach-toe, as well as at mid-reef. All scores of the model are given in Table 3.2

The accuracy of the model diminishes for the sensors located further away from the beach by again underestimating IG wave energy, though total wave heights increase in accuracy. This could be attributed to the fact that a wrong combination of offshore forcing, MSL and fore reef and reef crest bathymetry was used. A large part of the computed total and IG wave heights remain in the 25% confidence interval, and thus the model is assumed to be sufficiently accurate given the uncertainties in the dataset.

Table 3.2: Table with *SCI* and *RB* for computed wave height (total, HF and IG), as well as computed variance.

	sensor 1		sensor 3		sensor 5		sensor 6	
	SCI	RB	SCI	RB	SCI	RB	SCI	RB
$H_{s,total}$	0.2	0.082	0.31	0.22	0.22	0.12	0.28	0.2
$H_{s,HF}$	0.44	0.26	1	0.88	0.44	0.26	0.61	0.5
$H_{s,IG}$	0.24	0.036	0.31	0.027	0.24	0.077	0.43	0.015
$S_{high,water}$	0.82	-0.062	0.92	0.015	0.75	-0.065	0.83	-0.044
$S_{low,water}$	0.8	-0.053	0.87	-0.039	0.76	-0.04	0.8	-0.051

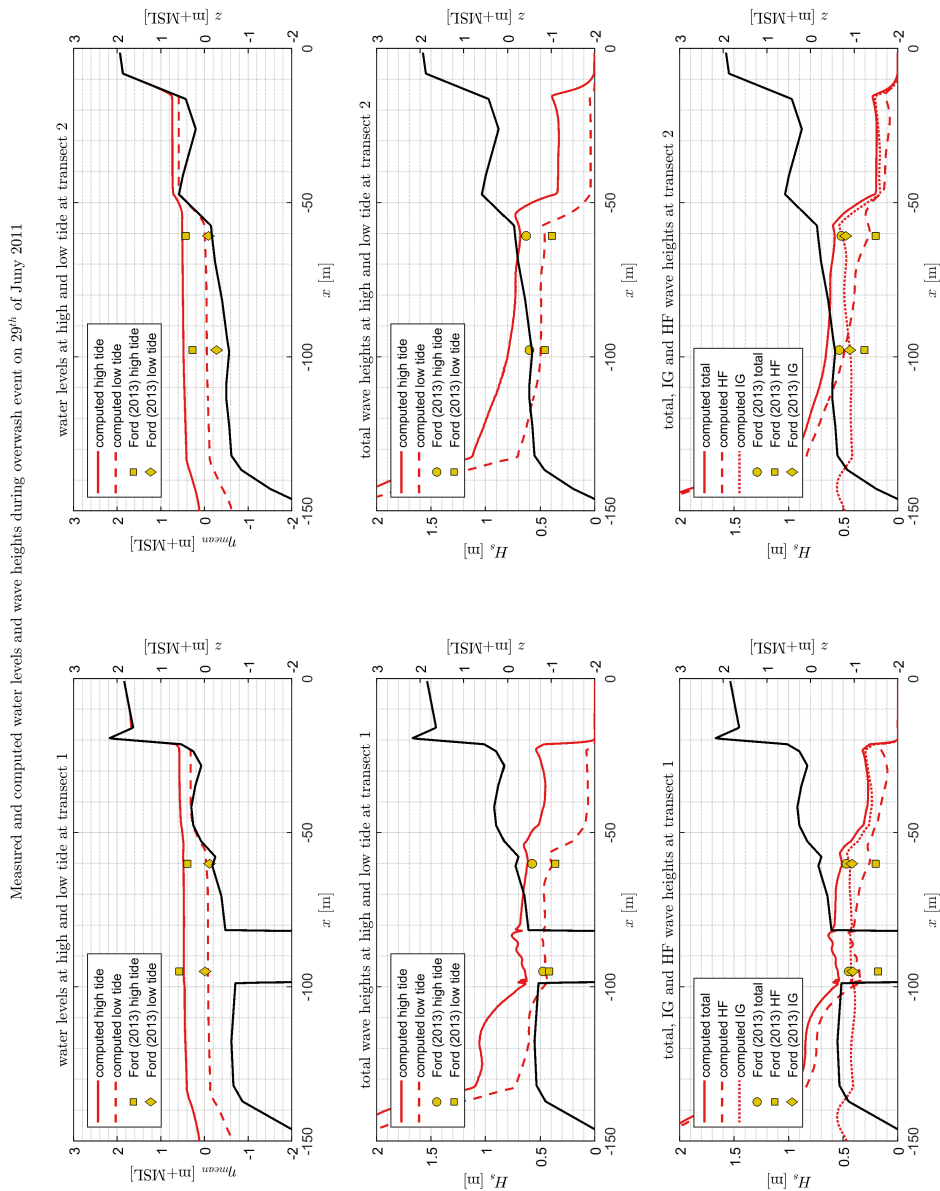


Figure 3.6: Comparison of measured and modelled water levels during high and low tide, total wave heights during high and low tide and a decomposition of total wave height into HF and IG frequencies, during the validation event on the 29th of June 2011. The model is able to describe relevant hydrodynamic processes such as a decrease in HF energy and an increase in IG energy towards the shoreline. Water levels and wave heights are not modelled very accurately at the location of the excavation, which is expected based on literature (Ford et al., 2013).

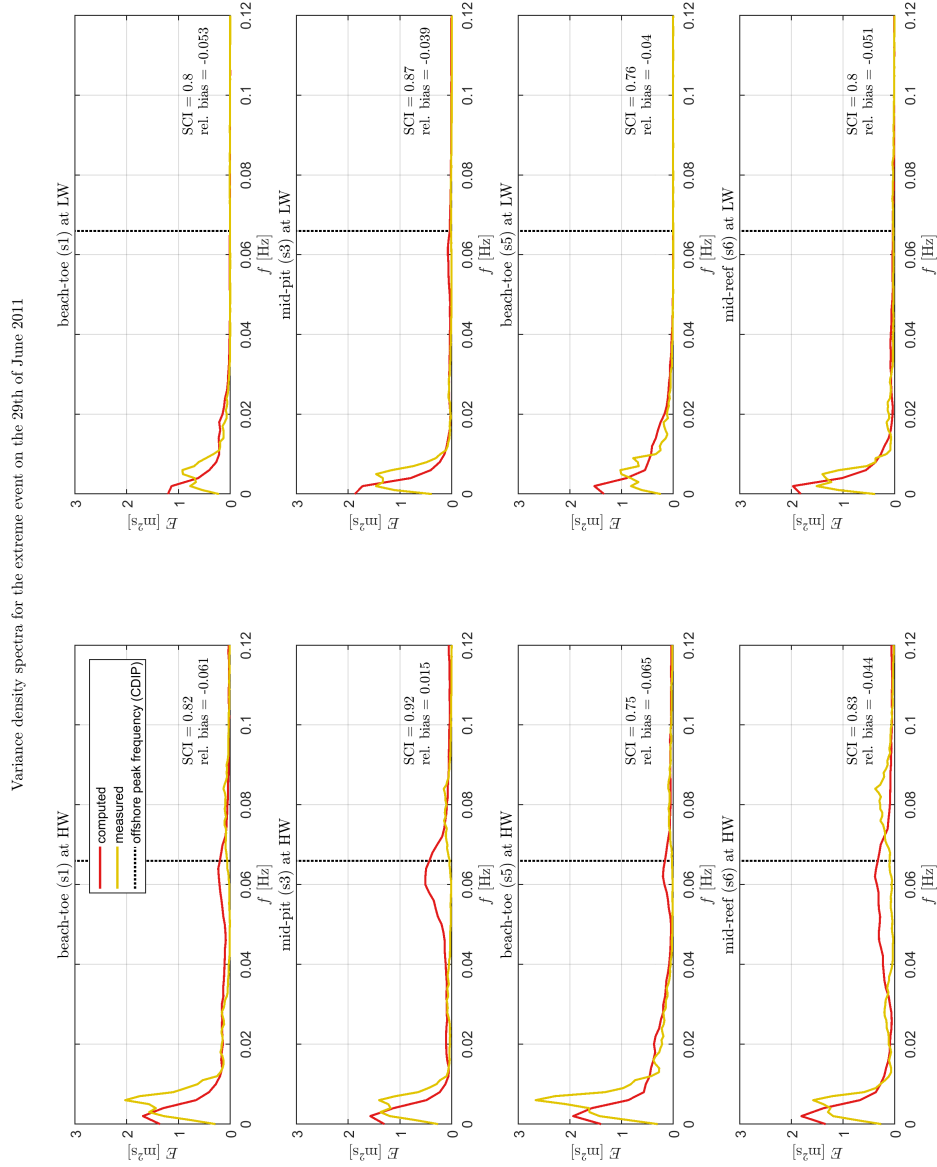


Figure 3.7: Comparison of measured and modelled variance density spectra at the location of each sensor, during high and low water for the validation event on the 29th of June 2011. The shift in peak frequencies is assumed to be related to the use of inaccurate offshore forcing and fore reef slope. See Figure 3.4 for sensor locations. As can be seen, there is still much energy present around $f = 0$ Hz. This is due to the presence of waves with a frequency lower than the minimum frequency used in the fast Fourier transform.

Scatter plots and regression values of computed and measured water levels and wave heights on the 29th of June, 2011

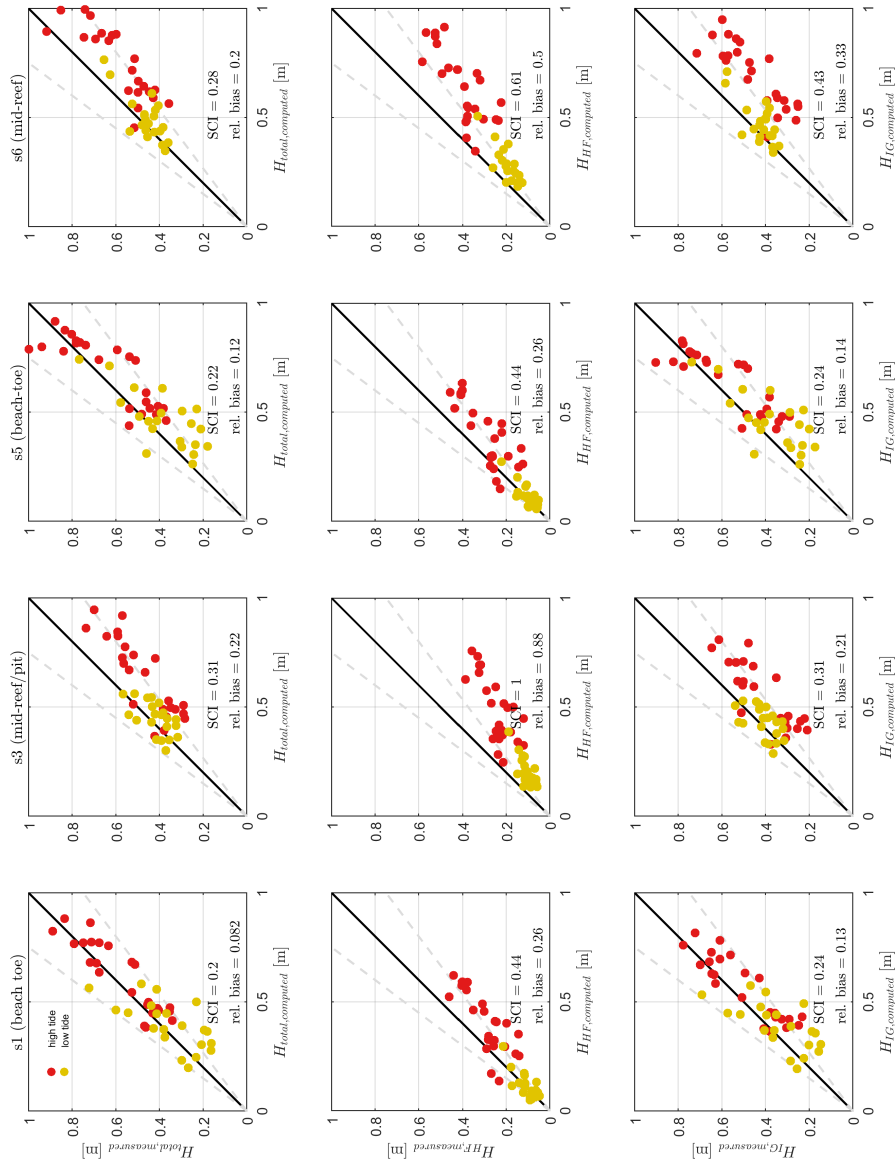


Figure 3.8: Comparison of measured and computed wave heights (total, HF and IG) at four different sensor locations, during high (red) and low (yellow) tide. For the validation event, IG waves are modelled most accurately, and waves at the excavation are modelled least accurately. (See Figure 3.4 for sensor locations.)

3.7. Conclusion

From the validation study, the following can be concluded:

- Currently, there is only one dataset available that includes the effect of excavation pits on fringing reef hydrodynamics. The validation study has shown that multiple parameters which have a significant impact on the simulated hydrodynamics are unknown in this dataset. Therefore, a conventional calibration method is unfeasible, and a detailed model validation is not possible.
- However, despite of these limitations, the XBNh+ model has shown reasonable results and accuracy in simulating near-shore hydrodynamics. The observed effects of excavation pits were modelled as well, which includes a decrease in IG wave energy and increase in HF wave energy due to the presence of the pit. Additionally, the model is able to simulate an overwash event that was observed during the measuring campaign.
- Moreover, XBNh+ has proven in the past to be a useful tool for simulating wave transformations on coral (fringing) reefs (Gawehn et al., 2016; Pearson, 2016; Quataert, 2015). The combination of a good historical record and reasonable results on the limited validation dataset gives confidence in its potential applicability on fringing reefs with excavation pits.

4

1D modelling study

4.1. Introduction

An assessment of the impact of excavation pits on reef hydrodynamics was performed in order to obtain a better understanding of the general implications of this practice. This chapter focuses on the hydrodynamic processes that are affected by the presence of a pit during daily wave conditions, as well as on the effects of reef excavations on runup of fringing reef beaches during extreme wave conditions. This was studied for a range of reef geometries, pit designs and wave conditions by using the XBeach non-hydrostatic+ model. A parameter space for hydrodynamic and reef structure related parameters was defined in Pearson (2016); Pomeroy (2011); Quataert et al. (2015) and has been expanded by studying satellite images of excavation pits in reefs of atolls. Based on eye-witness reports from Deltares employees and measurements of Ford et al. (2013), the range of pit depths has been estimated. This allowed for an assessment of the influence of individual parameters on wave runup during storm events and for future sea level rise. The objectives of the study were:

- To identify the effects that reef excavating has on the hydrodynamic processes of a fringing reef and to assess the influence of individual parameters relating to reef geometry, pit geometry and offshore forcing, on to assess the influence on these effects of individual parameters.
- To assess the impact of reef excavating on the wave runup for a range of fringing reef coasts as defined in the parameter space (see Table 4.1).

This chapter first deals with the methods used to obtain results that achieved these goals. These include two parameter sensitivity studies and descriptions of how wave heights and runup were estimated. Afterwards, the model setup is described. Finally, the results of both parameter sensitivity studies are presented and discussed, after which conclusions on the 1D modelling are presented.

4.2. Methodology

4.2.1. 1D model & setup

A one-dimensional XBNh+ model was used to assess the impact of reef excavations on the fringing reef hydrodynamics and effects on runup. Two studies were carried out with 1D models, a single parameter sensitivity study, and a multi-parameter sensitivity study.

See Figure 4.1 for a schematic visualization of the 1D XBNh+ models that were used. In total, six point outputs were used to analyse the model output. Of these, the first is located at the offshore boundary, to check the forcing conditions. The next four output locations represent characteristic components of a fringing reef, being the fore reef slope, reef crest, reef flat/center of pit and the beach-toe. Finally, a runup gauge was added near the shoreline.

The same minimal grid size was used as in the models used in the validation study. To speed up computation during the multi-parameter sensitivity study, grid size gradually increases (with a factor of 1.15 per grid cell) seaward of the fore reef slope at $z < -7$ m with respect to reef flat level, up to a maximum grid size of $\Delta x = 2$ m.

Beach slope was extended upward in order to only capture runup and no overwash. This resulted in a beach crest level at the closed boundary of $z = 4$ m above reef flat level for the single-parameter study and $z = 10$ m above reef flat level for the multi-parameter sensitivity study.

In all models, the fore reef slope is cut off at approximately $z = -30$ m, and extended in offshore direction for an additional 40 m. At this depth the waves generated at the boundary experience an intermediate water depth with $kh < 1$, $n < 0.79$ and a water depth larger than $4 \cdot H_{s,0}$. The bottom profile at the boundary is kept constant in order for the generated waves to adjust to this intermediate water depth. The XBNh+ model generates waves by forcing a velocity component at the boundary, which acts on both computational layers with equal magnitude. In theory this represents conditions of shallow water. By extending the constant bottom elevation in offshore direction, the waves can adjust to a velocity profile which corresponds to the local intermediate water depth.

At the boundary a unidirectional JONSWAP spectrum is forced with a peak period T_p and a significant wave height H_s . The peak enhancement factor was set at $\gamma = 3.3$ for all simulations.

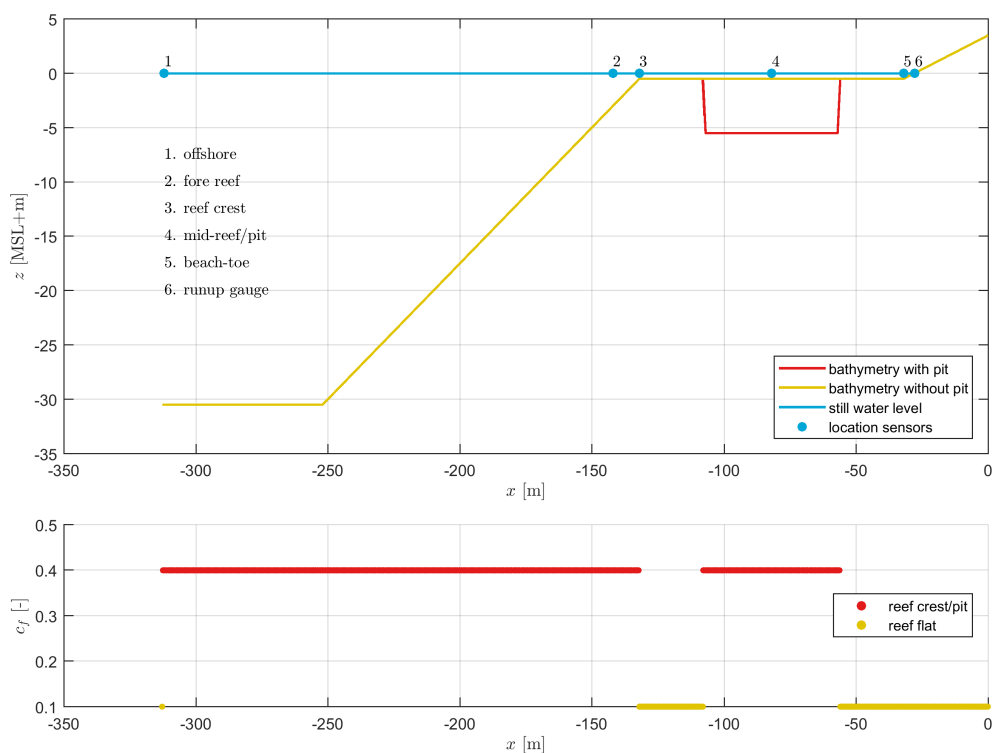


Figure 4.1: Schematization of the used 1D XBNh+ models, showing the locations of the five point outputs and runup gauge.

4.2.2. Single-parameter sensitivity study

A single-parameter sensitivity study was used to assess the influence of each individual parameter of the parameter space (Table 4.1) on the water levels and wave heights at different cross-shore locations on the reef obtained from point outputs (see Figure 4.1). This was done by running ten XBNh+ models in which each model has a different value for that particular parameter, isolating the effect of each parameter. Each simulation was carried out twice, once with reef excavation and once without. The remaining parameters were set to default values (see Table 4.1). The studied output parameters (water levels, wave heights, swash, runup) of the reef with pit are normalized with the outputs of the reef without pit. Values larger than 1 therefore correspond to an increase due to the presence of a pit and lower values indicate a decrease.

Additionally, global wave transformations and water level variations across the reef were studied for the maximum and minimum values of each parameter, while comparing models with and without a pit. This provided a more general understanding of the influence of each parameter across the entire reef.

This single parameter sensitivity study provided insights into the effects of reef excavating on reef hydrodynamics, such as changes in wave heights and water levels across the reef, but also provided detailed information on the effects of certain parameters on hydrodynamics of reefs without excavations. The generalized findings from this study are described in Section 4.3. The full parameter sensitivity study is described in Appendix B.4.

Additionally, the results of this parameter sensitivity study were used to determine the most sensitive and important parameters that affect the reef hydrodynamics and the effects of excavations. These were used in the second parameter sensitivity study, which was limited to a selection of parameters from the full parameter space due to the large quantity of simulations.

Full parameter space

The full parameter space as used in this research is given in Table 4.1. A distinction is made between parameters related to offshore forcing (top three), fringing reef geometry and hydrodynamic roughness (middle section) and pit geometry and hydrodynamic roughness (bottom five). This table lists the symbols that have been used throughout this report, the range in which this parameter occurs naturally in the world, according to literature, and a default value that was used during modelling in XBNH+. This parameter space covers a large portion of fringing reefs that exist around the globe and transforms these naturally occurring reefs into schematic models, such as depicted in Figure 4.1, with clear transitions between changing reef geometry and no gradual variations.

Table 4.1: Improved parameter space based on Pearson (2016); Pomeroy (2011); Quataert (2015), including default values used during 1D modelling. The range listed in the third column is obtained from literature. The default values were arbitrarily selected at the centre of this range.

Parameter	Symbol	Range	Default value	Unit
Reef submergence (MSL)	η_0 or MSL	-1:2	0.5	[m]
Offshore wave height	$H_{s,0}$	1:5	2	[m]
Offshore wave steepness	s_0	0.005:0.05	0.015	[-]
Fore reef slope	α_{reef}	1/2:1/20	1/4	[-]
Beach slope	α_{beach}	1/5:1/20	1/8	[-]
Reef flat width	W_{reef}	20:500	100	[m]
Reef flat roughness	$c_{f,flat}$	0.01:0.10	0.01	[-]
Reef crest roughness	$c_{f,crest}$	0.10:0.40	0.4	[-]
Pit width (x-direction)	W_{pit}	10:100	50% of W_{reef}	[m]
Pit depth	z_{pit}	1:5	5	[m]
Pit distance from shoreline (x-direction)	x_{pit}	10:100	50% of W_{reef}	[m]
Pit slope	α_{pit}	1/2:5/1	5/1	[-]
Pit roughness	$c_{f,pit}$	0.10:0.40	0.40	[-]

4.2.3. Multi-parameter sensitivity study

Next, a multi-parameter sensitivity study was used, which consisted of a large number of model runs (9750 in total), designed to study the relation between important parameters that had been defined in the single-parameter sensitivity study. Six parameters were identified as having a significant influence on the reef hydrodynamics and a significant influence on the effects of excavations on water levels and wave transformation across the reef, as well as swash and runup (Table 4.2). The selection of these parameters, as well as a detailed description of the effects of these parameters is discussed in Section 4.3. This study aimed to perform a more detailed assessment of possible effects of reef excavation on runup on fringing reef coasts during extreme events. In order to model extreme events, offshore wave heights were set to $H_{s,0} = 5.0$ m in the multi-parameter sensitivity analysis, the rest of the parameters were set to default (see Table 4.1). The models of this

study were setup in a similar way as those of the single-parameters sensitivity study. The results of this study give an approximation of the general effects that pits have on the runup of fringing reef coasts and indicate the possible effects that various parameters have on the probability of increase or decrease in runup due to an excavation.

The parameters were varied simultaneously during modelling in such a way that every possible combination of parameter values was modelled twice, once with pit and once without. Looking at Table 4.2, there are five variables with five different values and one variable with three different values. All simulations represented 375 different reefs with 25 different excavation pits, amounting to a total of 9375 runs.

The analysis of the large quantity of simulations has proved to be challenging. Empirical cumulative and probability distribution functions have been used to analyse the dataset.

Parameter space for multi parameter sensitivity study

The parameter space of Table 4.1 was narrowed down to six parameters in order to reduce computation time and facilitate analysis. These six parameters and their values used during modelling are shown in Table 4.2. Literature and modeling results indicate that these parameters have the largest influence on the fringing reef hydrodynamics, as well as on the effect of pits (Pearson, 2016). Section 4.3 & Appendix B.4 elaborate further on the selection of these parameters.

Table 4.2: Parameter space for the 1D models used in the multi-parameter sensitivity study, including all the modelled variable values. Every single combination of these values was modelled.

Parameter	Range					Unit
MSL	0.1	0.85	1.6	2.35	3.1	[m]
W_{reef}	50	150	250	350	450	[m]
α_{reef}	0.05	0.15	0.25	0.35	0.45	[-]
α_{beach}	0.05	0.125	0.20			[-]
W_{pit}	6	19	32	45	57	[% W_{reef}]
x_{pit}	30	40	50	60	70	[% W_{reef}]

4.2.4. Wave height & mean water level estimation

The estimation of wave heights followed the same method as presented in Section 3.3. Sampling of forcing time series and the short simulation period (1 hour) stored as output and used in the analysis, gives rise to errors in the estimation of hydrodynamics on reef and runup, compared to when longer simulation periods are used. These errors are explained in detail in Appendix B.1. The errors made by sampling 1 hour of output from a 24 hour simulation are given in Table 4.3. The errors are expressed in scatter index (SCI) and bias. An additional parameter is added that assesses the models predictive capability by taking into account the 95 % interval of the sample distribution:

$$\frac{2 \cdot \sigma_t}{E_{t=24hr}} \quad (4.1)$$

Where σ_t is the standard deviation of sample size t from the sample with $t = 24$ hr. $E_{t=24hr}$ is the expected value of (the wave height or mean water level) the 24 hr sample. This parameter represents a relative error with a range of two standard deviations, thereby including 95 % of all data (when assuming a normal distribution).

It's assumed here that a model simulation of 24 hours gives optimal results, as this simulation period contains sufficient information on all wave frequencies in order to be considered highly accurate. By using shorter simulations in the analysis, errors of estimating this "true" value become larger. The two left columns in the table show the computed model skill for the final simulation period of 1 hr.

However, since in both of the sensitivity studies the time series of the JONSWAP spectrum was reused for all runs (except for the forcing parameters in the single-parameter sensitivity study), the errors estimated by comparing smaller samples of a 24 hour run are not entirely accurate. More accurate estimates of the model

skill are computed by comparing the output that is analyzed, particularly the normalized mean water levels, wave heights, runup, etc. For the same reef, the runs with excavation and without excavation use identical forcing time series to assess the effects of the pit. As can be seen in the table, the resulting errors are lower.

The computed change in mean water levels, wave heights, swash and runup, is one order of magnitude larger than the estimated errors. Because of this, the model is assumed to be sufficiently accurate to describe relevant hydrodynamic processes.

Table 4.3: Model skill in wave height and mean water level estimation, expressed in SCI and bias. The left table under-represents the errors that the model makes by sampling a 1 hour output from a 24 hour run. The right table represents the error estimates of the normalized values (pit/no pit). The latter is lower due to the reuse of boundary condition time series. The third column in the left and right sub-table represent an estimate of the 95% interval of the error, measured by using standard deviation σ of all samples.

	SCI [-]	bias [m]	$\frac{2 \cdot \sigma_t}{E_{t=24hr}}$ [-]		SCI [-]	bias [-]	$\frac{2 \cdot \sigma_t}{E_{t=24hr}}$ [-]
$H_{s,total}$	0.03	0	0.06	$H_{s,total,pit}/H_{s,total,nopit}$	0.017	0	0.035
$H_{s,HF}$	0.02	0	0.045	$H_{s,HF,pit}/H_{s,HF,nopit}$	0.03	0	0.04
$H_{s,IG}$	0.04	0	0.08	$H_{s,IG,pit}/H_{s,IG,nopit}$	0.02	0	0.06
$\bar{\eta}$	0.01	0	0.018	$\bar{\eta}_{pit}/\bar{\eta}_{nopit}$	1.30E-03	0	0.0026

4.2.5. Wave runup estimation

Wave runup is computed by using special point outputs in the XBnh+ model, called runup gauges. These gauges record the horizontal and vertical displacement of the waterline at the shore and can therefore be used for an analysis of runup.

In many engineering applications, the highest 2% runup is used as a proxy for maximum runup. Runup of a single wave is defined as the highest surface elevation excursion at the waterline. In a time series of surface elevations of the water line, the $R_{n\%}$ is the threshold level for which $n\%$ of waves have a runup that exceed this value. For example, $R_{2\%}$ is defined as the threshold level which is exceeded by 2% of all wave peaks in the vertical elevation of the waterline. However, using the 2% value requires long time series with sufficient peaks in order to produce reliable runup estimates. Other runup values such as $R_{10\%}$ and $R_{33\%}$ (significant runup) can be used as well. A downside of using other runup values than $R_{2\%}$ is that the effect of the largest waves becomes less dominant for these lower runup values. Because overwash is generally caused by the higher waves in a storm, the use of a high quantile, and therefore low n -value is preferred.

A sample of an output time series of the vertical motions of a runup gauge is shown in Figure 4.2. The individual peaks in the output signal of the runup gauge are filtered with a filter period T_f , which is in this study equal to the offshore peak period $T_{p,0}$, taking only the highest peaks during a peak period into account. The runup is measured in this study from the reef flat level.

The same figure also shows a visual comparison of runup gauge outputs for a similar reef, one with pit and one without. Other than a phase shift, both signals show peaks at very similar locations. This is due to the fact that for both runs, the forcing time series at the boundary were reused.

For the multi-parameter sensitivity study, outputs of XBnh+ models with a simulation time of 1 hour were used. This corresponds to approximately 260 waves (with a peak frequency of $T_p = 14$ s). Only 5 individual runup events were taken into account in the estimate of the maximum runup, or $R_{2\%}$, while $R_{10\%}$ and $R_{33\%}$ take into account 25 and 85 respectively. To reduce the errors made caused by this so-called "sampling", while also still taking into account the largest portion of the runup, the $R_{10\%}$ values is used in this study. The $R_{10\%}$ is deemed to be a sufficiently accurate representation of the "extreme" runup that is likely to cause beach overtopping, as well as introduce minimal errors due to sampling. A more detailed argumentation of this selection is given in Appendix B.2. The model's skill for the estimation of runup is given in Table 4.4.

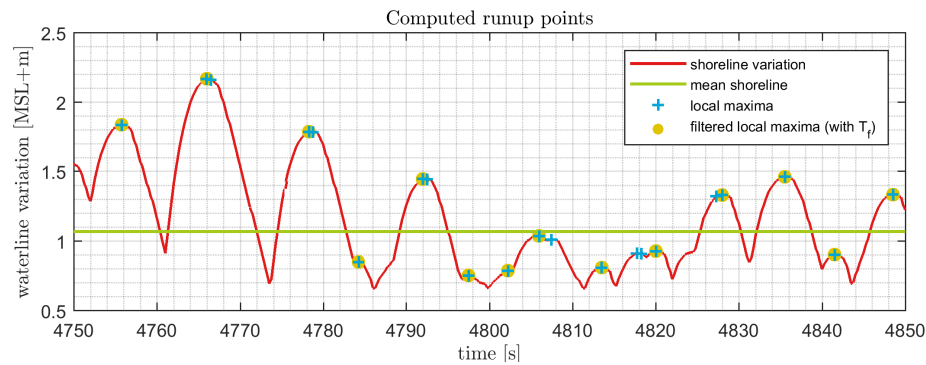


Figure 4.2: Visualization of the estimation of runup. The vertical motions of the shoreline (black) are characterized by individual peaks (green cross), or wave runup. These local maxima are filtered by only considering the largest peak if there are multiple peaks in the period of one offshore wave, taken here as $T_{p,0}$. The remainder of the peaks (red circles) are used to estimate runup levels.

Table 4.4: Model skill in runup estimation, expressed in SCI and bias. The three left columns under-represent the errors that the model makes by sampling a 1 hour output from a 24 hour run. The right three columns show the errors of the relative runup (pit/ no pit). The third column in the left and right sub-table represent an estimate of the 95% interval of the error, measured by using standard deviation σ of all samples.

	SCI [-]	bias [m]	$\frac{2 \cdot \sigma_t}{\bar{E}_{t=24hr}}$ [-]		SCI [-]	bias [-]	$\frac{2 \cdot \sigma_t}{\bar{E}_{t=24hr}}$ [-]
$R_{2\%}$	0.02	0	0.045	$R_{2\%,pit}/R_{2\%,nopit}$	0.023	0	0.045
$R_{10\%}$	0.02	0	0.028	$R_{10\%,pit}/R_{10\%,nopit}$	0.016	0	0.034
$R_{33\%}$	0.02	0	0.03	$R_{33\%,pit}/R_{33\%,nopit}$	0.01	0	0.02

4.3. General 1D model results

4.3.1. General hydrodynamic effects of excavation pits

In this section, the generic effect of an excavation pit on fringing reef hydrodynamics is explained using the output of a single model run. Firstly, the relevant hydrodynamic processes that are affected by the presence of the excavation pit are discussed. This is followed by an analysis of the changes in variance density spectra, which also deals with incoming and outgoing (reflected) wave signals. Finally, the changes in wave height and mean water level are explained in more detail.

4.3.1.1 Relevant processes

On the reef flat, three hydrodynamic processes dominate the exchange of wave energy between frequencies and the loss of wave energy. These are: wave dissipation, wave-wave (triad) interaction and resonant amplification. Figure 4.3 illustrates the change in variance density spectra due to these processes.

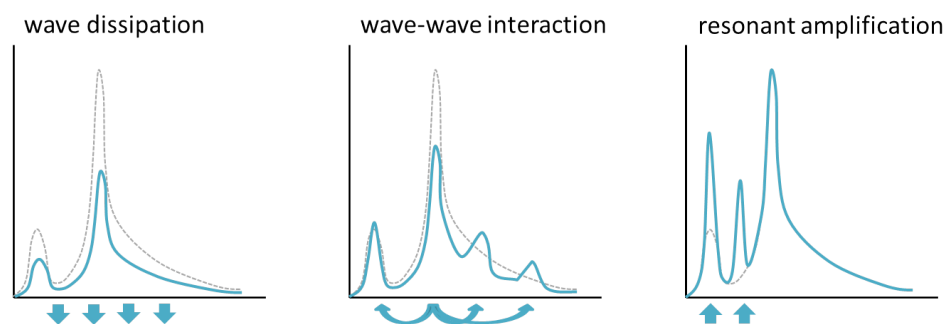


Figure 4.3: Schematic visualisation of the effect of relevant reef flat processes on variance density spectrum. From left to right: wave dissipation, wave-wave interaction (or triads) & resonant amplification. The original spectrum is represented by the dashed grey lines. Under the influence of these processes, the spectrum evolves into the function represented by the blue lines. Blue arrows indicate energy dissipation (directed outward) energy transfer (curved arrows) or energy input (directed inward).

Wave dissipation

Through wave dissipation, energy is lost and variance of all frequencies decreases. Depending on the wave length and other parameters discussed in Chapter 2, this mechanism can vary in efficiency. Waves dissipate through wave breaking (most efficient at higher frequencies) and bottom friction (most efficient at lower frequencies).

The presence of a pit will decrease the amount of wave energy that is dissipated, especially for the higher frequencies, due to an increase in water depth. This will result in larger peaks in the variance density spectrum.

Wave-wave interaction (triads)

Wave-wave interaction, or triads, causes transfer of wave energy from the peak frequency to multiples of the peak frequency at the near shore. Two freely propagating wave components (f_1 , f_2 & \vec{k}_1 , \vec{k}_2) are equal to the frequency and wave number, respectively, of a third freely propagating wave (f_3 , \vec{k}_3):

$$f_3 = f_1 \pm f_2 \quad \& \quad \vec{k}_3 = \vec{k}_1 \pm \vec{k}_2 \quad (4.2)$$

Triad interactions transfer energy to super-harmonics through summation at multiples of the peak frequency, but also to sub-harmonics through subtraction. This mechanism increases in efficiency for (extremely) shallow water, where waves are non-dispersive (Young and Van Vledder, 1993). The process of this triad interaction results in an energetic high-frequency tail.

Because of a larger water depth due to the presence of an excavation pit, locally, the waves will become less non-linear. This leads to a decrease in non-linear wave-wave interaction. Ultimately this will result in larger peaks around the peak forcing frequency, less energetic high-frequency tails and less IG wave energy.

Reflection/resonant amplification

Resonant amplification occurs when the forcing frequency is close to one of the natural frequencies of the reef, following the reflection of waves at the closed (shoreline) boundary (see Figure 4.4). Resonance will only occur for $f = f_{n,i}$, which is given by the equation:

$$f_{n,i} = \frac{(1 + 2i)}{4} \cdot \frac{\sqrt{gh}}{W_{reef}} \quad (4.3)$$

Waves are amplified for $f \approx f_{n,i}$ (see Figure 4.4 for an example of an amplification curve). In a damped system (such as a fringing reef), the fundamental modes ($f_{n,0}$ & $f_{n,1}$) cause the largest amplification.

As pointed out by Ford et al. (2013), an excavation pit can disrupt the quasi-standing wave pattern that is present on the reef flat. This is possibly due to the change of the natural frequencies of the reef, because the pit changes the structure of the reef, which acts as an open basin. As a result, there is less resonant amplification. The decrease in resonant amplification could also be related to a decrease in wave energy reaching the shoreline, due to partial reflection at the pit walls.

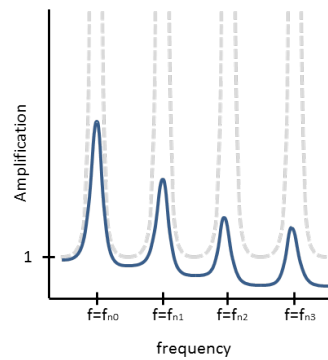


Figure 4.4: Schematic visualisation of an amplification curve for a damped system. The blue line indicates the degree of amplification of different wave frequencies, which have a maximum for forcing frequencies very close to one of the natural frequencies of the system. The fundamental modes are amplified the most. Full (undamped) resonance can only occur for $f = f_{n,i}$, represented by the dashed lines.

4.3.2. General modelled hydrodynamic effects of excavation pits

4.3.2.1 Cross-shore mean water level variation

The change in mean water level that is seen in model results (see subplot (d) of Figure 4.5) at the edge of the pit, where the mean water level abruptly increases, can be explained by a change in radiation stresses following an increase in water depth. The increase in water depth results in lower wave heights through energy conservation. This process of deshoaling is associated with an increase in mean water level, just like shoaling is associated with a decrease in mean water level. At the ocean-side pit wall, wave dissipation is low, and by neglecting this term in the momentum balance, the mean water level variation due to the sudden change is in the order of a couple of cm. This setup at the pit edge is also observed in the XBeach model runs.

Wave breaking accounts for the largest energy dissipation near the shoreline, followed by bottom friction. These two processes are also modelled in XBNh+. Waves break after a maximum steepness is obtained. XBNh+ then turns the non-hydrostatic pressure off and simulates the breaking wave as a bore while assuming hydrostatic pressure. This is the main energy dissipation mechanism at the reef crest and causes a mean setup in the order of 50 cm (see Figure 4.5 at $-140 \text{ m} < x < -120 \text{ m}$) for this specific case.

After wave breaking, bottom friction dominates energy dissipation of HF waves. This dissipation term causes a slight increase of mean setup over the reef flat. In the case of an excavation, this dissipation term becomes less due to an increase in water depths. This explains why the model results show a smaller setup at the shoreward side of the pit compared to an unmodified reef.

When traveling over the pit onto the reef flat, the waves shoal a second time due to the sudden decrease in water depth at the pit wall. This causes a small decrease in mean water level.

The difference in setup between a modified reef and an unmodified reef increases from the edge of the pit in shoreward direction. This difference is in the order of a few % and is a possible explanation for modelled 2D effects (see Chapter 5).

At the beach, waves shoal and cause a minor setdown, followed by a setup due to wave breaking. No apparent differences were found for the situation with and without a pit, other than the initial difference in mean water level that originates at the center of the reef flat.

4.3.2.2 Cross-shore HF wave transformation

The transformation of HF waves is shown in Figure 4.5 in subplot (b). The first notable difference in HF wave energy shoreward of the reef crest is after initial wave breaking ($-120 \text{ m} < x < -110 \text{ m}$). Here, larger wave heights are computed for the reef with pit. This is due to a change in the outgoing wave signal (see section 4.3.2.4).

As mentioned in the previous paragraph, HF waves deshoal when traveling over the pit and subsequently shoal when leaving the excavation. This causes the HF waves on the modified reef to become smaller than

Comparison of wave heights and water levels for a reef with and without a pit

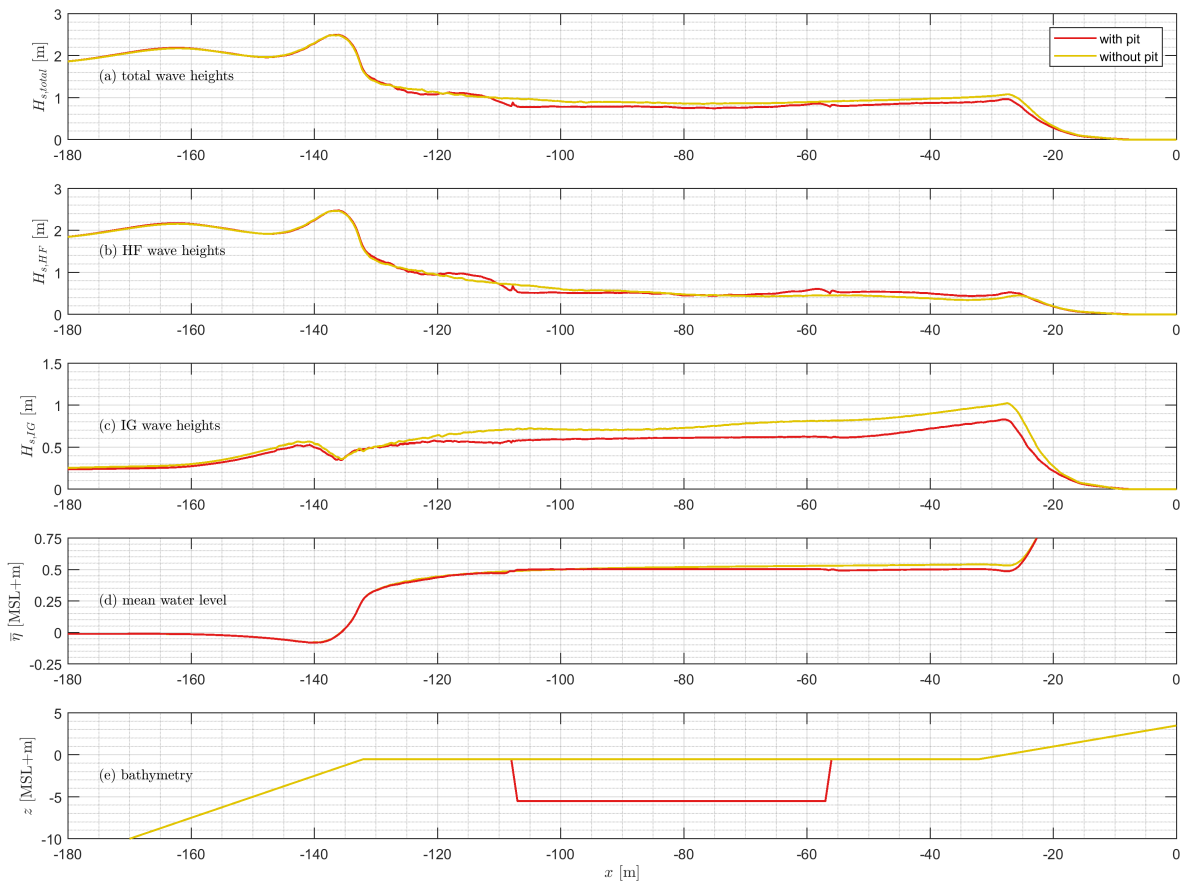


Figure 4.5: Computed total wave heights (a), HF wave heights (b), IG wave heights (c), mean water level (d) and bathymetry (e) of a generic XBnh+ model run. Each subplot shows the characteristic effect of pits on fringing reef hydrodynamics in cross-shore direction: a reduction in total wave height at the shoreline (a), caused by the combined effect of an increase in HF wave energy (b) and a decrease in IG wave energy (c) at the shoreline. Changes in radiation stresses cause a minor decrease in mean water level at the shoreline (d).

on the unmodified reef when entering the pit, but due to less frictional dissipation, these waves eventually become larger, especially at the pit edge. HF waves can remain significantly higher towards the shoreline, in the order of 20%. The modelled HF wave transformation is in agreement with observations and numerical modeling results (Ford et al., 2013; Yao et al., 2016).

4.3.2.3 Cross-shore IG wave transformation

IG waves on the reef are generated by the breakpoint-forcing mechanism due to an oscillating breakpoint (see Chapter 2). Through resonant amplification, IG waves are amplified.

The model results show that the effect of a pit is a decrease in IG wave heights (see subplot (c) of Figure 4.5. Yao et al. (2016) argues that this is due to a decrease in wave energy at the above mentioned wave lengths, suggesting that the pit alters the reef geometry which normally causes this IG wave amplification. The XBnh+ model results show that this decrease in IG wave heights is observed for different reef widths and offshore wave periods and is a very generic effects of reef excavating.

4.3.2.4 Incoming and outgoing wave signals

The reflective properties of the pit were studied by comparing incoming and reflected waves with the method described by Guza et al. (1984). Because the method described by Guza et al. (1984) is valid for shallow water conditions, post-processing of model output data at the location of the pit on the reef flat is potentially not

entirely accurate. At other locations on the reef flat, this method is valid and shows good results (see Figure 4.6). This section deals with the results obtained with Guza's method at locations around the pit.

The modeling results of the incoming signal (Figure 4.6 left), show that the pit causes a decrease in wave height over the pit, which is caused by an increase in water depth. Shoreward of the pit, HF wave height is larger than for a reef without excavation, due to smaller rates of bottom friction. The IG wave height has decreased shoreward to the pit, compared to a reef without excavation.

Figure 4.6 (right) shows that the excavation affects the outgoing wave signal seaward of the excavation. This explains the variation in wave heights (both HF & HF), that were observed in the total wave signal (see Figure 4.5, at $-130 \text{ m} < x < -110 \text{ m}$).

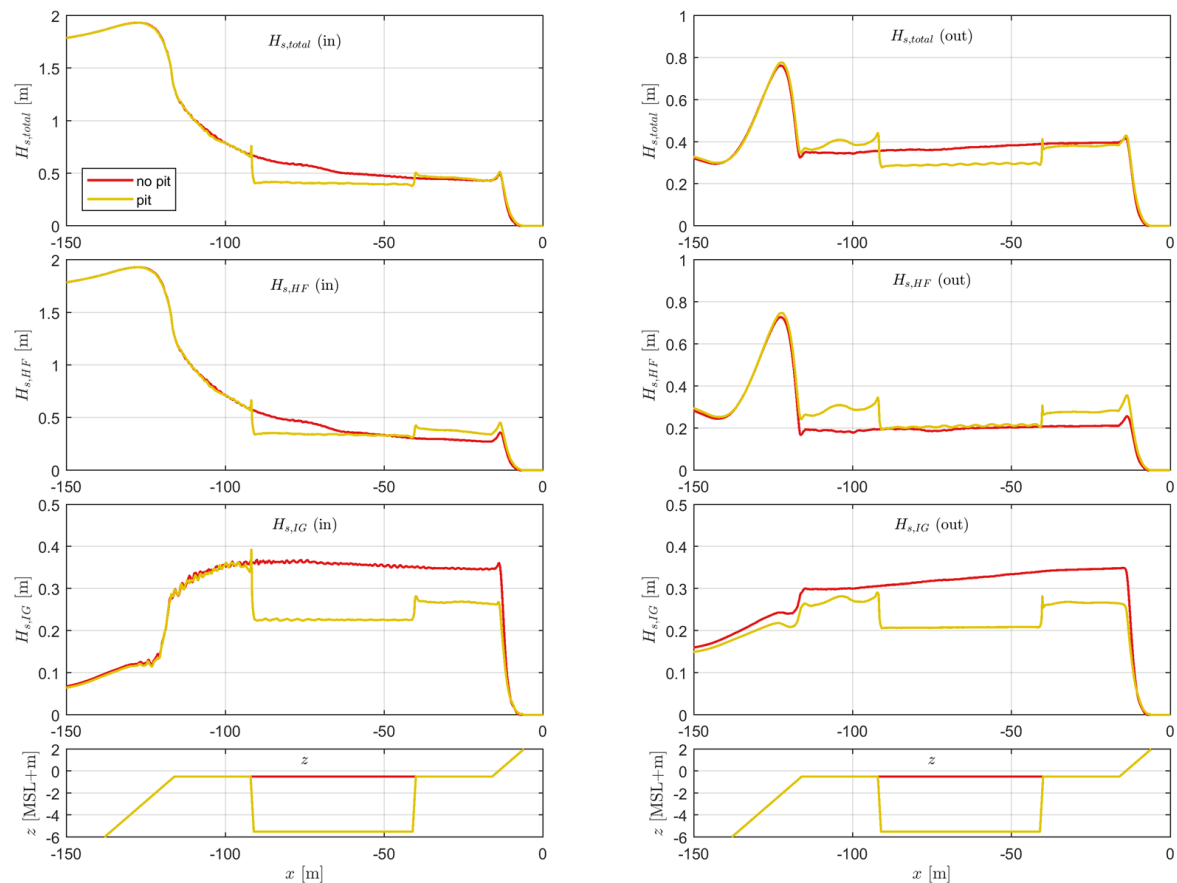


Figure 4.6: Incoming (left) and outgoing (right) wave heights across a reef with (yellow) and without (red) excavation, using the method of Guza et al. (1984). Total wave heights are shown in the upper two subplots, HF wave heights in the center two, and the lower two subplots show the IG wave heights.

4.3.2.5 Variance density spectrum

The model output generated with the reef of Figure 4.1 is used here to give an example of the changes in variance density between the reef crest and beach-toe, both for a reef with and without pit. Figure 4.7 shows the variance density spectra at the reef crest (left three subplots) and at the beach-toe (right three subplots). The top two subplots show the variance density of the total signal, from which the incoming (center) and outgoing (bottom) signals are derived, using the method of Guza et al. (1984).

The incoming wave signal shows a sharp decrease in HF energy from reef crest to beach-toe, and a slight increase in IG energy. For a reef with excavation pit, there is less incoming wave energy at the beach-toe at the IG band, and more at the HF band at the peak frequency.

The outgoing signal shows that there is a slight dissipation of (HF) wave energy from beach-toe to reef crest. There is IG wave energy dissipating for the reef without pit, while the reef with pit experiences an increase in IG energy in the outgoing signal. This can be related to partial reflection at the pit walls.

The incoming and outgoing signals combined result in slightly lower IG wave energy and higher (peak) HF energy at the reef crest, due to the presence of the pit. At the beach-toe the decrease in IG wave energy is more significant, as well as the difference in (peak) HF energy.

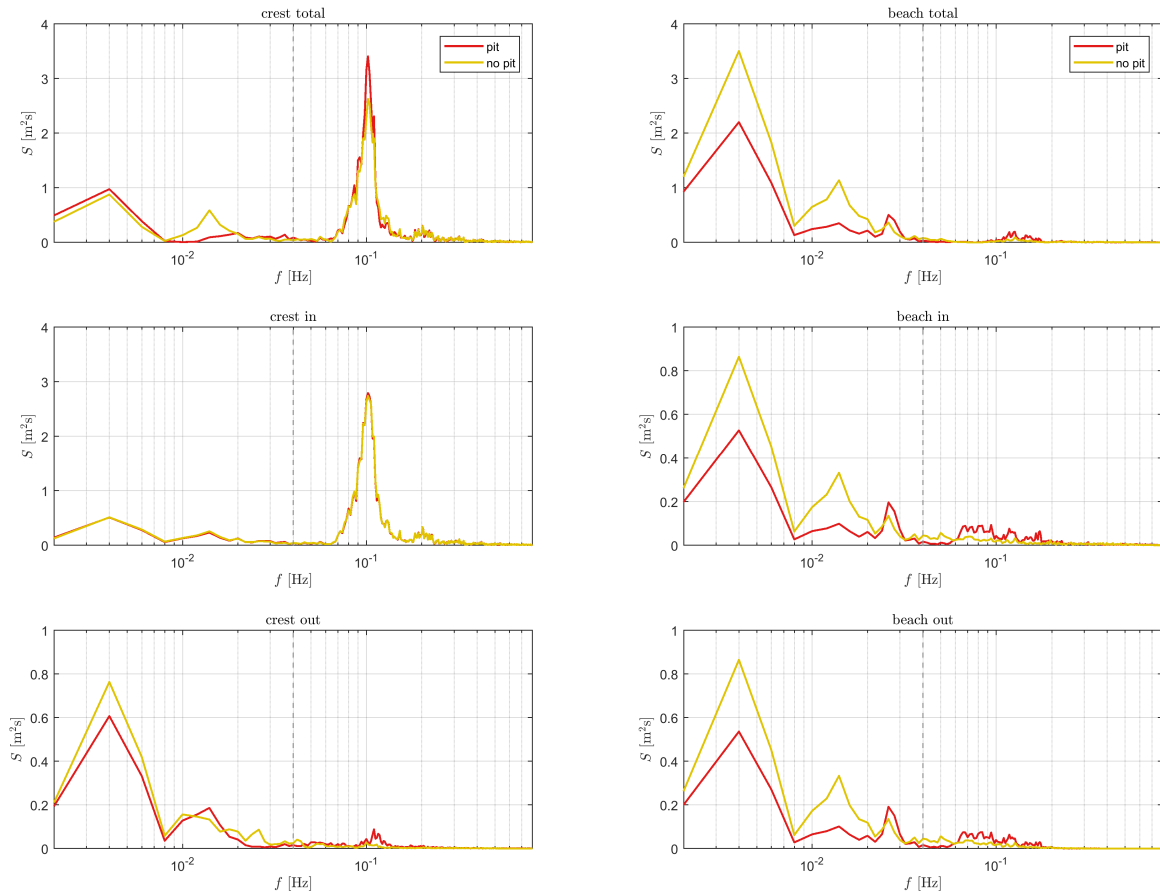


Figure 4.7: Variance density spectra of total (top two subplots), incoming (center two subplots) and outgoing (bottom two subplots) wave signals at the reef crest (left three subplots) and beach-toe (right three subplots), for a reef with (red lines) and without pit (yellow lines).

4.4. Results multi-parameter sensitivity analysis

The multi-parameter sensitivity study was used as a tool to study the impact of reef excavation on fringing reef hydrodynamics, including wave runup. Currently, six important parameters have been identified as having a major influence on reef hydrodynamic processes and the effect of pits on reef hydrodynamics (see Appendix B.4 for a detailed argumentation). The multi-parameter sensitivity analysis is limited to six parameters due to limited computational power. The six parameters used here will provide an initial, though detailed estimate of the effects of pits on hydrodynamics. This estimate is valid for a large portion of all fringing reefs in the world within the range of values that were used. The values of these parameters are given in Table 4.2:

- **Beach slope** (α_{beach}), which determines for a large part processes related to runup. Due to the nature of the effects of an excavation pit (increase in shoreline HF energy, decrease in shoreline IG energy) and the beach slope (IG dominance for gentle slopes, HF and IG equally important for steep slopes), the effect of beach slope on changes in runup due to pits can be significant.
- **Reef submergence** (MSL), which is related to storm events and sea level rise. Also, probability of flooding increases for increasing reef submergence.
- **Reef flat width** (W_{reef}) determines for a large part the wave dissipation on fringing reefs, as well as IG amplification through resonance or quasi-standing wave patterns.
- **Fore reef slope** (α_{reef}), which significantly affects the IG wave generation mechanisms of fringing reefs.
- **Excavation pit width** (W_{pit}) & **Cross-shore location of excavation** (x_{pit}) have the largest impact on the reef hydrodynamics. Also, varying these parameters offers the best insight into how to improve reef excavating with respect to the observed effects on runup.

In total, 375 reefs without excavation were modelled. These were compared with the outputs of the same reef, but with an excavation (25 variations). In total 9375 combinations of different reefs and excavation pits were modelled. This section discusses the changes in hydrodynamic processes due to the presence of a reef, that were observed in all these model runs. Additionally, the effects of excavation pits on runup is discussed.

4.4.1. Effect on hydrodynamic processes

The effects of excavation pits on the hydrodynamic processes are assessed by analysing the output of the modelled reefs in the multi-parameter sensitivity analysis. Only the output at the beach-toe will be considered here.

4.4.1.1 Variance density spectrum

Figure 4.8 shows the variance density spectra at the beach-toe of all modelled reefs by means of boxplots. The top subplot clearly shows the dominating peaks of IG wave energy at $f < 0.04$ Hz, caused by the combined effect breakpoint forcing and resonant amplification. Additionally, the peak of the original offshore forcing spectrum at $f = 0.07$ Hz is also clearly visible, but less pronounced on average. There is a well pronounced HF tail for a large part of all modelled reefs, which results from triad wave-wave interactions that transfer energy to superharmonics.

The lower subplot shows the difference in variance density spectra when subtracting the variance density of the reefs without pit from the variance density of the reef with pit. The resulting negative values indicate a decrease in wave energy at that frequency due to the presence of the pit, compared to an increase in wave energy at the peak frequency. Outliers exist both in the IG and in the HF, and can cause the opposite effect that was described in section 4.3. However, this is more significant for the HF band. This is because the combined effect of dissipation and wave-wave interactions results in a large spread in HF energy and change in HF energy.

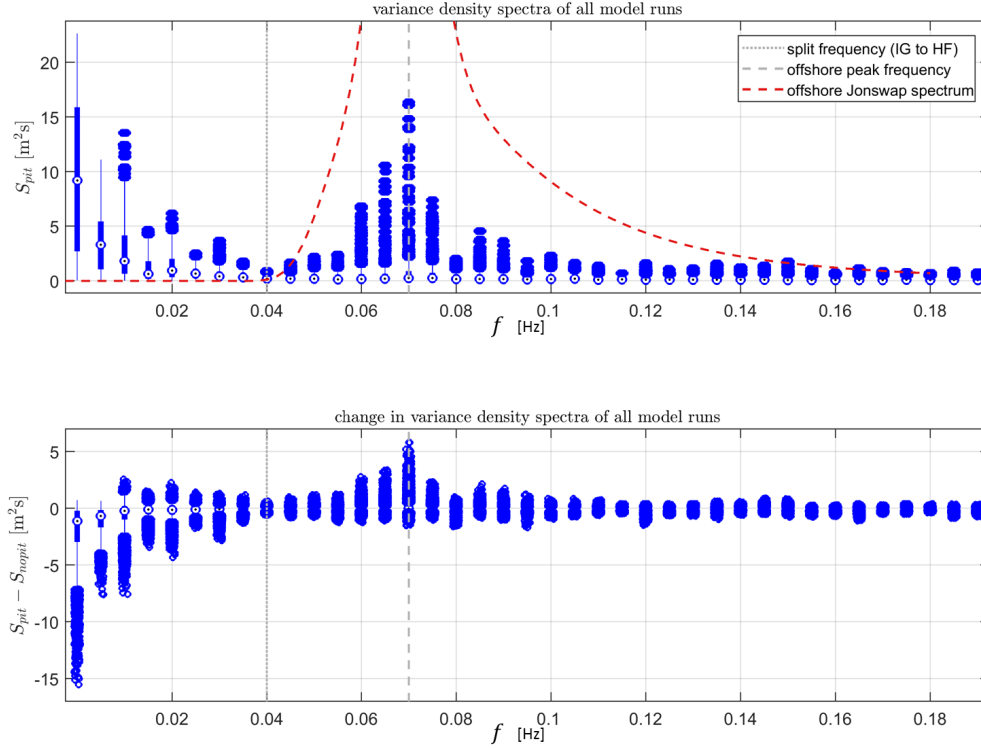


Figure 4.8: Boxplots of variance density spectra (top) & change in variance due to excavations (bottom), at the beach-toe, for all modelled reefs. The median value is depicted by a blue encircled dot. The bold solid line represents the "box" that covers the 25 to 75 % intervals. The thin solid line extends to 1.5 times the interquartile ranges. All blue circles outside these whiskers are considered outliers. The gray dotted line represents the frequency that splits IG and HF bands. The offshore JONSWAP spectrum at the boundary is depicted by the red dashed line, with its peak frequency at the dashed gray line. The top plot shows the variance density ($\Delta f = 0.005$ Hz) of every single modelled reef. The lower plot shows the difference in variance density at the beach-toe, by subtracting the variance of the reef without pit from the reef with pit. Frequency is on the x-axis on both subplots.

4.4.1.2 Infra-gravity energy

Nearly all modelled reefs experience a decrease in IG wave energy. The most significant cause for this is likely a change in the natural frequencies of the reef. This causes a decrease in resonant amplification at frequencies that match these original natural frequencies. In this study, the wave height around the four fundamental modes of the reef without excavation pit were compared with the wave height around the same frequencies of a reef with excavation pit. The definition of these wave heights used here is:

$$H_{s,f_{n,i}} = 4 \cdot \sqrt{m_{0,i}} \quad (4.4)$$

Where $m_{0,i}$ is a newly defined zeroth-order moment of the variance density spectrum, computed around the i^{th} natural frequency of the reef without excavation:

$$m_{0,i} = \int_{f_{n,i}-0.5}^{f_{n,i}+0.5} E(f) df \quad (4.5)$$

For each modelled reef, the wave height from equation 4.4 and the IG wave height were computed. These were used to estimate the change in wave height due to the presence of a pit. Figure 4.9 shows the empirical cumulative distribution functions (ECDFs) of the changes in these wave heights at the natural frequencies. The majority of these wave heights are lower, due to the presence of the pit. Higher natural frequencies have smaller probabilities of a decrease in wave height. The first two fundamental modes are located in the IG band for the majority of the modelled reefs.

Figure 4.10 shows a scatter plot of the changes in $H_{s,IG}$ and in $H_{s,f_{n0}}$ for each modelled reef. The plot shows that these two wave heights are significantly correlated (Pearson's $r = 0.65$) and the root-mean-squared-error (RMSE) is also very low (0.07). This relation shows that IG wave heights are determined in large part by the first fundamental mode of the reef, which is subjected to resonant amplification. These results therefore support previous findings that an excavation pit disrupts the quasi-standing wave pattern by changing the spatial structure of reef, which simplifies to an open basin (Ford et al., 2013; Yao et al., 2016).

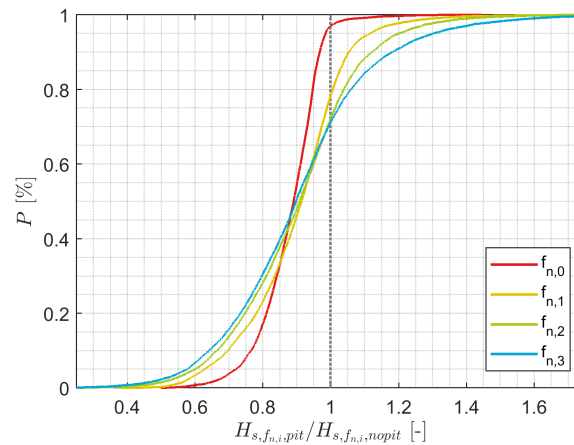


Figure 4.9: ECDFs of changes in wave heights at the four natural frequencies of the original reef. The median change in wave height at the natural frequencies stays approximately the same for higher fundamental modes. Though the average change in wave height decreases, as an increasing amount of reefs experience an increase in wave height at these higher natural frequencies.

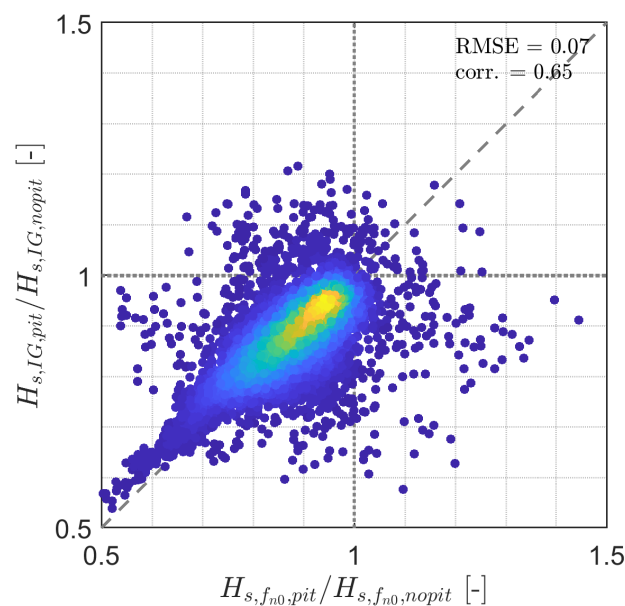


Figure 4.10: Density scatter plot of changes in wave height at the zeroth fundamental mode and in IG wave height at the beach-toe. The change in wave energy around the zeroth natural frequency (f_{n0}) of the reef is correlated significantly to the change in total IG wave energy (corr. = 0.65) and has a low RMSE of 0.07. The colors (indicating density) show that the majority of the data is located near the diagonal (1:1).

Controls of pit geometry on natural frequencies

The two modelled parameters relating to excavation pit geometry are pit width (W_{pit}) and cross-shore pit location (x_{pit}). The effect of these two parameters on the wave height at the natural frequencies is shown in

Figure 4.11. The figure shows the clear relationship that the width of the pit has on the wave height at the first two natural frequencies, as wider pits cause a larger decrease in wave height. Additionally, the location of the pit also has an effect, though less intense, as excavations located close to the reef crest also cause larger decreases in the wave height at the first fundamental mode.

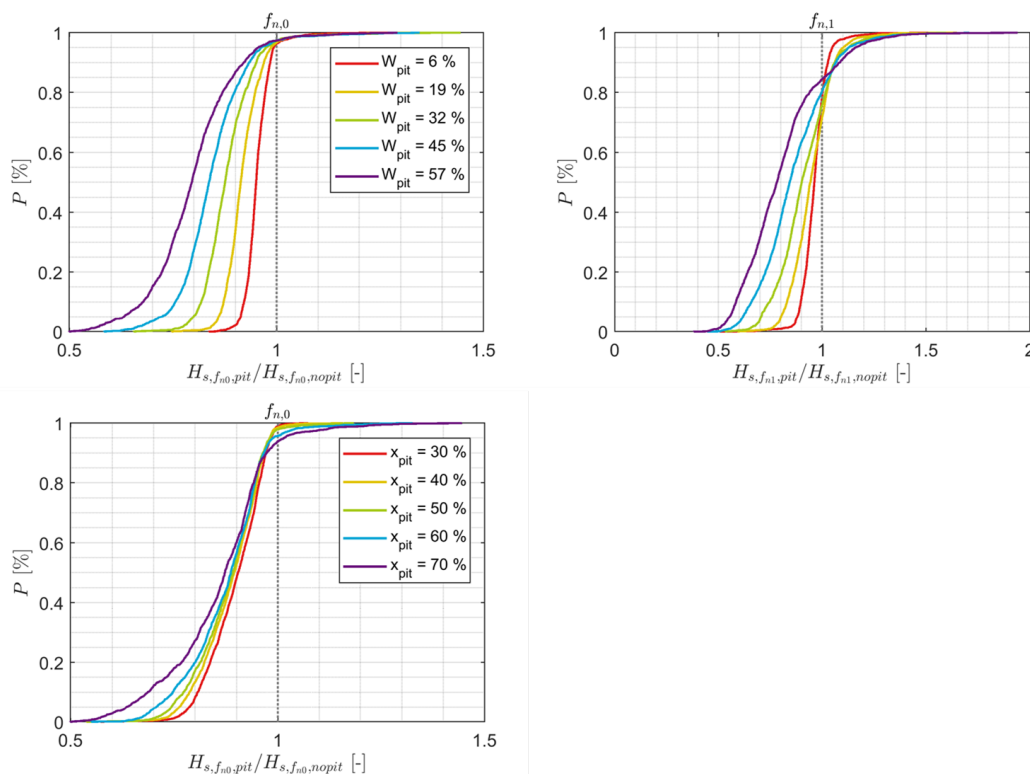


Figure 4.11: ECDFs of changes in $H_{s,f_{n,i}}$ at the beach-toe as a function of pit width (top subplots, left represents wave heights around the 0^{th} -natural frequency, right represents wave heights around the 1^{th} -natural frequency) and cross-shore location (bottom subplot). Values on the x-axis lower than 1 indicate a decrease in wave height due to the presence of a pit. Both pit width and location are expressed as a % of reef flat width.

4.4.1.3 High frequency energy

The energy in the HF band changes due to the presence of pit because it mainly affects two processes: wave dissipation and wave-wave (triad) interaction. Both of these mechanisms are most effective in (very) shallow water.

Figure 4.12 shows the change in wave heights at the HF tail (left, $f > 0.12$ Hz) and peak frequency (right, 0.04 Hz $< f < 0.12$ Hz). In this study, this split frequency for HF peak and HF tail is arbitrary, but it satisfies the relation $f_{0,peak} < f_{split} < 2 \cdot f_{0,peak}$, where $f_{0,peak}$ is the peak of the offshore spectrum. Since all runs had the same forcing conditions, the split frequency is set in this study at $f_{split} = 0.12$ Hz.

For wider pits, there is a larger probability of increase in peak wave height due to the presence of a pit, which follows from lower wave dissipation rates. Additionally, wider pits also introduce a decreased wave-wave interaction, and therefore lower wave heights are expected to be present in the HF tail. The results show the opposite, as wider pits also increase the wave height in the HF tail, which can possibly be explained by lower dissipation rates of HF tail energy, similarly to HF energy.

Remarkably, the majority of modelled reefs shows a decrease in total HF wave height, and to a lesser extent this is also seen for wave heights at the HF peak and HF tail (see Figure 4.13). On average, the change in wave height at the HF peak is smaller than at the HF tail, which supports the statements made above. This could be due to a combination of multiple processes: decreased resonant amplification of the higher natural

frequencies (in HF band), less wave-wave interaction and dissipation.

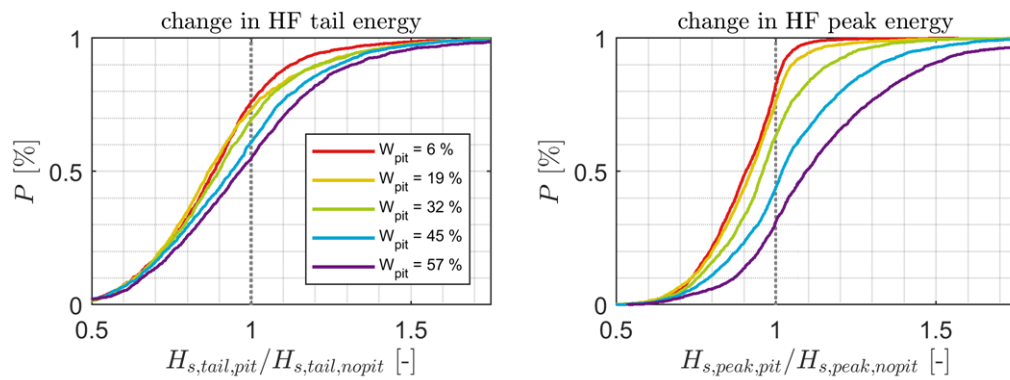


Figure 4.12: ECDFs of change in wave height at the HF peak (right) and HF tail (tail), as a function of pit width.

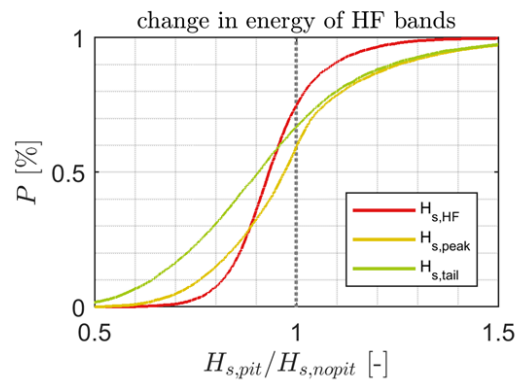


Figure 4.13: ECDF of change in wave height at the HF band, HF peak and HF tail.

It can be seen in Figure 4.14 that the wave heights of the HF peak and HF tail bands have a high correlation. Based on the theoretical and modelled effects of pits, it is expected that an excavation pit causes both an increase in the HF peak due to decreased dissipation and wave-wave interaction and a decrease in the HF tail due to the latter. The right subplot shows that there is no correlation between the change in wave height at these frequency bands. It is remarkable that the relation between the HF peak and HF tail that follows from this theory is not visibly present in the modelling results. This is probably due to other effects simultaneously significantly contributing to the hydrodynamics.

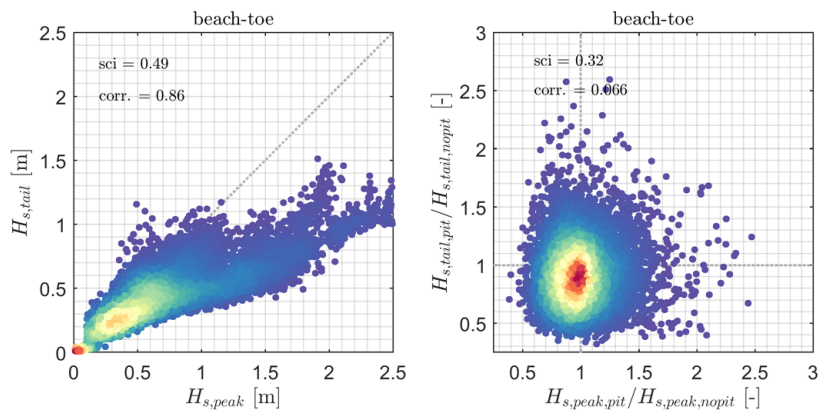


Figure 4.14: Density scatter plots of relation between wave heights in the HF peak (horizontal) and HF tail (tail). The wave heights are shown in the left subplot, the changes in wave heights in the right subplot.

4.4.2. Effect on wave runup

4.4.2.1 Modelled wave runup on fringing reefs

The direct relation of each of the five studied parameters and computed runup levels is shown in figure 4.15 by means of boxplots.

The figure clearly shows that reef submergence has a linear relation to runup (top left). This follows from the used definition of runup, which is here measured from the reef flat. Also, larger water depths on the reef result in lower dissipation rates due to wave breaking at the reef crest and due to bottom friction at the reef flat.

An increase in fore reef slope also results in larger runup of reefs (top right). This is due to an increase in IG wave generation at the fore reef and reef crest due to breakpoint forcing.

A larger reef width results in lower runup (center left). For reefs wider than approximately 250 m, this decrease becomes minimal and runup stays nearly constant for wider reefs. The decrease in runup can be due to a number of processes. Firstly, wave dissipation rates on the reef flat increase. This also leads to a decrease in IG wave amplification. Wider reefs also require longer waves to become resonant, which could alter the quasi-standing wave pattern for similar wave conditions.

Beach slope has a large role in processes dominating wave runup (center right). For gentle slopes, wave runup is lower than for steep slopes. This can be related to the fact that gentle slopes dampen out HF waves.

Both the width and the cross-shore location of the pit do not have a significant effect on the total runup, though a very slight decrease in mean runup can be observed for wider pits and pits located further from shoreline (bottom subplots).

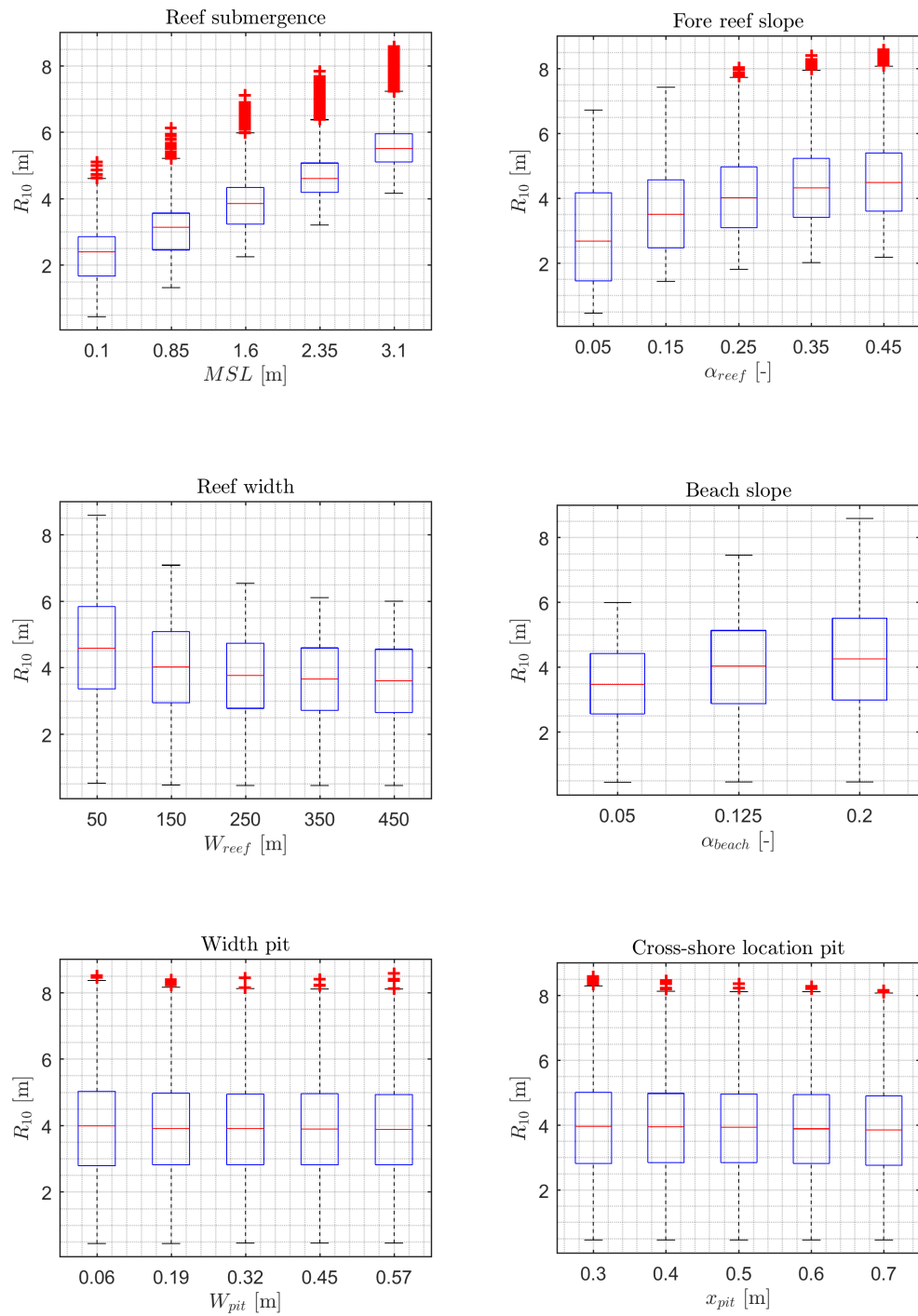


Figure 4.15: Boxplots of computed runup for all modelled reefs, as a function of the used variables: reef submergence, fore reef slope, reef width, beach slope, pit width and cross-shore location of pit.

4.4.2.2 Modelled effect of excavation pits on wave runup

Figure 4.16 shows the probability density functions (EPDFs) of all input variables and the resulting cumulative distribution function and probability distribution function of the normalized runup ($R_{10\%}$) of all model outputs. The six subplots on the left show the probability distribution functions of the values of each used variable. Every single combination of these values was modelled in XBNh+. Of all these runs, the ECDF and EPDF of the change in runup due to the presence of a pit are plotted on the right two subplots. Values on the x-axis higher than 1 indicate an increase in runup due to the presence of a pit.

On average, the runup decreased by 4% due to the presence of a pit. Maximum increase and decrease are approximately 10% and 20% respectively. The percentage of reefs that experienced an increase in runup was 15.5%. Of those 15.5%, the mean increase in runup was approximately 2.6%.

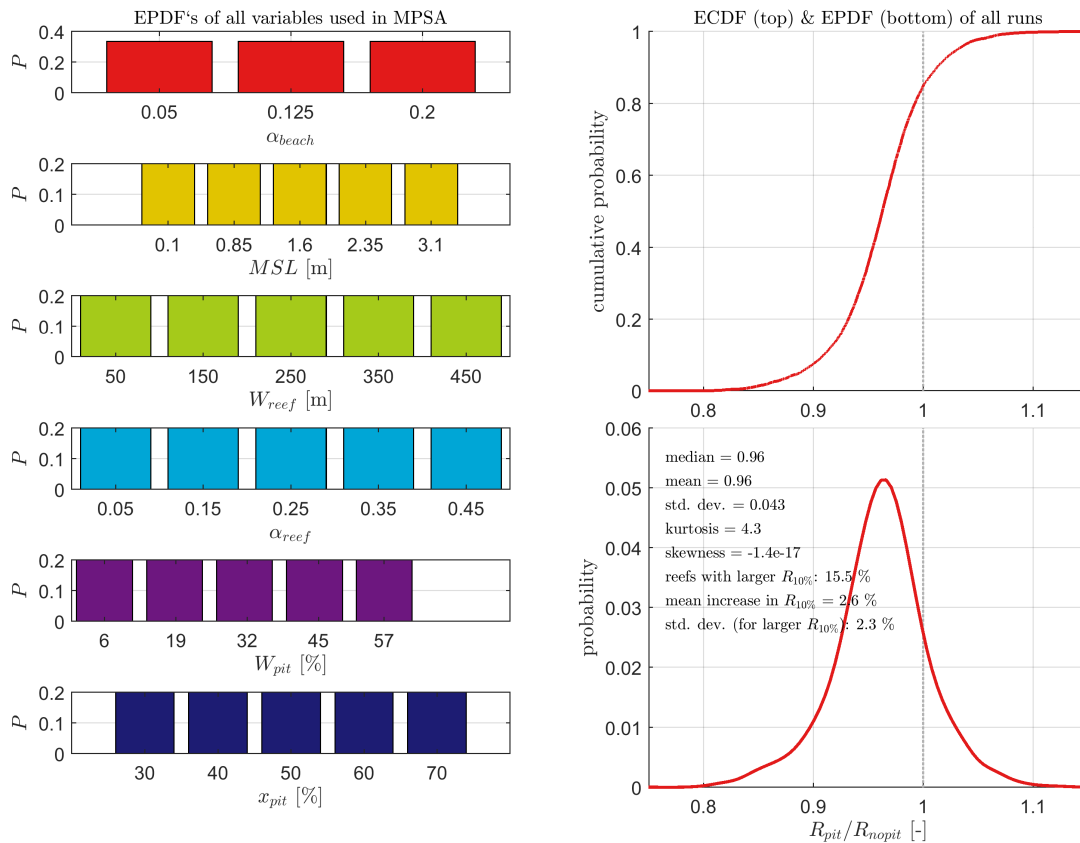


Figure 4.16: PDF's of input variables used in the multi-parameter sensitivity study (left) and ECDF and EPDF of the normalized runup. In the study, all possible combinations of the input variables were modelled. Results show that for 15.5% of all modelled reefs, an excavation pit will lead to an increase in runup. The EPDF of the total output is a near Gaussian distribution.

4.4.2.3 Mean change in variance density spectrum

The changes in runup can be explained with Figure 4.17. This figure shows the change in mean variance density for each frequency (light gray dots, $\Delta f \approx 0.25 \cdot 10^{-3}$ Hz). The solid yellow line shows the moving average of this change in mean variance density. The red and blue lines represent the same moving averages, but for reefs experiencing an increase in runup and a decrease in runup, respectively.

On average, reefs experience a decrease in IG energy, an increase in HF peak energy and a decrease in HF tail energy. This is caused by the combined effect that pits have on the processes of resonant amplification, wave dissipation and wave-wave (triad) interaction.

For reefs that experience an increase in runup, there is a significantly more pronounced HF peak and even less energy in the HF tail, which is likely caused by the combined effect of wave-wave (triad) interaction and wave dissipation. Also, IG wave energy is higher compared to reefs that do not experience an increase in runup. The opposite is seen for these reefs (blue line).

From this graph it follows that an increase in runup is caused mainly by an increase in energy around the HF peak. The decrease in wave height at the HF tail does not cause any decrease of the runup, just as the decrease in IG wave energy.

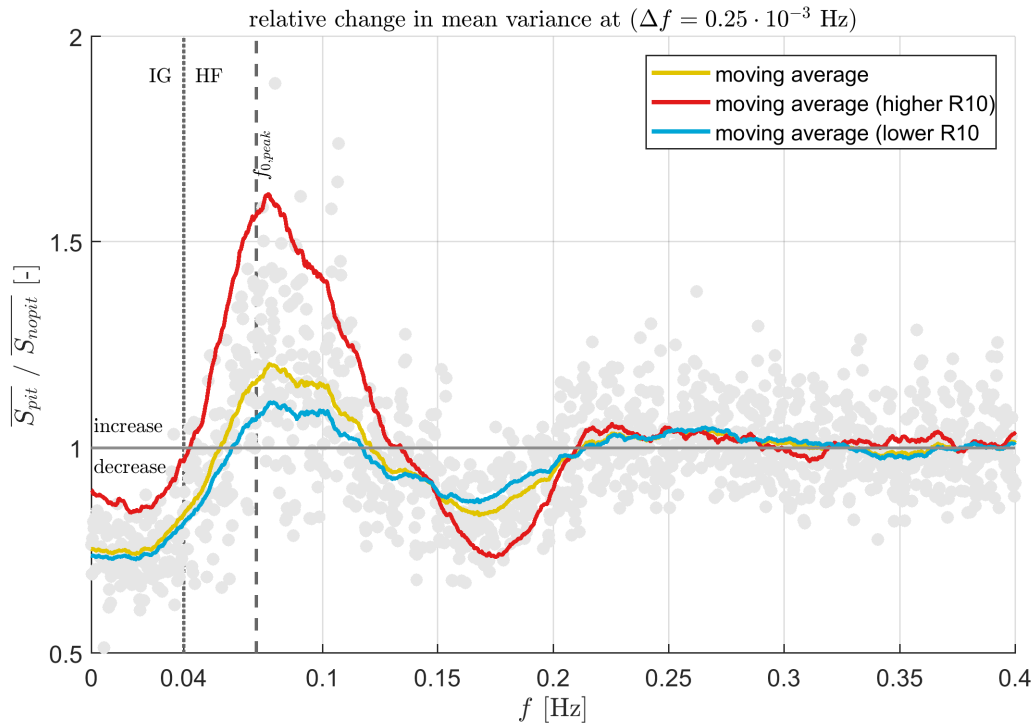


Figure 4.17: Changes in mean variance density due to pit are presented by light gray dots, which shows a significant spread and scatter for different frequencies. The moving average, represented by solid yellow line, is easier to interpret. For reefs with an increase (solid red line) and decrease in runup (solid blue line), these average trends change. Split and offshore peak frequency are shown in gray dotted and dashed lines respectively. Values on the y-axis > 1 indicate an increase in wave energy at that frequency, compared to a decrease for values < 1 .

4.4.2.4 Effect of parameters on change in wave runup

Figure 4.18 shows the ECDF's of the normalized runup of all modelled reefs per parameter. Each subplot shows the ECDF's for each modelled parameter value. For normalized runup of $R_{10,pit}/R_{10,nopit} > 1$, the chance of an increased runup can be deducted. Also, wide distributions resemble larger spread in results.

These distributions show which change in runup occurs most frequently, and also what effect each parameter has on the change in runup. The total probability of an increase in runup for each parameter value is plotted in Figure 4.19. The y-axis shows the probability of an increase in runup due to the presence of an excavation. On the x-axis represents the number (n) of each variable, corresponding to the value in the n^{th} column of Table 4.2.

Probabilities of increased runup increase for steeper beach slopes. This is expected, as steeper slopes are characterized by larger HF components in swash. The effect of a pit is to increase HF wave height, thus leading to larger chances of increased runup. Beach slope is the most significant parameter in this dataset, as the largest and smallest probabilities of increased runup occur for the steepest and most gentle beach slope respectively.

The reef submergence has a decreasing effect on changes in runup for larger values. This is because for larger reef submergence, the relative change in water depth at the pit decreases, thus resulting in a relatively smaller impact. Also, both IG and HF waves are dampened less due to larger water depth on the reef flat. This results in a relative decrease in significance of the pit on the reef hydrodynamics, thus also leading to lower probabilities of an increase in runup.

The probability of an increase in runup becomes larger for wider reefs. This is probably partly due to the fact that the excavation width was taken as a fraction of the reef width, thus increasing in size for wider reefs. This increase in size could explain the larger probabilities of increased runup. As was also seen in Figure 4.15, the effect of larger reef width dampens out for reefs larger than $W_{reef} > 250$ m (or $n > 3$). For these values of n , the changes in probabilities are less apparent.

Fore reef slope causes lower probabilities of increased runup when steeper (large n). However, there is a clear turning point, for fore reef slopes gentler than $\alpha_{reef} < 0.15$ ($n < 2$), the probability of increased runup becomes minimal. Looking at Figure 4.18, it can be observed that for $\alpha_{reef} = 0.05$, the distribution becomes bimodal and has a significantly less pronounced peak.

The width of the excavation has a very clear relationship when it comes to probabilities of increased runup. For wider pits, chances of increased runup becomes larger. This is because larger pits have a larger impact than smaller pits, therefore also increasing the probability of larger runup. Figure 4.18 shows that for wider reefs, the distribution becomes wider, indicating that the effect of the excavation is spreaded.

The cross-shore location of the excavation causes decreased probabilities of increased runup for larger distances from the shoreline (large n). From Figure 4.18 it can be seen that the distribution shifts to the right for excavations located closer to the shoreline.

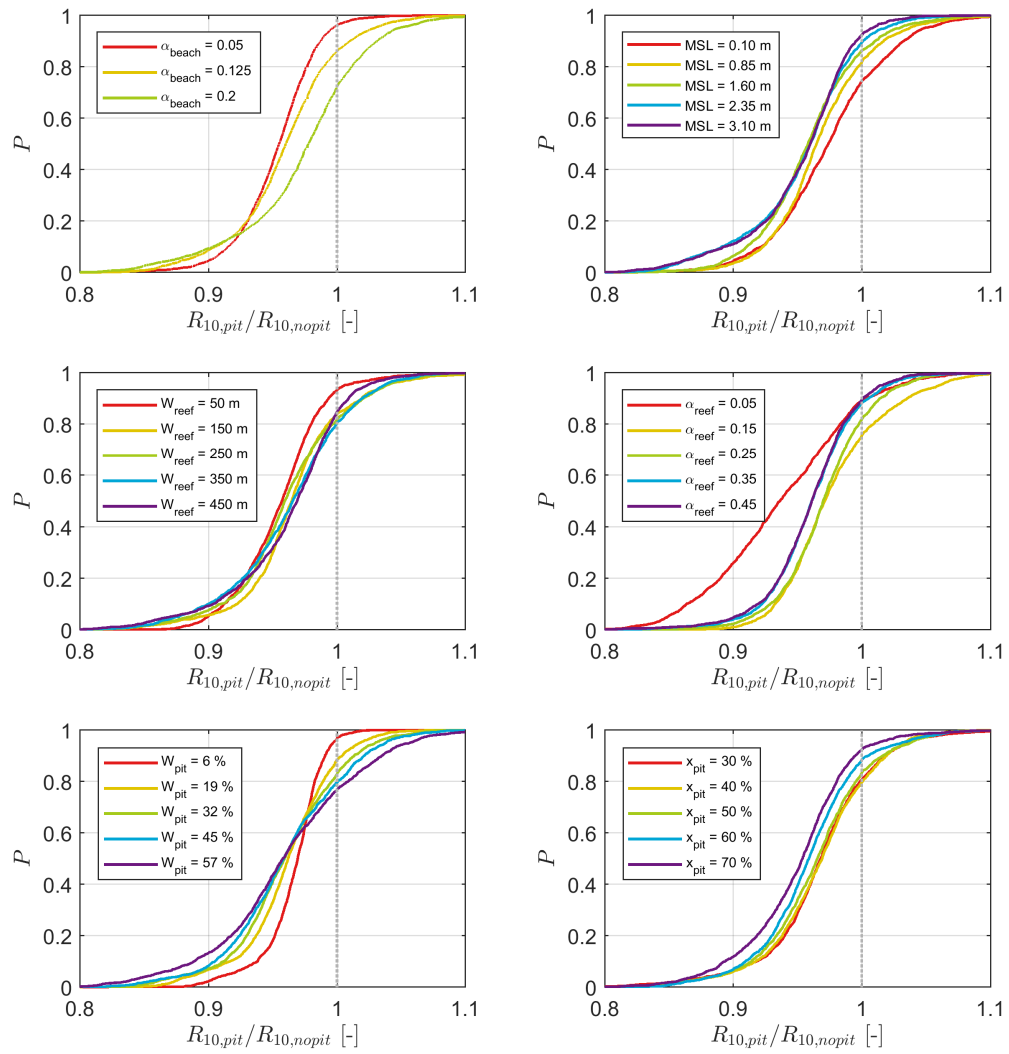


Figure 4.18: EPDF's of the normalized runup for each of the modelled variable values. The figures clearly show that each of the six variables has a direct influence on the distribution of the change in runup due to an excavation.

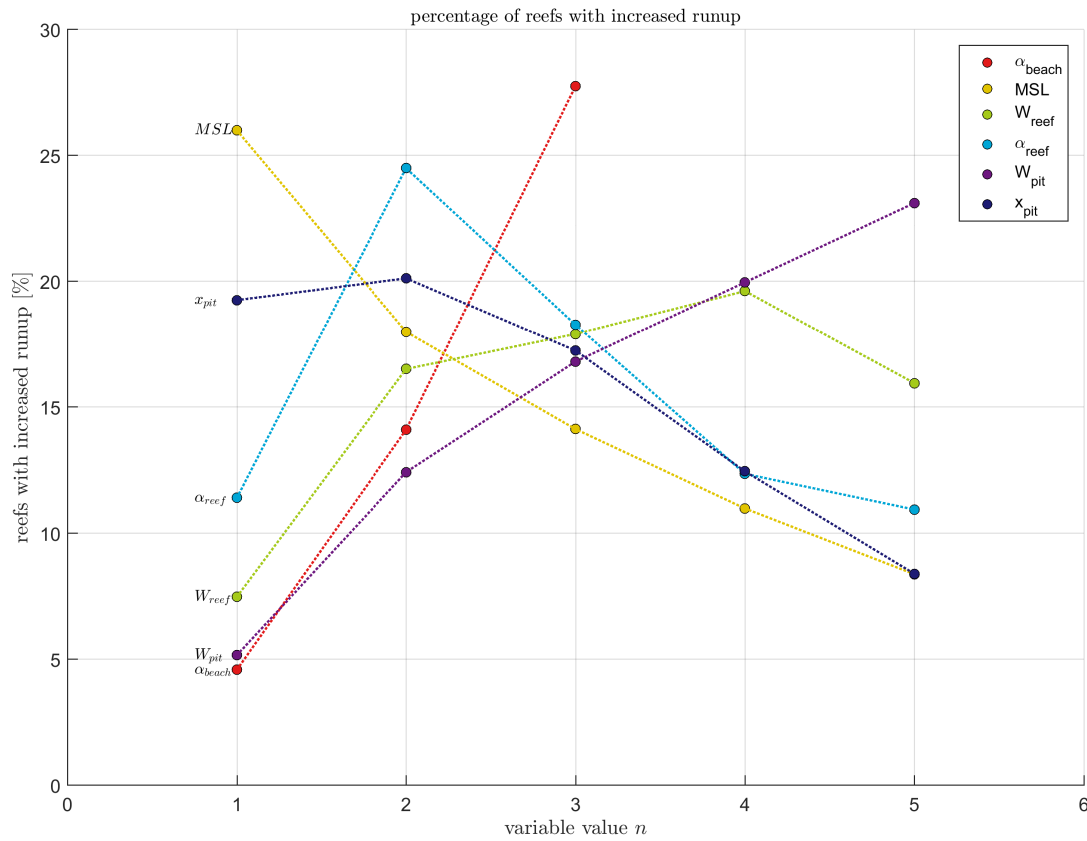


Figure 4.19: Percentage of modelled reefs experiencing an increase in runup due to presence of a pit, as function of the six parameters of the multi-parameter sensitivity study. The x-axis of the figure represents the n^{th} value of the variable, see Table 4.2. The probability of an arbitrary reef to experience increased runup due to a reef excavation depends on all modelled parameters. Large probabilities of increased runup are found for reefs with steep beaches (large n), low submergence (low n) and gentle fore reefs (though not gentler than $\alpha_{reef} = 0.15$, $n = 2$). Additionally, a large width of excavation pits (large n) and a close proximity to the shoreline (low n) increases the probability of a negative impact on runup. The wider reefs modelled also experienced larger probabilities of an increase in runup, but this could be related to the fact that excavation width was defined as a fraction of reef width, thus resulting in wider pits.

4.4.2.5 Effect of sea level rise

Figure 4.20 show the same relations as Figure 4.19, but for an offshore mean sea level of $MSL = 3.1$ m. Reef submergence is used here as a proxy for sea level rise, as this will lead to an increase of the water depth on the reef. The figure shows that for large reef submergence, the effect of excavations can be quite different than for other water levels. In general, the potential negative impact of reefs decrease for increasing water depth on the reef flat, which will be the case for a rising sea level.

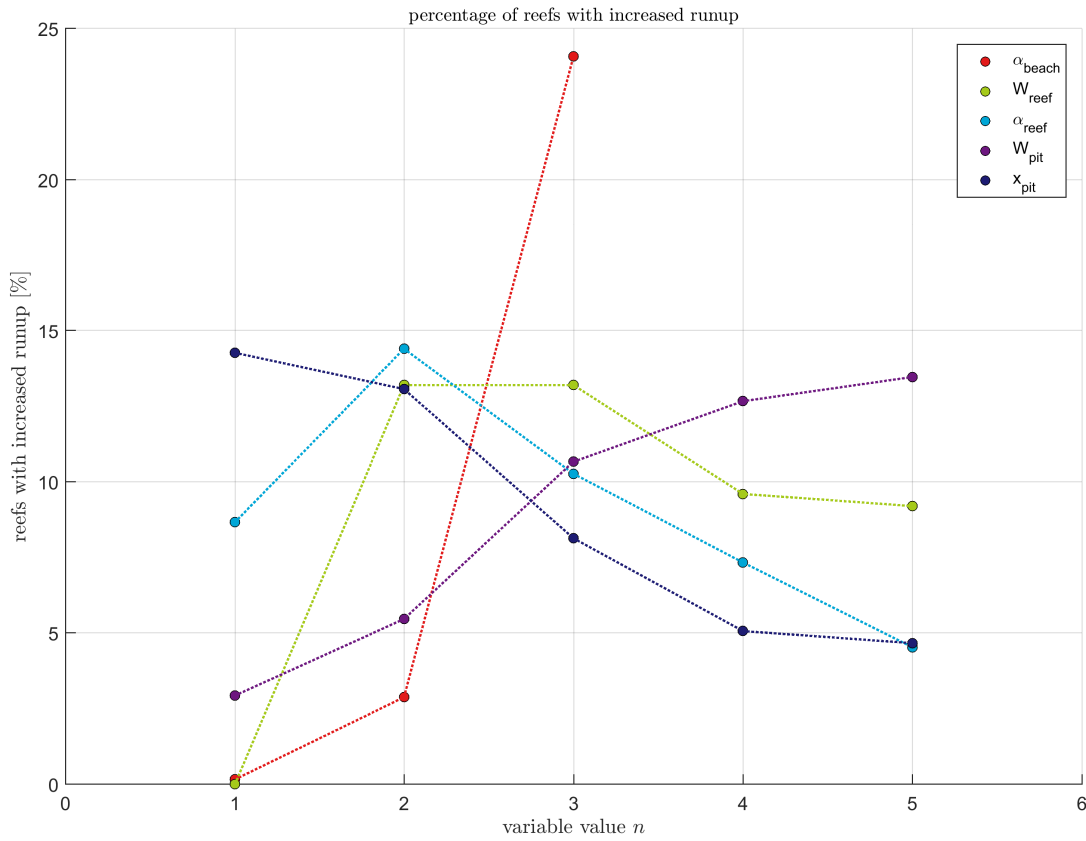


Figure 4.20: Percentage of modelled reefs experiencing an increase in runup due to presence of a pit, as function of the six parameters of the multi-parameter sensitivity study, for high MSL.

4.5. Conclusion

Effects on hydrodynamics

Based on the modelling studies performed in 1D with XBNH+, the following can be concluded regarding the effects of excavation pits on fringing reef hydrodynamics:

- Based on a single-parameters sensitivity study, involving the full parameter space, four parameters were selected that contributed most to changes in reef hydrodynamics & wave runup. These were: reef submergence, fore reef slope, reef width & beach slope. Two parameters were found to be most significant regarding the design of different excavation pits: pit width and cross-shore location.
- Based on a hypothesis and modelling results, three near-shore hydrodynamic processes are assumed to be significantly contributing to changing reef hydrodynamics due to the presence of a pit. These are: 1. wave dissipation on the reef flat (mainly through bottom friction), 2. wave-wave (triad) interaction and 3. resonant amplification. According to the hypothesis, there is less wave dissipation due to the presence of a pit, as well as less wave-wave (triad) interaction. This mainly causes changes in the HF band, such as an increase of wave energy in the HF peak and a decrease in wave energy in the HF tail. The excavation pits disrupts the spatial structure of the fringing reef, and therefore alters the natural frequencies. This in turn causes a decrease in resonant amplification, leading to less wave energy in the IG band. A large spread in modelling results is expected, partially due to the large amount of simulations (~ 10.000), but also due to the combined effects of the contributing hydrodynamic processes.
- Model results show that there is mainly a decrease in HF energy due to the presence of a pit. For wider pits, wave energy in the HF peak increases, but also a minor increase in wave energy in the HF tail is present. This indicates that there are also decreased dissipation rates for waves in the HF tail band, in addition to a decrease in wave-wave (triad) interaction causing a less pronounced HF tail.
- The model results also show that there is a large correlation between the changes in IG wave energy and the wave energy around the zeroth natural frequency of the reef. This indicates that the changes in IG wave energy are a result of changing resonant amplification. This supports previous findings of Yao et al. (2016). Wider pits and pits located closer to the reef crest have a larger decrease in resonant amplification and thus IG wave energy.
- Moreover, it is expected based on the momentum balance that a decrease in wave dissipation due to the presence of the pit results in an increase in mean water level behind the excavation pit. This hydrodynamic effect of the pit is also confirmed by the model results.

Effects on wave runup

Similarly, on the effects of excavation pits on wave runup the following can be concluded:

- On average, model simulations show an increase in wave runup of +5 %, with extremes lying between +10 % and -20 %. Fringing reefs with narrow reef flat, very gentle or very steep fore reef slopes, gentle beach slopes and high reef submergence experienced the lowest probabilities of an increase in runup due to the presence of an excavation. Excavation pits have the lowest probability of an increase in runup when they are characterized by a small width and are located close to the reef crest.
- For 84 % of the simulations a decrease in wave runup due to the presence of the pit is observed.. This occurred for 84 % of all simulations. The decrease in wave runup is a result of a decrease in wave energy in the IG band and a decrease in wave energy in the HF tail.
- For the remaining simulations (16 %) an increase in wave runup is observed. An increase in wave runup is driven by an increase in HF peak energy, which was associated with a further decrease in wave energy in the HF tail, due to decreased wave-wave (triad) interactions.

5

2D modelling study

5.1. Introduction

A two-dimensional XBNh+ model was used to make a first assessment of the 2D-effects associated with reef excavating, such as alongshore variations of wave heights, water levels and runup, and current circulation patterns. The 2D model was also used to make a comparison between the 1D and 2D results, in order to assess the numerical and physical effects of introducing a new dimension. The objectives of this 2D modelling study are:

- Assess the two-dimensional effects of pits on reef hydrodynamics and runup;
- Assess the numerical and physical effects of the introduction of an extra horizontal dimension.

5.2. Methodology & 2D Model setup

The 2D XBNh+ model was setup in the same way as the 1D models (see Figure 4.1), using the same grid spacing and numerical settings. The ratio of width/length of the pit (x-/y-direction, respectively) was set to a value of approximately 1/2.5. The long-shore (y-) direction was discretized with a grid size of $\Delta x = 5$ m. In alongshore direction, the bathymetry was extended several 100 m away from the excavation pit, in order to minimize boundary effects. At the lateral boundaries, cyclic conditions were used. On the offshore boundary, the same JONSWAP spectrum was forced as those that were used in 1D simulations, but with a JONSWAP spreading parameter of $s = 15$, which corresponds to a directional spreading $\sigma = 20^\circ$. Significant wave height at the boundary was set at $H_{s,0} = 2$ m, with a peak period of $T_p = 9.8$ s. Still water level on the reef flat is $MSL = 0.5$ m.

In order to reduce the effect of sampling and produce a "smooth" long-shore variation, the 2D model was run for a duration of $T = 3$ hr. The model was run in parallel mode, by using a Message Passing Interface (MPI), which subdivides the computational domain into 8 sections, all perpendicular to the coastline. This increases computational speed, but does not reduce the model's accuracy. Six cross-shore and three along-shore transects were used in post-processing analysis, as well as a runup gauge at every grid cell in y-direction. The outputs of two identical reefs (1D & 2D) are compared here. Both reefs are run with and without excavation pit. The output of these six cross-shore transects of the 2D model are compared with the output of the 1D model. Additionally, long-shore variation in wave height and runup is assessed in 2D, as well as spatial variations in wave height and mean water levels and currents.

5.3. 2D Model results & discussion

5.3.1. Comparison of 1D and 2D output

Figure 5.1 shows a comparison of the wave height and water level transformation in x-direction, for a 1D model and a transect including excavation pit of the 2D model. A similar output figure is included in Appendix C.1, without excavation pit.

The 2D model is characterized by slightly higher energy dissipation on the reef crest and flat, causing the HF waves to become lower than in 1D.

The IG wave height is significantly lower offshore for the 2DH mode, which is caused by smaller groupiness of waves, associated with the directional spreading of the incoming waves. This results in a lower BLW. This difference is also seen on the reef flat, where IG waves that originate from the breakpoint forcing mechanism dominate. The lower IG wave energy is also observed at the beach-toe (see Figure 5.2), however this is limited possibly to the VLF range. The large peak shown in red is located around the longest natural frequency of a reef without excavation. This could indicate that in 2D there is less resonant amplification for multi-directional waves.

Because of larger dissipation rates of HF waves in 2D, a larger wave-induced setup is also seen, which follows from the momentum balance.

Figure 5.3 shows the variation of runup as a function of n , both for a 1D and a 2D run. In 2D there is not such a distinctive difference in runup for high n , when comparing the reef with and without pit. For this reef this indicates that there is a larger change in $R_{10\%}$ when modelled in 1D, compared to when modelled in 2D. This could be related to errors that result from sampling.

The normalized mean water level and wave heights at four different locations on the reef are compared for 1D and 2D in Figure 5.4. The resulting changes due to the presence of the pit are very comparable in 1D and 2D. The change in runup can be explained with both models in a qualitative way (e.g. higher or lower runup due to the presence of a pit), but accurately quantitatively estimating actual runup levels remains challenging.

From a single 2D run it is difficult to deduct the impact of the second horizontal dimension on the physical processes. Modelling errors (e.g. sampling) could also contribute to the differences that are seen between 1D and 2D.

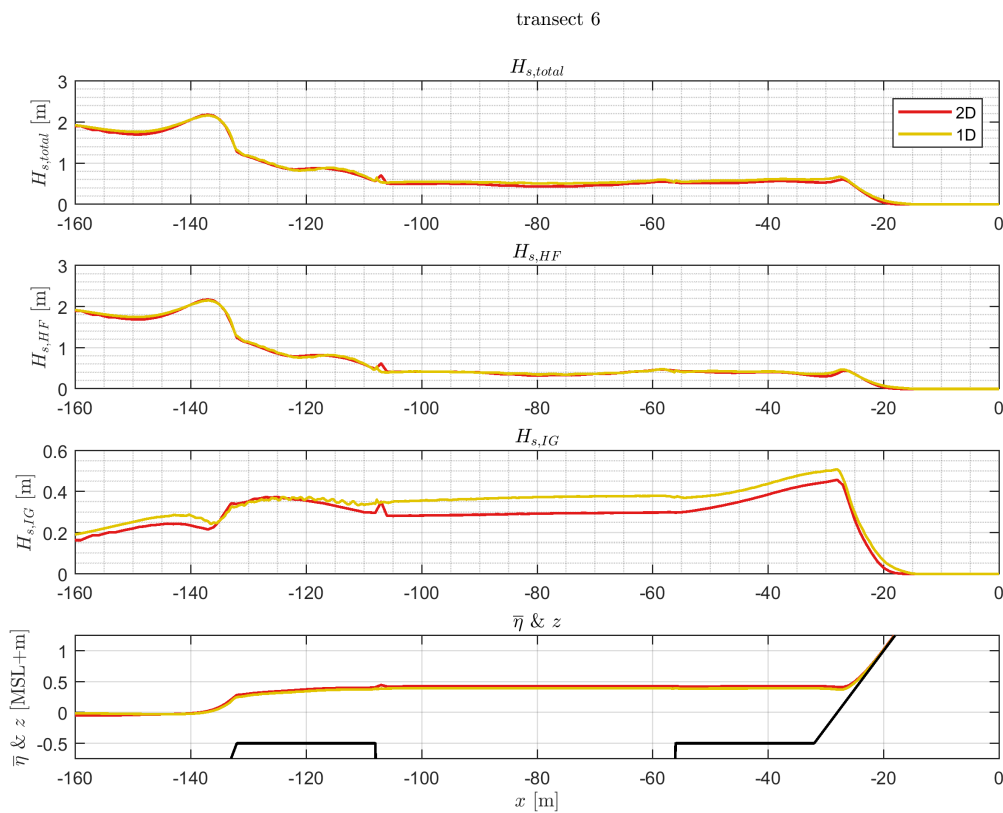


Figure 5.1: Comparison of wave heights and mean water levels of a 1D (yellow lines) and 2D (red lines) run.

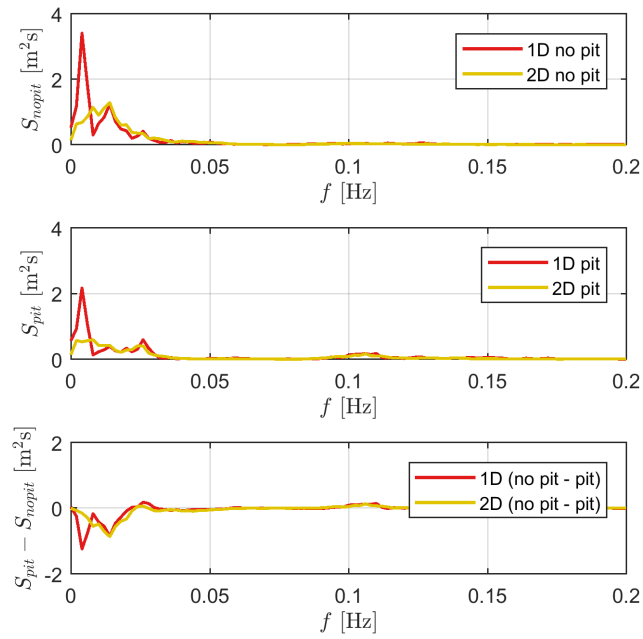


Figure 5.2: Comparison of variance density spectra at the beach-toe, for the 1D (red) & 2D (yellow) model. The top subplot shows the variance density of the reefs without pit, the centre shows this for the reef with pit, and the bottom subplot shows the difference in variance due to the presence of the pit.

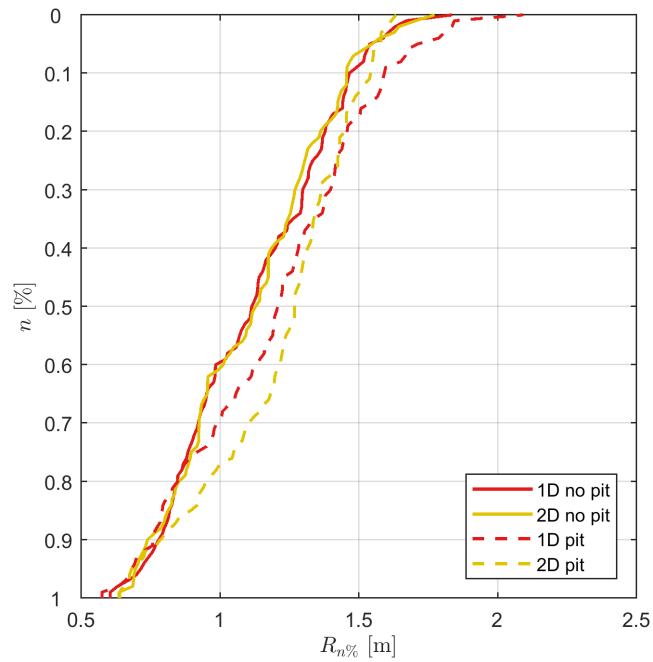


Figure 5.3: Runup as a function of n , a comparison between 1D (red) and 2D (yellow) model outputs. Both the reef with (dashed lines) and without (solid lines) pit are shown.

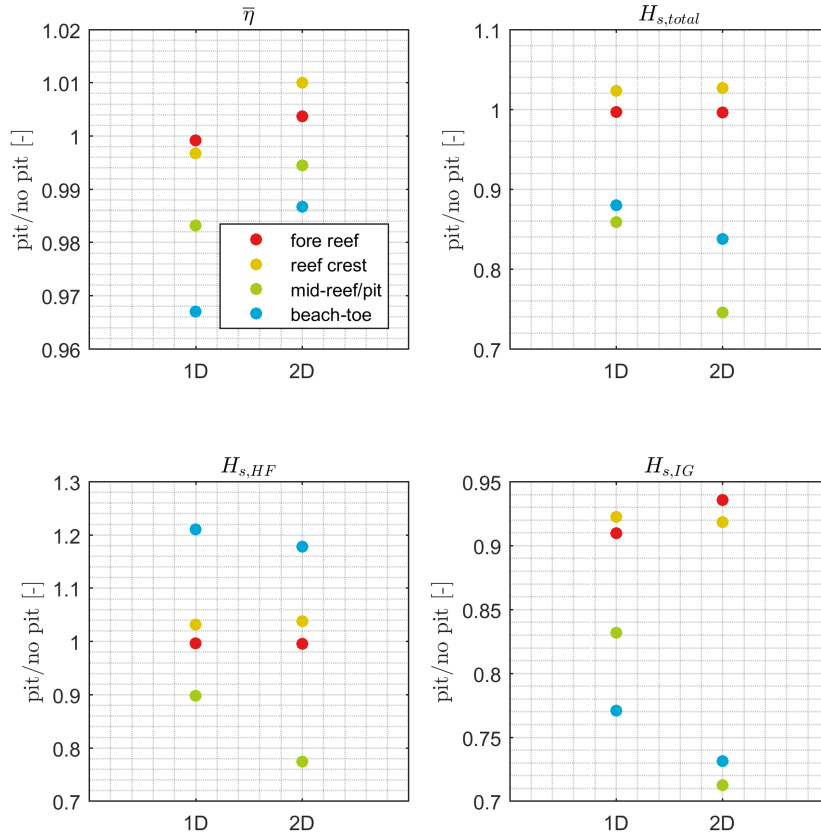


Figure 5.4: Comparison of normalized wave heights and mean water level for 1D & 2D, at four different cross-shore locations of the reef.

5.3.2. Observed 2D effects

Figure 5.5 shows the spatial variation in significant wave height, mean water level and resulting currents. The excavation pit has an impact on wave height in an area that extends to a wider stretch of coastline than the bathymetry itself. At the center behind the pit, larger wave heights can be observed than behind the lateral walls of the excavation.

The variations in wave height cause a mean water level that is lower behind the pit, compared to surrounding area. This causes a mean circulation pattern to form, which directs towards the back of the excavation and then in offshore direction. No effects on morphology were modelled. But as sediment dynamics is linked directly to hydrodynamics, it is assumed that a circulation pattern like this can cause erosion and accretion at certain locations along the coast. Additionally, sediment that is transported in offshore direction may be trapped in the excavation pit. This could initiate long-term erosion. These patterns exist during daily wave conditions ($H_{s,0} = 2$ m), and suggest that this indicates the presence of a very generic effect, with a higher frequency than extreme flooding events.

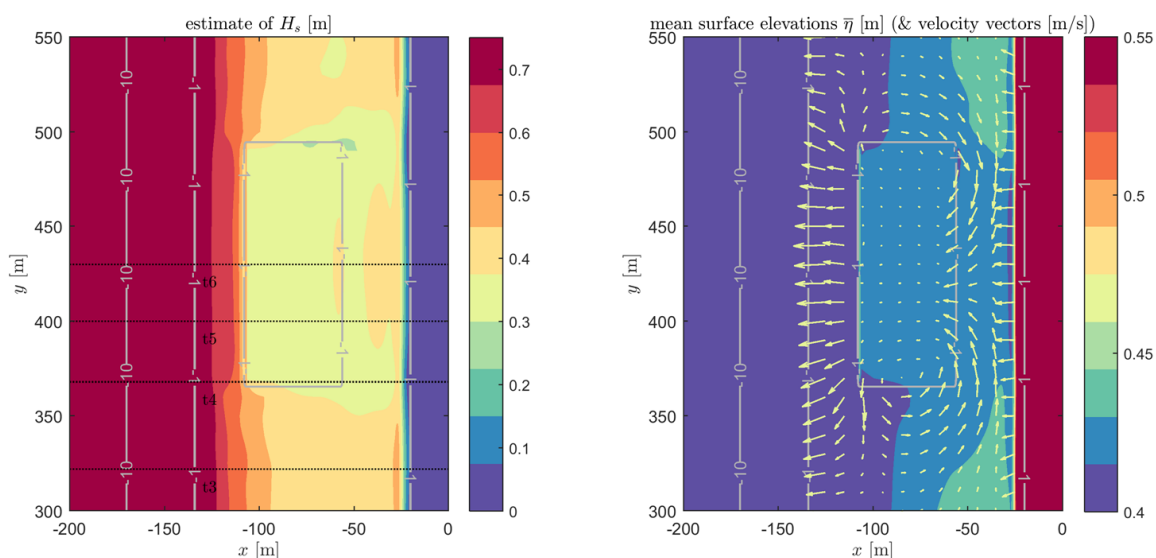


Figure 5.5: Spatial variation of wave height (left) and mean water level & resulting currents (right). Depth contours of $z = -10/-1/1$ m are shown in gray solid lines. The black dotted lines represent the transects mentioned in Figures 5.1 & 5.6

Figure 5.6 shows the long-shore variation of wave heights and mean water level, for a cross-section at the beach-toe, as well as the variation of runoff. Two distinctive patterns are observed, that of the HF wave height and that of the IG wave height. The effect of the excavation on HF wave height reverses at the lateral pit boundaries, and extends significantly in y -direction (approximately with a similar length as l_{pit}). This spatial variation also has a visible impact on the variation in runoff, even though it is not as pronounced as in the total wave height. The effect on IG wave height is similar to that modelled in 1D. It is expected that these long-shore effects of excavation pits vary with offshore forcing (e.g. directional spreading, wave steepness), as well as reef dimensions and pit design (e.g. cross-shore location). There is a notable difference in the computed runoff in 1D and 2D. This could be related to the use of different samples of wave time series in both runs. Additionally, the mean circulation current could induce extra near-shore processes which cause waves to steepen and break further away from the waterline, compared to 1D. This could decrease runoff and explain why there are no visible difference at a location where there is no effect of the excavation.

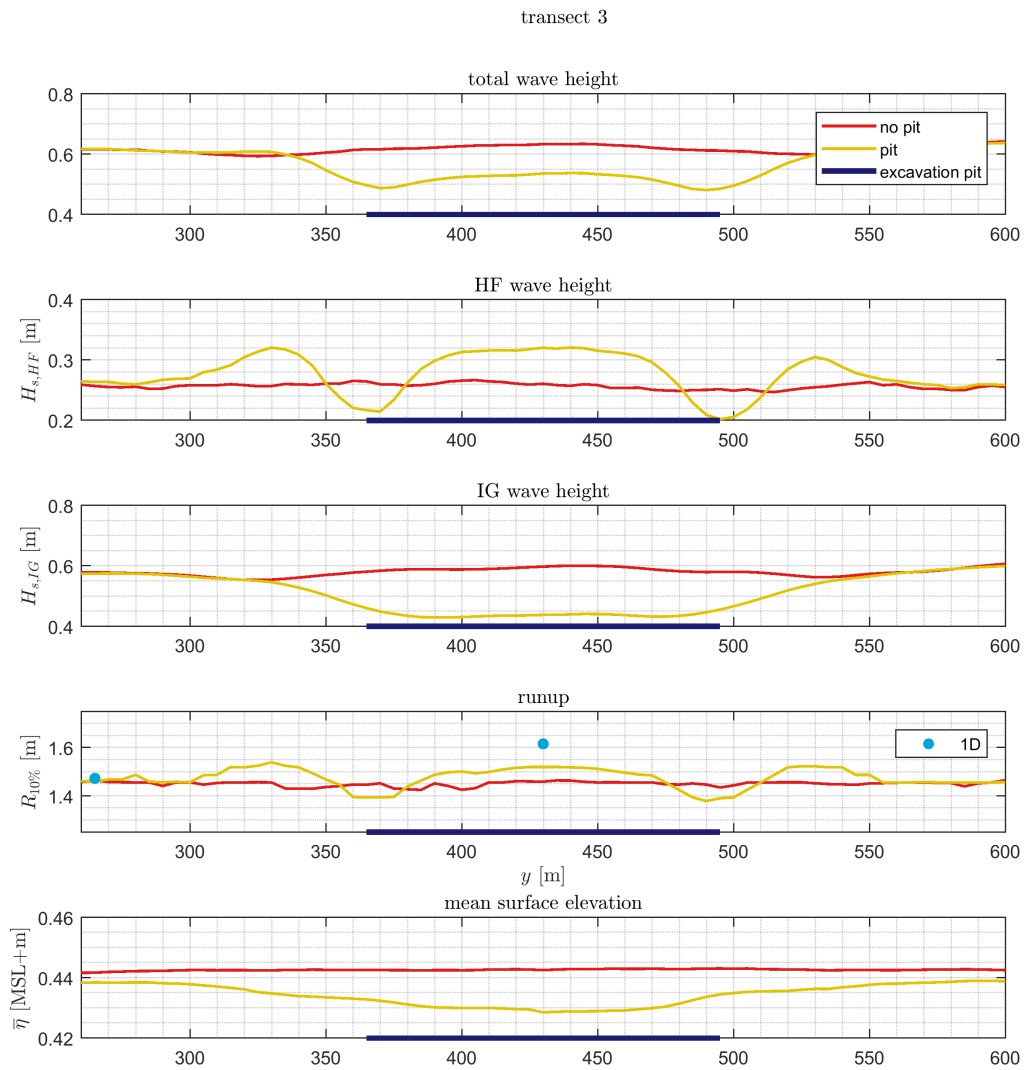


Figure 5.6: Long-shore variation in wave height, mean water level and runup. A comparison is made between a 2D run with (yellow line) and without (red line) pit. The runup values computed in the 1D run are plotted as well (blue dots). The blue solid line in the bottom subplot represents the lateral extent of the excavation pit.

5.4. Conclusion

A 2D modelling study was conducted in order to make a comparison between 1D and 2D and assess the differences, as well as to gain insights on possible 2D effects associated with excavation pits. Based on this study, the following can be concluded:

- The main difference between 1D and 2D model results is the difference in wave energy. 1D simulations have more short wave groupiness compared to 2D simulations, which is related to the fundamental difference of directional spreading in an 1D versus 2D model.
- The modelled effects of an excavation pit are comparable in 1D and 2D. Changes in wave heights due to the pit (increase in HF wave height and decrease in IG wave height) were observed in both models. The largest difference observed in 1D and 2D, related to the effects of pits, is a smaller decrease in mean water level at the beach-toe.
- The spatial variation in mean water level around the excavation pit induces a mean circulation current around the pit, which is eventually directed offshore over the pit.
- The model results show long-shore variations in wave heights and resulting wave runup, which extend to approximately one time the length of the excavation. Moreover, at the edges of the excavation, the wave-driven runup can reduce compared to the situation without a pit.

6

Discussion & limitations

6.1. Limitations of XBnh+

Unknown parameters of dataset

As was mentioned in Chapter 3, there is currently one dataset available on near-shore fringing reef hydrodynamics that includes an excavation pit. Using this dataset is currently the only possibility of calibrating and validating a hydrodynamic model such as XBnh+.

Unfortunately, there are some drawbacks to this dataset, as was discussed in Chapter 3. Some unknown parameters are found to have a significant impact on the hydrodynamic processes in the reef, which resulted in a conventional calibration to be impractical and unrealistic. This has caused that the validation study that has been presented in this thesis is flawed, because it is not highly accurate. However, the XBnh+ model is able to simulate relevant processes in a fringing reef coast, as well as the effect of pits. The outcome is that quantitative results can not be interpreted as reality, although the modelled processes are assumed to be sufficiently accurate.

Additionally, there are no data on runup on fringing reefs. Therefore, this study solely relies on the predictive capabilities of the XBnh+ model. Although these contain a good representation of actual physical processes, a validation for the runup is still lacking. The model was able to simulate the overwash that occurred during the validation event, and therefore produced sufficient confidence for the rest of this study.

Errors due to 3D hydrodynamic properties of excavations

Locally, around the excavation, there is a steep bathymetric change. In flow over steps or weirs, with comparable bathymetric characteristics as an excavation pit, there is a certain adaptation length before the flow reattaches itself to the bottom. It could be that a similar process is present at the edge of the excavation, due to the orbital velocity of the water particles. Because the XBnh+ model only has 2 vertical layers, any impact of this effect is expected not to be simulated accurately. However, as is seen in Appendix A.1, the XBnh+ model produces far more realistic results than its predecessors, which do not have this extra layer incorporated in their computations. Any visible effects that result from simplifying vertical hydrodynamics around the pit walls are not found across the reef and are assumed to be negligible. For the modelling of sediment dynamics, this could introduce additional errors.

6.2. Model simplifications

In this study, a number of model simplifications have been introduced that facilitated the progress and scope of this study, but also reduced the accuracy and reliability of the model and its results. All of these have been studied in more detail in order to assess and estimate the errors corresponding to the simplifications (see Appendices A.1, A.2, B.1, B.2 & B.3). The impact of these simplifications is assumed to be sufficiently small when one order of magnitude smaller than the modelled effect of excavation pits. Some model simplifications are: sampling, boundary conditions, reef geometry and parameter selection.

Sampling

This has been discussed briefly in Chapter 4 and is explained in more detail in Appendix B.1 & B.2. In order to limit computational efforts and facilitate the progress of this thesis, the simulations have been limited to a duration of $T = 1$ hr (excluding spinup time, currently set at $T_{spinup} = 10$ min). This allowed for an extensive analysis of hydrodynamics of a large number of different reefs (9375), which contributed to the value of this thesis. The used simulation time introduces a (minor) sampling error that is responsible for inaccuracies in the computation of hydrodynamics and runup (in the order of a few percent). Because boundary conditions are reused, this error decreases further. The errors made in the computation of changes in wave height and runup are also in the same order, which is sufficiently small compared to the effects of the excavation pits that are studied.

Because of less extremes present in the surface elevation signal of the runup gauges, and a larger variability for the upper runup quantiles, it has been opted to use a different runup than $R_{2\%}$ in this study, namely $R_{10\%}$. Appendix B.2 discusses the impact of including runup values other in addition to the extreme runup levels. Because the $R_{2\%}$ $R_{10\%}$ are highly correlated and sufficiently low errors ($sci < 0.05$) are made, the 10 % quantile is assumed to be a good representation of the extreme runup. This quantile actually shows to give conservative estimates for changes in runup, since for higher quantiles a (slightly) larger decrease is expected.

The negative effects of sampling are therefore assumed to be limited and do not affect the results significantly.

Reef simplifications

In this research, the physical characteristics of a fringing reef were schematized into a simplified version, consisting of specific components. In reality, fringing reefs have more continuous transitions and larger variability. However, this schematization proved to be a useful method to model the hydrodynamic processes of fringing reefs in the past (Pearson et al., 2017). In Appendix B.3 a comparison (in XBnh) of a natural reef and a simplified reef is shown. From this comparison it follows that the simplified reef is a sufficiently accurate representation of a natural reef.

Parameter selection

In this study, a parameter space has been defined based on real fringing reefs occurring throughout the world. Therefore, the results of this thesis give a good approximation of the possible effects of excavation pits. However, the resulting probabilities of increases in runup should not be interpreted as a representation of the real world, since the parameter space does not include a weighing factor or distribution for each parameter which represents actual worldwide reef distributions.

The parameter space was reduced to six in the multi-parameter sensitivity analysis, with a uniform distribution of the possible values of each parameter. These six parameters represent the most sensitive and relevant parameters that were modelled, any impact of other parameters is neglected. The remainder was set on default value, which is assumed to be a common value for reefs around the world. This allowed for the simulation of a large amount of reefs with specific parameter values, which contained the most important factors of influence of reef hydrodynamics.

Both of these aspects (reef distribution & parameter selection) form limiting factors in this study, and the possible impact on the modelled results is complex. The parameter selection process has taken into account the possible effects of these and was aimed at alleviating any errors.

6.3. Model results

Relation between wave height at beach-toe and swash motion

Additionally, the modelled relation between changes in wave height at the beach-toe (both HF and IG) and swash components does not seem as straightforward as would be expected. Figure 6.1 shows the relation of the wave height (left) and changes in wave height (right) at the beach-toe (x-axis) and water line (y-axis), both for IG (top) and HF (bottom) frequency bands, in the form of density scatter plots.

There is an amplitude increase for IG band energy from beach-toe to the water line (see runup gauge). This can be related to shoaling of waves on the beach slope and the influence of reflected IG waves, causing an increased quasi-standing wave pattern at the water line.

The change in IG wave height (top right subplot) at beach-toe correlates significantly less to the change in IG wave height included in the swash.

The same holds for the HF band (bottom left figure). The swash is split into three, corresponding to the three different bottom slopes, which modulates the dampening of HF waves on the beach. Even though this distorts the comparison, the correlation remains significant.

But for the change in HF wave height from beach-toe to shore line, the data is far more cloudy.

This figure shows that changes in wave height at the beach-toe do not directly relate to the change in swash (and ultimately runoff). In previous studies, near-shore wave height has generally been used as a prediction for wave runoff and overtopping. The results of the XBnh+ model show that the processes involved in wave propagation on the beach slope on fringing reefs with excavation pits are too complex to be simplified in such a manner. This requires sufficient confidence in the model's capacity of simulating runoff on beach slopes with sufficient accuracy. XBnh+'s capacity of simulating runoff has been studied in the past, and proved to be sufficiently accurate on different coasts, including fringing reefs (Beer, 2017; Pearson, 2016; Quataert, 2015). The confidence in the model for this study is also present, as the results presented in Figure 4.19 reflect the hypothesis.

However, it has been pointed out that there is a low number of datasets on runoff of fringing reefs available (Pearson, 2016). This is even more the case for fringing reefs with excavation pits.

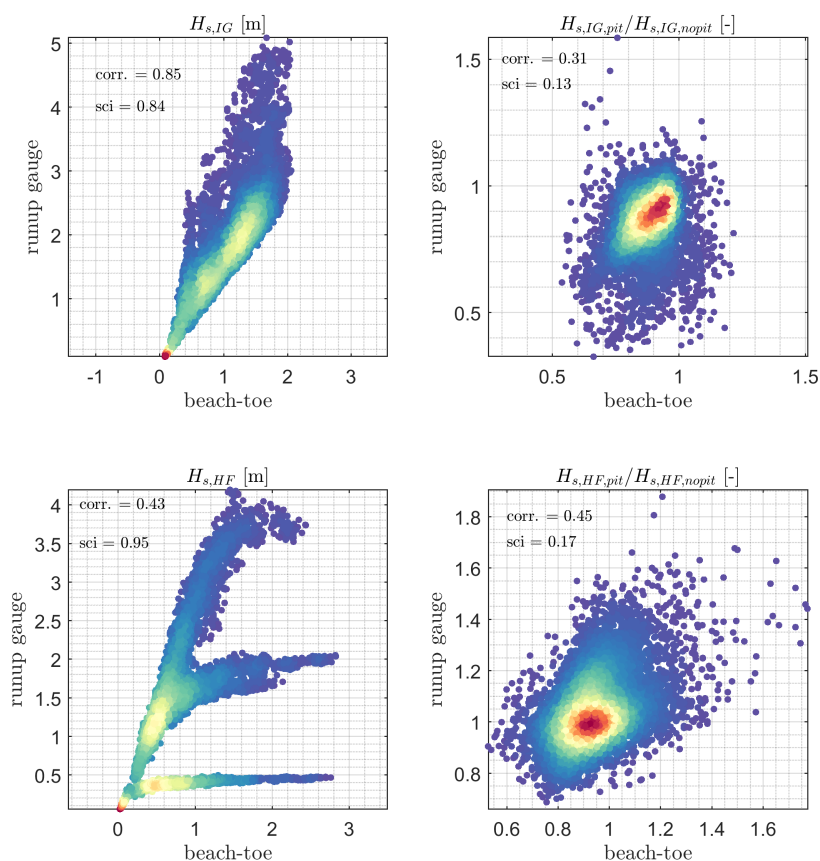


Figure 6.1: Density scatter plots of wave height and change in wave height at the beach-toe and swash. The subplots include the correlation and scatter index between beach-toe (x-axis) and swash (y-axis). Wave heights are shown in the left subplots (top left: IG, bottom left: HF). The change in wave height due to the pit is shown in the two right subplots (top right: IG, bottom right: HF).

7

Conclusions

7.1. Modelling with XBeach non-hydrostatic+

- The results of modelling activities with XBnh+ of two events recorded in 2011 at the nearshore of Majuro Atoll, Marshall Islands, show that the model is sufficiently capable of capturing relevant hydrodynamic processes on fringing reefs, as well as the effect of reef flat excavation. Additionally, the model is able to reproduce the overwash which was observed on the 29th of June 2011.
- Three different XBeach modules have been compared briefly, which resulted in the evident advantage of using XBnh+ over other modules. This is because it resolves all frequencies, resulting in a more accurate estimate of runup. The extra computational layer in z-direction increases its applicability on steep bottom profiles, such as fore reef slope and excavation pit walls.
- Due to the current limited availability of detailed datasets of surface elevations and wave transformations over a fringing reef with reef flat excavations, the validation of using a numerical model to simulate these hydrodynamic processes proves to be challenging. The availability of datasets remains an issue when studying the effects of excavation pits on fringing reefs. The dataset that was used had some unknown parameters, which were needed to accurately validate a numerical model that simulates the effects of pits on reef hydrodynamics. This introduced complications in the efforts to accurately calibrate an XBnh+ model. The effect of conventional calibration parameters such as hydraulic roughness were overshadowed by the effects of the missing parameters in the dataset, such as offshore water level and fore reef slope.

7.2. Effects of excavation pits on fringing reef hydrodynamics

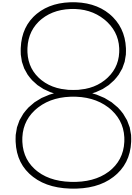
- The large number of 1D XBnh+ simulations that have been included in this study (~ 10.000) show that there is a large spread in the computed hydrodynamics and effects of excavation pits.
- Reef excavating can cause an increase in HF peak wave energy reaching the shoreline. This is due to a decrease in HF wave dissipation caused by an increase in water depth due to the pit. A decreased intensity of wave-wave interaction can also contribute to this increased HF peak, while also causing a decrease in wave height at frequencies in the HF tail. Model results indicate that these two processes are most likely responsible for the observed changes in HF wave height at the beach-toe. In theory, these two processes are likely to cause a decrease of the HF tail and an increase of the HF peak in the variance density spectrum. However, the majority of the modelled reefs experiences a decrease in HF wave energy at the beach-toe, due to the combined effect decreases in wave energy at the HF peak and HF tail bands. The model results also show that the width of the excavation has a large impact on the HF peak, as this increases for increasing pit width. The same effect is seen for the HF tail, though less pronounced.

- Reef excavating causes a decrease in IG wave energy reaching the shoreline. A possible explanation for this is that the excavation pit disrupts the spatial structure of the reef, which is similar to that of an open basin. Model results show that the decrease in IG wave height is correlated with the change in wave height around the zeroth fundamental mode of the reef. This suggests that resonant amplification is altered by the presence of the pit, which is in turn caused by a change in the natural frequencies of the reef. This confirms findings from previous studies (Ford et al., 2013; Yao et al., 2016). The wave height around the first two fundamental modes is affected most by the presence of a pit. Both pit width and cross-shore location affect the resonant amplification of the reef. Wider pits and pits located closer to the reef crest cause the largest drop in wave height around the zeroth (and first in the case of pit width) fundamental mode.
- Reef excavating causes changes in mean water level on the reef due to changes in momentum in cross-shore direction. Ultimately this leads to a lower mean water level shore-ward of the pit, compared to a reef without excavation. In a two-dimensional case, this will lead to mean circulation patterns directed offshore over the excavation, which was confirmed by a 2DH model. This suggests that there is a possibility of systematic erosion due to the presence of excavation pits (e.g. entrapment of sediments). However, the morphological effects of excavation pits were not incorporated in this study.
- Of all modelled forcing parameters, reef submergence has the most significant impact on reef hydrodynamics, as it increases the HF energy that reaches the shoreline. This is the result of a decrease in wave dissipation rates on both reef crest and reef flat. Additionally, IG wave generation reaches an optimum for median values of reef submergence. This is because the breakpoint forcing mechanism decreases in efficiency, while the resonant amplification increases in efficiency for larger water depths. These findings are in agreement with previous research (Pearson, 2016).
- Significant parameters related to reef geometry affecting reef hydrodynamics are: fore reef slope, reef width and beach slope.
 - The fore reef slope has a large impact on the generation of IG waves through the breakpoint forcing mechanism. Steep slopes give rise to larger IG waves on the reef flat.
 - Reef width affects the resonant modes of the fringing reef by changing the amount of frictional dissipation and the 1/4 and 3/4 wave length modes of the reef.
 - Beach slope has a significant impact on the distribution of HF and IG swash components, which directly affects runup.

7.3. Effects of excavation pits on wave runup

- The multi-parameter sensitivity study shows that the effect of excavation pits on the wave runup of fringing reefs during storm conditions ($H_{s,0} = 5$ m) differs for each reef. The general effect is that pits decrease runup (84 % of all modelled reefs) by an average of 5%. Therefore, no significant direct risks involved with reef excavating and inundation through overtopping are expected in most cases. However, there is a large spread in results, showing that that reefs can potentially experience an increase of up to 10 % and a decrease in runup of up to 20 %. Of all modelled reefs, 16% experienced an increase in runup. For these reefs, the average increase in runup was 3%, which shows that any potential negative impact is generally limited. From the modelled parameters, reef submergence is the most important factor influencing runup of fringing reefs. Fore reef slope, reef width and beach slope also determine the runup.
- Of all modelled reefs, the probabilities of an increase in runup are lowest for reefs with:
 - Gentle beach slopes;
 - Large reef flat submergence;
 - Either a very gentle or a very steep fore reef slope;
 - Narrow reef flats, though it is unsure whether this is due to the model setup or actual physical processes;
 - Narrow excavation pits;

- Excavation pits located close to the reef crest.
- Reef submergence is a large contributor to the relation between change in runup and other modelled parameters. For larger reef submergence, the probability of an increase in runup decreases. This suggests that sea level rise reduces any potential negative effect of pits on runup.
- In all simulations that computed an increase in runup due to the presence of the pit, there was significantly more wave energy at IG and HF peak frequencies than those reefs that experienced a decrease in runup. This contrasts with the variance at the HF tail, which showed a decrease for reefs with increasing runup. The latter can be a possible result of decreased wave-wave (triad) interaction. These effects suggest the change in runup is affected most by the HF peak, and to a lesser extent by the IG band.
- There is a long-shore variability in runup associated with an excavation pit on a long-shore uniform fringing reef. The effect of the excavation pit extends significantly beyond the longitudinal scale of the excavation, and is of approximately the same scale as the length of the excavation, parallel to the coast.



Recommendations

8.1. Modelling with Xbeach non-hydrostatic+

- As discussed in Chapter 3, the validation of the XBnh+ model has some shortcomings. With an improved dataset on near-shore hydrodynamics, the model could be calibrated and validated more accurately. It would be beneficial to have additional observations on swash, runup and velocity profiles at locations on the reef flat and in the pit.
- An improved validation study could lead to the identification and quantification of flaws in the XBnh+ model. Although in theory and based on model results it is an improvement compared to the original XBnh model, the extra computational layer the XBnh+ model is still a relatively new feature and possibly requires additional improvements and testing.

8.2. Reef excavation practices & designs

The practice of reef excavating has a significant impact on the coastal systems of coral (atoll) islands. Some of the hydrodynamic effects of these excavations have been identified in previous research (Ford et al., 2013; Yao et al., 2016), although impact on runup has remained unknown prior to this research. Based on the effect of reef excavating on wave runup of fringing reef coasts that were found in this present research, recommendations can be made on excavation practices. It must be noted that these recommendations must only be interpreted with respect to wave runup.

- The geometry and cross-shore location of the excavation have a significant effect on the probability of an increase/decrease in wave runup. Based on the XBnh+ model results, the design of a reef excavation should be sufficiently narrow (smaller than $0.2 \cdot W_{reef}$) and located near the reef crest (center of excavation pit at a distance of $0.7 \cdot W_{reef}$ of the beach), in order to reduce negative effects of an increase in runup. As these designs will result in the lowest probabilities of such an increase.

8.3. Future research

This research only covers one of several aspects that are assumed to experience a significant impact of reef excavating. As mentioned in previous research, there remains a knowledge gap on the ecological and morphological impact of reef excavating.

- The 1D modelling study used ranges of values for the different reef parameters that originate from the real world. However, the frequency of occurrence of each of these reefs has not been accounted for. As stated by Pearson et al. (2017), a database of fringing reefs of SIDS, that includes values of these parameters could improve the estimates made in this report on potential hazards related to runup. This could also facilitate the identification of islands that face increased risks related to reef excavating.
- Assessing the impact on morphology is the next step after establishing the impact on hydrodynamics. This requires observations on shoreline advances/retreats around excavation pits, data on when pits

were excavated, but also more datasets with detailed (near-shore) wave data. Observations of sediment generating species (e.g. Parrotfish) and their fluxes could also benefit such a study.

- Regarding ecological impact, the excavating itself could cause increased turbidity of the ocean water, thereby possibly resulting in a negative impact on the ecosystem. The excavation pits themselves can offer new accommodation space for growing coral, as conditions are able to improve due to permanent submergence and lower wave impact. However, excavation pits also form traps for debris and human pollution, which is abundant in the densely populated islands. This could cause contamination of the ocean water and subsoil, as well as degradation of the coral and the surrounding ecosystem. Excavation methods and environmental impact on water quality should therefore be studied. Possibly, a (vertical) two-dimensional (2DV) or three-dimensional (3D) model would be required to assess the impact of reef excavating on these processes.

Bibliography

- Atkinson, M. J. and Bilger, R. W. (1992). Effects of water velocity on phosphate uptake in coral reef-hat communities. *Limnology and Oceanography*, 37(2):273–279.
- Atkinson, M. J. and Falter, J. L. (2003). Biogeochemistry of marine systems. *Coral Reefs*. Blackwell, Oxford, pages 40–64.
- Baird, M. E. and Atkinson, M. J. (1997). Measurement and prediction of mass transfer to experimental coral reef communities. *Limnology and Oceanography*, 42(8):1685–1693.
- Baldock, T. E. (2012). Dissipation of incident forced long waves in the surf zone-Implications for the concept of "bound" wave release at short wave breaking. *Coastal Engineering*, 60(1):276–285.
- Baldock, T. E., Golshani, A., Callaghan, D. P., Saunders, M. I., and Mumby, P. J. (2014). Impact of sea-level rise and coral mortality on the wave dynamics and wave forces on barrier reefs. *Marine Pollution Bulletin*, 83(1):155–164.
- Baldock, T. E., Huntley, D. A., Bird, P. A. D., Bullock, G. N., and Hare, T. O. (2000). Breakpoint generated surf beat induced by bichromatic wave groups. *Coastal Engineering*.
- Banner, A. (1968). A Fresh-Water "Kill" on the Coral Reefs of Hawaii. *University of Hawaii, Institute of Marine Biology*.
- Battjes, J. A. (2004). Shoaling of subharmonic gravity waves. *Journal of Geophysical Research*, 109(C2):C02009.
- Becker, J. M., Merrifield, M. A., and Ford, M. (2014). Water level effects on breaking wave setup for Pacific Island fringing reefs. *Journal of Geophysical Research: Oceans*, 119(2):914–932.
- Becker, J. M., Merrifield, M. A., and Yoon, H. (2016). Infragravity waves on fringing reefs in the tropical Pacific: Dynamic setup. *Journal of Geophysical Research: Oceans*, 121(5):3010–3028.
- Beer, A. F. D. (2017). The influence of incident waves on runup. Msc thesis.
- Beetham, E., Kench, P. S., O'Callaghan, J., and Popinet, S. (2016). Wave transformation and shoreline water level on Funafuti Atoll, Tuvalu. *Journal of Geophysical Research: Oceans*, 121(1):311–326.
- Berkhoff, J. C., Booy, N., and Radder, A. C. (1982). Verification of Numerical Wave Propagation Models for Simple Harmonic Linear Water Waves. *Coastal Engineering*, 6:255–279.
- Blacka, M. J., Flocard, E., Splinter, K. D., and Cox, R. J. (2015). Estimating Wave Heights and Water Levels inside Fringing Reefs during Extreme Conditions. *Coast and Ports 2015*, (September):1–7.
- Boers, M. (2005). Surf zone turbulence. PhD thesis TU Delft.
- Bosserelle, C., Kruger, J., Movono, M., and Reddy, S. (2015). Wave inundation on the Coral Coast of Fiji.
- Brander, R. W., Kench, P. S., and Hart, D. (2004). Spatial and temporal variations in wave characteristics across a reef platform, Warraber Island, Torres Strait, Australia. *Marine Geology*, 207(1-4):169–184.
- Brown, B. E. and Dunne, R. P. (1988). The Environmental Impact of Coral Mining on Coral Reefs in the Maldives. *Environmental Conservation*, 15(02):159.
- Cheriton, O. M., Storlazzi, C. D., and Rosenberger, K. J. (2016). Observations of wave transformation over a fringing coral reef and the importance of low-frequency waves and offshore water levels to runup, overwash, and coastal flooding. *Journal of Geophysical Research: Oceans*, 121(5):3121–3140.
- Church, J. A., White, N. J., and Hunter, J. R. (2006). Sea-level rise at tropical Pacific and Indian Ocean islands. *Global and Planetary Change*, 53(3):155–168.

- Daly, C., Roelvink, D., van Dongeren, A., van Thiel de Vries, J., and McCall, R. (2012). Validation of an advective-deterministic approach to short wave breaking in a surf-beat model. *Coastal Engineering*, 60(1):69–83.
- Darwin, C. (1842). The Structure and Distribution of Coral Reefs, Being the first part of the geology of the voyage of the Beagle, under the command of Capt. Fitzroy, R.N. during the years 1832 to 1836.
- Dollar, S. J. (1982). Wave stress and coral community structure in Hawaii. *Coral Reefs*, 1(2):71–81.
- Dollar, S. J. and Tribble, G. W. (1993). Recurrent storm disturbance and recovery: a long-term study of coral communities in Hawaii. *Coral Reefs*, 12(3-4):223–233.
- Dulby, N. K., Stanwell-smith, D., Darwall, W. R., and Horrill, C. J. (2016). Coral Mining at Mafia Island, Tanzania: A Management Dilemma. 29(3):167–173.
- Falter, J. L., Atkinson, M. J., and Merrifield, M. A. (2004). Mass-transfer limitation of nutrient uptake by a wave-dominated reef flat community. *Limnology and Oceanography*, 49(5):1820–1831.
- Ferrario, F., Beck, M. W., Storlazzi, C. D., Micheli, F., Shepard, C. C., and Airoidi, L. (2014). The effectiveness of coral reefs for coastal hazard risk reduction and adaptation. *Nature Communications*, 5(May):1–9.
- Filipot, J. F. and Cheung, K. F. (2012). Spectral wave modeling in fringing reef environments. *Coastal Engineering*, 67:67–79.
- Foda, M. A. and Mei, C. C. (1981). Nonlinear excitation of long-trapped waves by a group of short swells. *Journal of Fluid Mechanics*, 111:319–345.
- Ford, M. R., Becker, J. M., and Merrifield, M. a. (2013). Reef Flat Wave Processes and Excavation Pits: Observations and Implications for Majuro Atoll, Marshall Islands. *Journal of Coastal Research*, 288(3):545–554.
- Gawehn, M., van Dongeren, A., van Rooijen, A., Storlazzi, C., Cheriton, O., and Reniers, A. (2016). Identification and classification of very low frequency waves on a coral reef flat. (November).
- Gerritsen, F. (1980). Wave attenuation and wave set-up on a coastal reef. *Coastal Engineering Proceedings*, 17:444–461.
- Gourlay, M. R. (1996a). Wave set-up on coral reefs. 1. Set-up and wave-generated flow on an idealised two dimensional horizontal reef. *Coastal Engineering*, 27(3-4):161–193.
- Gourlay, M. R. (1996b). Wave set-up on coral reefs. 2. Set-up on reefs with various profiles. *Coastal Engineering*, 28(1-4):17–55.
- Grady, A. E., Moore, L. J., Storlazzi, C. D., Elias, E., and Reidenbach, M. A. (2013). The influence of sea level rise and changes in fringing reef morphology on gradients in alongshore sediment transport. *Geophysical Research Letters*, 40(12):3096–3101.
- Grigg, R. W. (1998). Holocene coral reef accretion in Hawaii: a function of wave exposure and sea level history. *Coral Reefs*, 17(3):263–272.
- Grinsted, A., Moore, J. C., and Jevrejeva, S. (2010). Reconstructing sea level from paleo and projected temperatures 200 to 2100 AD. *Climate Dynamics*, 34(4):461–472.
- Gunasekara, K. H., Tajima, Y., and Shimoazono, T. (2014). Variation of Impact along the East Coast of Eastern Samar Due to Typhoon Haiyan in the Philippines. *Journal of Japan Society of Civil Engineers*, 70(2):I_241–I_245.
- Guza, R., Thornton, E., and Holman, R. (1984). Swash on steep and shallow beaches. *Coastal Engineering Proceedings*, 1(19):708–723.
- Guza, R. T. and Feddersen, F. (2012). Effect of wave frequency and directional spread on shoreline runup. *Geophysical Research Letters*, 39(11):1–5.
- Hardy, T. A. and Young, I. R. (1996). Field study of wave attenuation on an offshore coral reef. *Journal of geophysical research*, 101(C6):14311–14326.

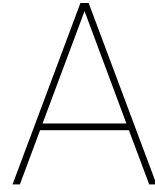
- Herbers, T. H. C., Elgar, S., Guza, R. T., Herbers, T. H. C., Elgar, S., and Guza, R. T. (1994). Infragravity-Frequency (0.005–0.05 Hz) Motions on the Shelf. Part I: Forced Waves.
- Herbers, T. H. C., Elgar, S., Guza, R. T., Herbers, T. H. C., Elgar, S., Guza, R. T., and O'Reilly, W. (1995). Infragravity-Frequency (0.005–0.05 Hz) Motions on the Shelf. Part II: Free Waves.
- Hoegh-Guldberg, O., Mumby, P. J., Hooten, A. J., Steneck, R. S., Greenfield, P., Gomez, E., Harvell, C. D., Sale, P. F., Edwards, A. J., Caldeira, K., Knowlton, N., Eakin, C. M., Iglesias-Prieto, R., Muthiga, N., Bradbury, R. H., Dubi, A., and Hatziolos, M. E. (2007). Coral Reefs Under Rapid Climate Change and Ocean Acidification. *Science*, 318(5857):1737–1742.
- Hoeke, R. K., McInnes, K. L., Kruger, J. C., McNaught, R. J., Hunter, J. R., and Smithers, S. G. (2013). Widespread inundation of Pacific islands triggered by distant-source wind-waves. *Global and Planetary Change*, 108:1–11.
- Holthuijsen, L. H., Booij, N., and Herbers, T. H. C. (1989). A prediction model for stationary, short-crested waves in shallow water with ambient currents. *Coastal Engineering*, 13(1):23–54.
- Hopley, D. (2011). Encyclopedia of modern coral reefs; structure, forms and process. *Springer-Verlag*, page 1205pp.
- Huntley, D. A., Guza, R. T., and Thornton, E. B. (1981). Field observations of surf beat: 1. Progressive edge waves. *Journal of Geophysical Research: Oceans*, 86(C7):6451–6466.
- Jaramillo, S. and Pawlak, G. (2011). AUV-based bed roughness mapping over a tropical reef. *Coral Reefs*, 30(1):11–23.
- Kench, P. S., Brander, R. W., Parnell, K. E., and O'Callaghan, J. M. (2009). Seasonal variations in wave characteristics around a coral reef island, South Maalhosmadulu atoll, Maldives. *Marine Geology*, 262(1-4):116–129.
- Kennedy, A. B., Mori, N., Zhang, Y., Yasuda, T., Chen, S.-E., Tajima, Y., Pecor, W., and Toride, K. (2016). Observations and modeling of coastal boulder transport and loading during super typhoon haiyan. *Coastal Engineering Journal*, 58(01):1640004.
- Kolijn, D. J. (2014). Effectiveness of a multipurpose artificial underwater structure as a coral reef canopy. Msc thesis.
- Kraines, S. B., Isobe, M., and Komiyama, H. (2001). Seasonal variations in the exchange of water and water-borne particles at Majuro Atoll, the Republic of the Marshall Islands. *Coral Reefs*, 20(4):330–340.
- Kunkel, C. M., Hallberg, R. W., and Oppenheimer, M. (2006). Coral reefs reduce tsunami impact in model simulations. *Geophysical Research Letters*, 33(23):n/a—n/a.
- List, J. H. (1992). A model for the generation of two-dimensional surf beat. *Journal of Geophysical Research: Oceans*, 97(C4):5623–5635.
- Longuet-Higgins, M. and Stewart, R. (1964). Radiation stresses in water waves; a physical discussion, with applications. *Deep Sea Research and Oceanographic Abstracts*, 11(4):529–562.
- Longuet-Higgins, M. S. and Stewart, R. W. (1962). Radiation stress and mass transport in gravity waves, with application to 'surf beats'. *Journal of Fluid Mechanics*, 13(4):481–504.
- Lowe, R. J. and Falter, J. L. (2015). Oceanic Forcing of Coral Reefs. *Annual Review of Marine Science*, 7(1):43–66.
- Lowe, R. J., Falter, J. L., Bandet, M. D., Pawlak, G., Atkinson, M. J., Monismith, S. G., and Koseff, J. R. (2005). Spectral wave dissipation over a barrier reef. *Journal of Geophysical Research C: Oceans*, 110(4):1–16.
- Lowe, R. J., Hart, C., and Pattiaratchi, C. B. (2010). Morphological constraints to wave-driven circulation in coastal reef-lagoon systems: A numerical study. *Journal of Geophysical Research: Oceans*, 115(C9):n/a—n/a.
- Lowe, R. J., Leon, A. S., Symonds, G., Falter, J. L., and Gruber, R. (2015). The intertidal hydraulics of tide-dominated reef platforms. *Journal of Geophysical Research C: Oceans*, 120(7):4845–4868.

- Lugo-Fernández, A., Roberts, H. H., Wiseman Jr., W. J., and Carter, B. L. (1998). Water level and currents of tidal and infragravity periods at Tague Reef, St. Croix (USVI). *Coral Reefs*, 17(4):343–349.
- MacCormack, R. (1969). The effect of viscosity in hypervelocity impact cratering. *4th Aerodynamic Testing Conference*.
- Massel, S. R. and Gourlay, M. R. (2000). On the modelling of wave breaking and set-up on coral reefs. *Coastal Engineering*, 39(1):1–27.
- Masselink, G. (1995). Group bound long waves as a source of infragravity energy in the surf zone. *Continental Shelf Research*, 15(13):1525–1547.
- Merrifield, M. A., Becker, J. M., Ford, M., and Yao, Y. (2014). Observations and estimates of wave-driven water level extremes at the Marshall Islands. *Geophysical Research Letters*, 41(20):7245–7253.
- Monismith, S. G., Rogers, J. S., Kowalik, D., and Dunbar, R. B. (2015). Frictional wave dissipation on a remarkably rough reef. *Geophysical Research Letters*, 42(10):4063–4071.
- Montaggioni, L. F. (2005). History of Indo-Pacific coral reef systems since the last glaciation: Development patterns and controlling factors. *Earth-Science Reviews*, 71(1-2):1–75.
- Munk, W. H., Miller, G. R., Snodgrass, F. E., and Barber, N. F. (1963). Directional Recording of Swell from Distant Storms. *Philosophical Transactions of the Royal Society A: Mathematical, Physical and Engineering Sciences*, 255(1062):505–584.
- Munk, W. H. and Sargent, M. C. (1948). Adjustment of Bikini Atoll to ocean waves. *Eos, Transactions American Geophysical Union*, 29(6):855–860.
- Nairn, R., Roelvink, J. A., and Southgate, H. (1990). Transition zone width and implications for modeling surfzone hydrodynamics. *Proceedings 22th International Conference on Coastal Engineering*, pages 68–81.
- Nakaza, E. and Hino, M. (1991). Bore-like surf beat in a reef zone caused by wave groups of incident short period waves. *Fluid Dynamics Research*, 7(2):89.
- Narayan, S., Beck, M. W., Reguero, B. G., Losada, I. J., Van Wesenbeeck, B., Pontee, N., Sanchirico, J. N., Ingram, J. C., Lange, G. M., and Burks-Copes, K. A. (2016). The effectiveness, costs and coastal protection benefits of natural and nature-based defences. *PLoS ONE*, 11(5):1–17.
- Nelson, R. (1997). Height limits in top down and bottom up wave environments. *Coastal engineering*, 32(2-3):247–254.
- Nelson, R. C. (1996). Hydraulic roughness of coral reef platforms. *Applied Ocean Research*, 18(5):265–274.
- Nwogu, O. and Demirbilek, Z. (2010). Infragravity Wave Motions and Runup over Shallow Fringing Reefs. *Journal of Waterway, Port, Coastal, and Ocean Engineering*, 136(December):295–305.
- Pandolfi, J. M., Connolly, S. R., Marshall, D. J., and Cohen, A. L. (2011). Projecting Coral Reef Futures Under Global Warming and Ocean Acidification. *Science*, 333(6041):418–422.
- Pearson, S., Storlazzi, C., van Dongeren, A., Tissier, M., and Reniers, A. (2017). A Bayesian-Based System to Assess Wave-Driven Flooding Hazards on Coral Reef-Lined Coasts. *Journal of Geophysical Research*, pages 1–20.
- Pearson, S. G. (2016). Predicting Wave-Induced Flooding on Low-Lying Tropical Islands. MSc thesis.
- Péquignet, A. C., Becker, J. M., Merrifield, M. A., and Boc, S. J. (2011). The dissipation of wind wave energy across a fringing reef at Ipan, Guam. *Coral Reefs*, 30(SUPPL. 1):71–82.
- Péquignet, A. C. N., Becker, J. M., and Merrifield, M. A. (2014). Energy transfer between wind waves and low-frequency oscillations on a fringing reef, Ipan, Guam. *Journal of Geophysical Research C: Oceans*, 119(10):6709–6724.
- Péquignet, A. C. N., Becker, J. M., Merrifield, M. A., and Aucan, J. (2009). Forcing of resonant modes on a fringing reef during tropical storm Man-Yi. *Geophysical Research Letters*, 36(3):20–23.

- Pistrika, A. K. and Jonkman, S. N. (2010). Damage to residential buildings due to flooding of New Orleans after hurricane Katrina. *Natural Hazards*, 54(2):413–434.
- Pomeroy, A. (2011). Low Frequency Wave Resonance on Fringing Reefs. (June):152.
- Pomeroy, A., Lowe, R., Symonds, G., van Dongeren, A., and Moore, C. (2012a). The dynamics of infragravity wave transformation over a fringing reef. *Journal of Geophysical Research: Oceans*, 117(11):1–17.
- Pomeroy, A., van Dongeren, A. R., Lowe, R. J., van Thiel de Vries, J. S. M., and Roelvink, D. J. A. (2012b). Low-frequency wave resonance in fringing reef environments. *Coastal Engineering 2012*, pages 1–10.
- Pomeroy, A. W. M., Lowe, R. J., Van Dongeren, A. R., Ghisalberti, M., Bodde, W., and Roelvink, D. (2015). Spectral wave-driven sediment transport across a fringing reef. *Coastal Engineering*, 98:78–94.
- Quataert, E. (2015). Wave runup on atoll reefs. MSc thesis.
- Quataert, E., Storlazzi, C., Van Rooijen, A., Cheriton, O., and Van Dongeren, A. (2015). The influence of coral reefs and climate change on wave-driven flooding of tropical coastlines. *Geophysical Research Letters*, 42(15):6407–6415.
- Rawat, A., Arduin, F., Ballu, V., Crawford, W., Corela, C., and Aucan, J. (2014). Infragravity waves across the oceans. *Geophysical Research Letters*, 41(22):7957–7963.
- Roberts, C. M. (1997). Connectivity and Management of Caribbean Coral Reefs. *Science*, 278(5342):1454–1457.
- Roeber, V. and Bricker, J. D. (2015). Destructive tsunami-like wave generated by surf beat over a coral reef during Typhoon Haiyan. *Nature Communications*, 6:7854.
- Roelvink, J., McCall, R., Mehvar, S., Nederhoff, C., and Dastgheib, A. (2017). Improving predictions of swash dynamics in XBeach: The role of groupiness and incident-band runup. *Coastal Engineering*, (July):1–21.
- Roelvink, J., Reniers, A., van Dongeren, A., van Thiel de Vries, J., McCall, R., and Lescinski, J. (2009). Modelling storm impacts on beaches, dunes and barrier islands. *Coastal Engineering*, 56(11-12):1133–1152.
- Roelvink, J., van Dongeren, A., McCall, R., Hoonhout, B., van Rooijen, A., van Geer, P., de Vet, L., Nederhoff, C., and Quataert, E. (2015). XBeach Technical Reference : Kingsday Release. pages 1–141.
- Roelvink, J. A. (1993). Dissipation in random wave groups incident on a beach. *Coastal Engineering*, 19(1-2):127–150.
- Rogers, J. S., Monismith, S. G., Dunbar, R. B., and Kowalik, D. (2013). Hydrodynamics of spur and groove formations on a coral reef. *Journal of Geophysical Research: Oceans*, 120(1):145–160.
- Rogers, J. S., Monismith, S. G., Kowalik, D. A., and Dunbar, R. B. (2015). Wave dynamics of a Pacific Atoll with high frictional effects. *Journal of Geophysical Research: Oceans*, 119(1):2813–2825.
- Sanderson, P. G. (2000). A comparison of reef-protected environments in Western Australia: the central west and Ningaloo coasts. *Earth Surface Processes and Landforms*, 25:397–419.
- Seelig, W. N. (1983). Laboratory study of reef-lagoon system hydraulics. 109(4):380–391.
- Sheppard, C., Dixon, D. J., Gourlay, M., Sheppard, A., and Payet, R. (2005). Coral mortality increases wave energy reaching shores protected by reef flats: Examples from the Seychelles. *Estuarine, Coastal and Shelf Science*, 64(2-3):223–234.
- Sheremet, A., Kaihatu, J. M., Su, S. F., Smith, E. R., and Smith, J. M. (2011). Modeling of nonlinear wave propagation over fringing reefs. *Coastal Engineering*, 58(12):1125–1137.
- Shimozono, T., Tajima, Y., Kennedy, A. B., Nobuoka, H., Sasaki, J., and Sato, S. (2015). Combined infragravity wave and sea-swell runup over fringing reefs by super typhoon Haiyan. *Journal of Geophysical Research: Oceans*, (490):2121–2128.
- Smit, P. B., Stelling, G., Roelvink, J. A., van Thiel de Vries, J. S. M., McCall, R., van Dongeren, A., and Zwinkels, J. R. (2014). XBeach: Non-hydrostatic model. Validation, verification and model description.

- Smithers, S. G. and Hoeke, R. K. (2014). Geomorphological impacts of high-latitude storm waves on low-latitude reef islands - Observations of the December 2008 event on Nukutoa, Takuu, Papua New Guinea. *Geomorphology*, 222:106–121.
- Stelling, G. and Zijlema, M. (2003). An accurate and efficient finite-difference algorithm for non-hydrostatic free-surface flow with application to wave propagation. *International Journal for Numerical Methods in Fluids*, 43(1):1–23.
- Stive, M. J. F. and de Vriend, H. J. (1994). Shear Stresses and Mean Flow in Shoaling and Breaking Waves. *Coastal Engineering 1994*.
- Stockdon, H. F., Holman, R. A., Howd, P. A., and Sallenger, A. H. (2006). Empirical parameterization of setup, swash, and runup. *Coastal Engineering*, 53(7):573–588.
- Storlazzi, C. D., Elias, E., Field, M. E., and Presto, M. K. (2011). Numerical modeling of the impact of sea-level rise on fringing coral reef hydrodynamics and sediment transport. *Coral Reefs*, 30(1):83–96.
- Storlazzi, C. D., Ogston, A. S., Bothner, M. H., Field, M. E., and Presto, M. K. (2004). Wave- and tidally-driven flow and sediment flux across a fringing coral reef: Southern Molokai, Hawaii. *Continental Shelf Research*, 24(12):1397–1419.
- Suhayda, J. N. (1974). Standing waves on beaches. *Journal of Geophysical Research*, 79(21):3065–3071.
- Svendsen, I. A. (1984). Wave heights and set-up in a surf zone. *Coastal Engineering*, 8(4):303–329.
- Symonds, G., Huntley, D. A., and Bowen, A. J. (1982). Two-dimensional surf beat: Long wave generation by a time-varying breakpoint. *Journal of Geophysical Research: Oceans*, 87(C1):492–498.
- Terry, J. P. and Chui, T. F. M. (2012). Evaluating the fate of freshwater lenses on atoll islands after eustatic sea-level rise and cyclone-driven inundation: A modelling approach. *Global and Planetary Change*, 88–89:76–84.
- Thomas, F. I. M. and Atkinson, M. J. (1997). Ammonium uptake by coral reefs: Effects of water velocity and surface roughness on mass transfer. *Limnology and Oceanography*, 42(1):81–88.
- UN-Habitat (2015). Urbanization and Climate Change in Small Island Developing States. page 52.
- Van Dongeren, A., Lowe, R., Pomeroy, A., Trang, D. M., Roelvink, D., Symonds, G., and Ranasinghe, R. (2012). Numerical modeling of low-frequency wave dynamics over a fringing coral reef. *Coastal Engineering*, 73:178–190.
- Van Dongeren, A., Reniers, A., and Battjes, J. (2003). Numerical modeling of infragravity wave response during DELILAH. *Journal of Geophysical Research*, 108(C9):3288.
- Vermeer, M. and Rahmstorf, S. (2009). Global sea level linked to global temperature. *Proceedings of the National Academy of Sciences of the United States of America*, 106(51):21527–21532.
- Vetter, O., Becker, J. M., Merrifield, M. A., Pequignet, A. C., Aucan, J., Boc, S. J., and Pollock, C. E. (2010). Wave setup over a Pacific Island fringing reef. *Journal of Geophysical Research: Oceans*, 115(12):1–13.
- Wunsch, C. and Gill, A. E. (1976). Observations of equatorially trapped waves in Pacific sea level variations. *Deep-Sea Research and Oceanographic Abstracts*, 23(5):371–390.
- Wyatt, A. S. J., Lowe, R. J., Humphries, S., and Waite, A. M. (2010). Particulate nutrient fluxes over a fringing coral reef: Relevant scales of phytoplankton Production and mechanisms of supply. *Marine Ecology Progress Series*, 405(Hatcher 1997):113–130.
- Xue, C. (2001). Coastal Erosion and Management of Majuro Atoll, Marshall Islands. *Journal of Coastal Research*, 17(4):909–918.
- Yahel, G., Post, A. F., Fabricius, K., Marie, D., Vaulot, D., and Genin, A. (1998). Phytoplankton distribution and grazing near coral reefs. *Limnology and Oceanography*, 43(4):551–563.

- Yao, Y., Becker, J. M., Ford, M. R., and Merrifield, M. A. (2016). Modeling wave processes over fringing reefs with an excavation pit. *Coastal Engineering*, 109:9–19.
- Yao, Y., Huang, Z., Monismith, S. G., and Lo, E. Y. M. (2012). 1DH Boussinesq modeling of wave transformation over fringing reefs. *Ocean Engineering*, 47:30–42.
- Young, I. and Van Vledder, G. P. (1993). A review of the central role of nonlinear interactions in wind-wave evolution. *Philosophical Transactions of the Royal Society of London A: Mathematical, Physical and Engineering Sciences*, 342(1666):505–524.
- Young, I. R. (1989). Wave transformation over coral reefs. *Journal of Geophysical Research: Oceans*, 94(C7):9779–9789.
- Zhang, Z., Lowe, R., Falter, J., and Ivey, G. (2011). A numerical model of wave- and current-driven nutrient uptake by coral reef communities. *Ecological Modelling*, 222(8):1456–1470.
- Zijlema, M., Stelling, G., and Smit, P. (2011). SWASH: An operational public domain code for simulating wave fields and rapidly varied flows in coastal waters. *Coastal Engineering*, 58(10):992–1012.



Validation

A.1. Comparison of XBeach modules

A.1.1. Introduction & background

The following is obtained from Roelvink et al. (2017, 2009); Smit et al. (2014).

XBeach is an open-source numerical model which originally was developed to simulate hydrodynamic and morphodynamic processes and impacts on sandy coasts with a domain size of kilometers and on the time scale of storms. Since then, the model has been applied to other types of coasts and purposes.

The model includes the hydrodynamic processes of short wave transformation (refraction, shoaling and breaking), long wave (infragravity wave) transformation (generation, propagation and dissipation), wave-induced setup and unsteady currents, as well as overwash and inundation. The morphodynamic processes include bed load and suspended sediment transport, dune face avalanching, bed update and breaching. Effects of vegetation and of hard structures have been included. The model has been validated with a series of analytical, laboratory and field test cases using a standard set of parameter settings.

XBeach has two modes: a hydrostatic and a non-hydrostatic mode. In the hydrostatic mode, the short wave amplitude variation is solved separately from the long waves, currents and morphological change. This saves considerable computational time, with the expense that the phase of the short waves is not simulated. A more complete model is the non-hydrostatic model which solves all processes including short wave motions, but with more computational demand.

The original application (surfbeat mode), funded by the U.S. Corps of Engineers in the framework of the Morphos project and the U.S. Geological Survey, was to be able to assess hurricane impacts on sandy beaches. Since then with funding from the Rijkswaterstaat, part of The Netherlands Ministry of Infrastructure and the Environment, the model has been extended, applied and validated for storm impacts on dune and urbanized coasts for the purpose of dune safety assessments. With support from the European Commission XBeach has been validated on a number of dissipative and reflective beaches bordering all regional seas in the EU.

Beyond sandy coasts, the model has been applied to coral fringing and atoll reefs, in cooperation with and with funding by the University of Western Australia, the USGS and the Asian Development Bank. The model now also includes vegetative damping effects, with support of the U.S. Office of Naval Research.

The non-hydrostatic model has been developed initially by the TU Delft (as a prototype version of the SWASH model (Zijlema et al., 2011)). For the purpose of simulating the morphodynamic processes on gravel beaches, the model was extended and validated with support from the University of Plymouth. In this mode, ship-induced waves can be simulated as well, demonstrating the flight that the model has taken since its first inception.

Surfbeat mode (instationary)

The short-wave motion is solved using the wave action equation which is a time-dependent forcing of the HISWA equations (Holthuijsen et al., 1989). These equations solve the variation of short-waves envelope (wave height) on the scale of wave groups. It employs a dissipation model for use with wave groups (Daly et al., 2012; Roelvink, 1993) and a roller model (Nairn et al., 1990; Stive and de Vriend, 1994; Svendsen, 1984) to represent momentum stored at the surface after breaking. These variations, through radiation stress gradients (Longuet-Higgins and Stewart, 1964, 1962) exert a force on the water column and drive longer period waves (infragravity waves) and unsteady currents, which are solved by the nonlinear shallow water equations. Thus, wave-driven currents (longshore current, rip currents and undertow), and wind-driven currents (stationary and uniform) for local wind set-up, long (infragravity) waves, and runup and rundown of long waves (swash) are included.

Using the surfbeat mode it is necessary when the focus is on swash zone processes rather than time-averaged currents and setup. This assumption is valid on dissipative beaches, where the short waves are mostly dissipated by depth-induced wave breaking. On intermediate beaches and during extreme events the swash motions are still predominantly in the infragravity band and so is the wave runup.

Non-hydrostatic mode (wave resolving)

For non-hydrostatic XBeach calculations. depth-averaged flow due to waves and currents are computed using the non-linear shallow water equations, including a non-hydrostatic pressure. The depth-averaged dynamic pressure (q) is derived in a method similar to a onelayer version of the SWASH model (Zijlema et al., 2011). The depth averaged dynamic pressure is computed from the mean of the dynamic pressure at the surface and at the bed by assuming the dynamic pressure at the surface to be zero and a linear change over depth. Under these formulations dispersive behavior is added to the long wave equations and the model can be used as a short-wave resolving model. Wave breaking is implemented by disabling the non-hydrostatic pressure term when waves exceed a certain steepness, after which the bore-like breaking implicit in the momentum-conserving shallow water equations takes over.

In case the non-hydrostatic mode is used, the short wave action balance is no longer required. However, in the wave-resolving mode we need much higher spatial resolution and associated smaller time steps, making this mode much more computationally expensive than the surfbeat mode.

The main advantages of the non-hydrostatic mode are that the incident-band (short wave) runup and overwashing are included, which is especially important on steep slopes such as gravel beaches. Another advantage is that the wave asymmetry and skewness are resolved by the model and no approximate local model or empirical formulation is required for these terms. Finally, in cases where diffraction is a dominant process, wave-resolving modeling is needed as it is neglected in the short wave averaged mode.

The non-hydrostatic module is based upon Stelling and Zijlema (2003). Vertically a compact scheme is used which allows a very natural inclusion of the boundary condition of the dynamic pressure at the free surface. In this way dispersive waves can be modelled using a depth average flow model with similar accuracy to that of lower order Boussinesq models.

The application of momentum conservative numerical schemes allows the accurate modelling of wave breaking without the need of a separate breaking model. Second order accuracy in space and time has been achieved by the implementation of a flux limited variant of the scheme by MacCormack (1969).

Verification of linear dispersion and the balance between non-linearity and dispersion was done by comparison to analytical solutions for an oscillating basin and a solitary wave. Momentum conservation and the capability to capture shock waves were verified using the analytical solution for the dam break problem.

The model was validated using experimental results by Berkhoff et al. (1982) and Boers (2005). The elliptic shoal from the Berkhoff experiment was used to validate refraction and diffraction for monochromatic waves. The Boers case 1C was used to validate the propagation and breaking of irregular waves.

Results show that the model performs well when waves remain in relatively shallow water. This is as expected as the numerical dispersion relation for a depth averaged model only approximates the linear dispersion relation for relatively shallow water. The Boers experiment furthermore showed that initiation of the breaking process is well captured but the dissipation rate of wave energy is underestimated. This is probably due to an inaccurate balance between non-linearity and dispersion.

An improvement of the non-hydrostatic module, is the non-hydrostatic+ module, which includes an extra (hydrostatic) computational layer in the vertical. This results in better solutions of the advection-diffusion equation, leading to increased model skill for steep bathymetry, e.g. fore reef slopes and/or excavation pits.

A.1.2. Output analysis

In this subsection a comparison is made between the three tested XBeach modules: XBeach Surfbeat (XBSB), XBeach non-hydrostatic (XBnh) and XBeach non-hydrostatic+ (XBnh+). Through this analysis, the outputs of the models are compared visually. Three 1D models were setup, with identical boundary conditions, bathymetry and bottom roughness.

Figures A.2, A.3 & A.4 show the transformations of wave heights (total, IG and HF), as well as the mean water level over an arbitrary schematized reef, for the incoming wave signal (Figure A.3), outgoing wave signal (Figure A.4) and total wave signal (Figure A.2). XBnh+ is characterized by the least amount of numerical oscillations, or "wiggles", at the pit walls. Additionally, XBnh computes unrealistically high HF wave heights over the pit, compared to the improved XBnh+ model. The XBSB mode is not capable of capturing all frequencies that contribute to runup levels, because it does not resolve all frequencies at the boundary. The non-hydrostatic modes produce very similar results when compared.

Figure A.1 compares the instantaneous surface elevation of the three modules. The XBnh+ mode visibly has the least numerical interference at the steep bathymetric gradients of the pit walls.

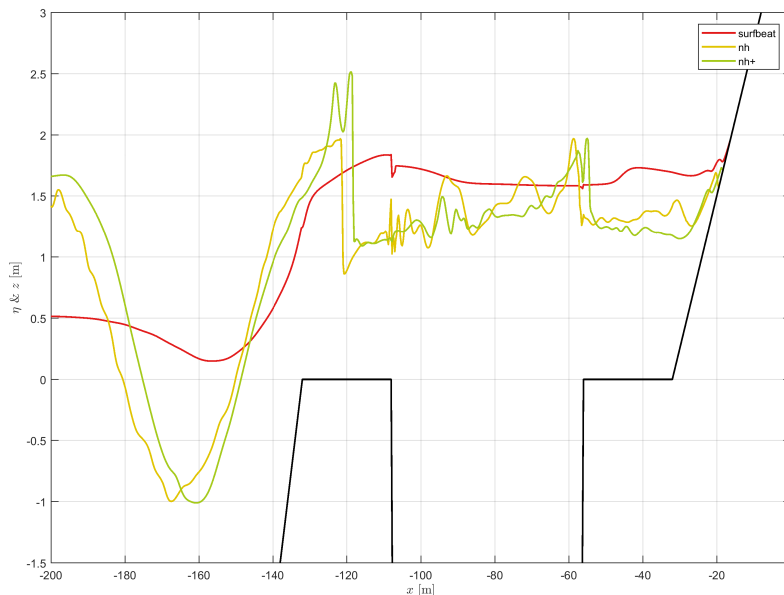


Figure A.1: Comparison of the instantaneous water level, for XBSB (red), XBnh (yellow) & XBnh+ (red).

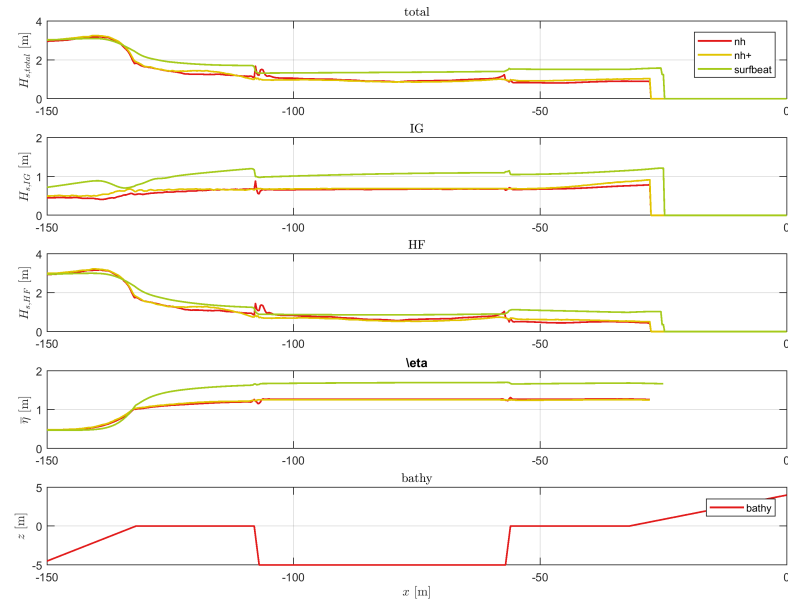


Figure A.2: Comparison of cross-shore wave transformations of the full wave signal and mean water level, for XBSB (green), XBNh (red) & XBNh+ (yellow).

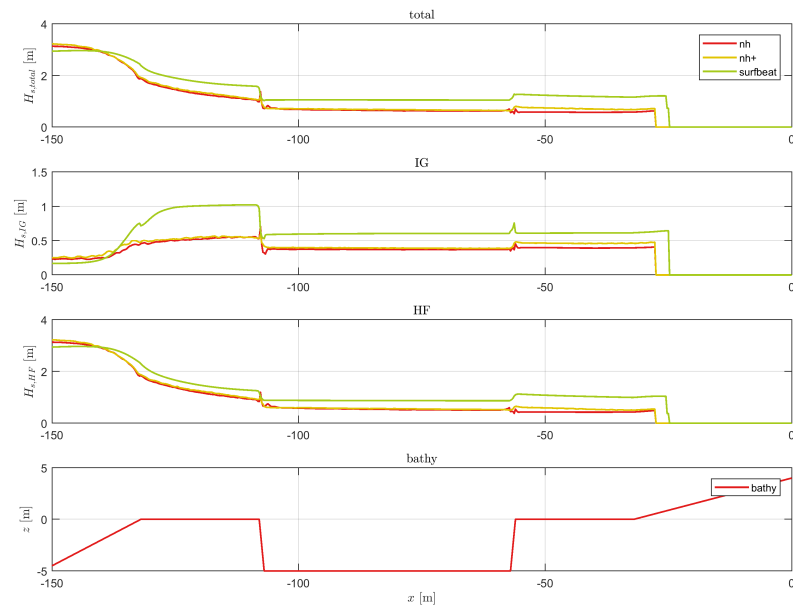


Figure A.3: Comparison of cross-shore wave transformations of the incoming wave signal for XBSB (green), XBNh (red) & XBNh+ (yellow).

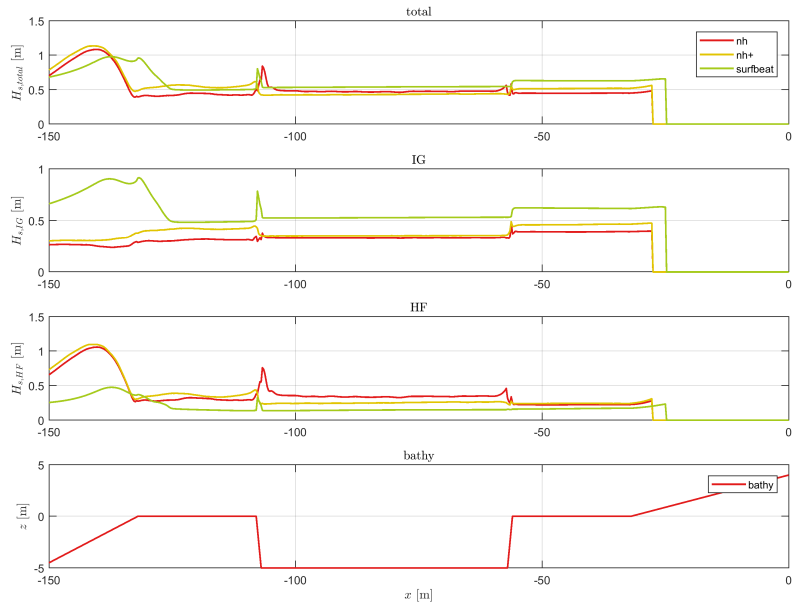


Figure A.4: Comparison of cross-shore wave transformations of the outgoing wave signal for XBSB (green), XBNh (red) & XBNh+ (yellow).

A.2. Grid discretisation

An optimal grid size has been chosen based on the following grid discretisation analysis. Figure A.5 shows the normalized change in wave heights, mean water levels and runoff, for grid sizes larger than $dx = 0.1$ m. It is assumed that a grid size of $dx = 0.1$ m is sufficiently small and requires no further optimization. This is true for the majority of the grid cells, e.g. the beach-toe, represented in the figure by the blue dots. Errors due to discretisation at the beach-toe become significantly small ($\approx O(1\%)$) or near negligible for grid sizes smaller than $dx < 0.3$ m. Figure A.6 (left) also confirms this, as the timeseries of the surface elevations at the beach-toe show negligible change for grid sizes smaller than $dx < 0.3$ m. Figure A.6 (right) shows that there is a minor underestimation of HF wave energy for larger grid sizes, but this effects diminishes for sufficiently smaller grid sizes, e.g. $dx < 0.3$ m.

At the pit walls, "wiggles" are found in the results, which is in part caused by numerical HF oscillations due to steep changes in bathymetry and by output frequency (see Appendix A.1). The effect of pit wall slopes on these numerical oscillations was studied as well, and this effect seemed to decrease for gentler pit walls. However, it was observed that these oscillations dampen out over the reef and have no significant impact on the modelled reef hydrodynamics (see Figure A.7). Steep slopes were therefore used in all model runs.

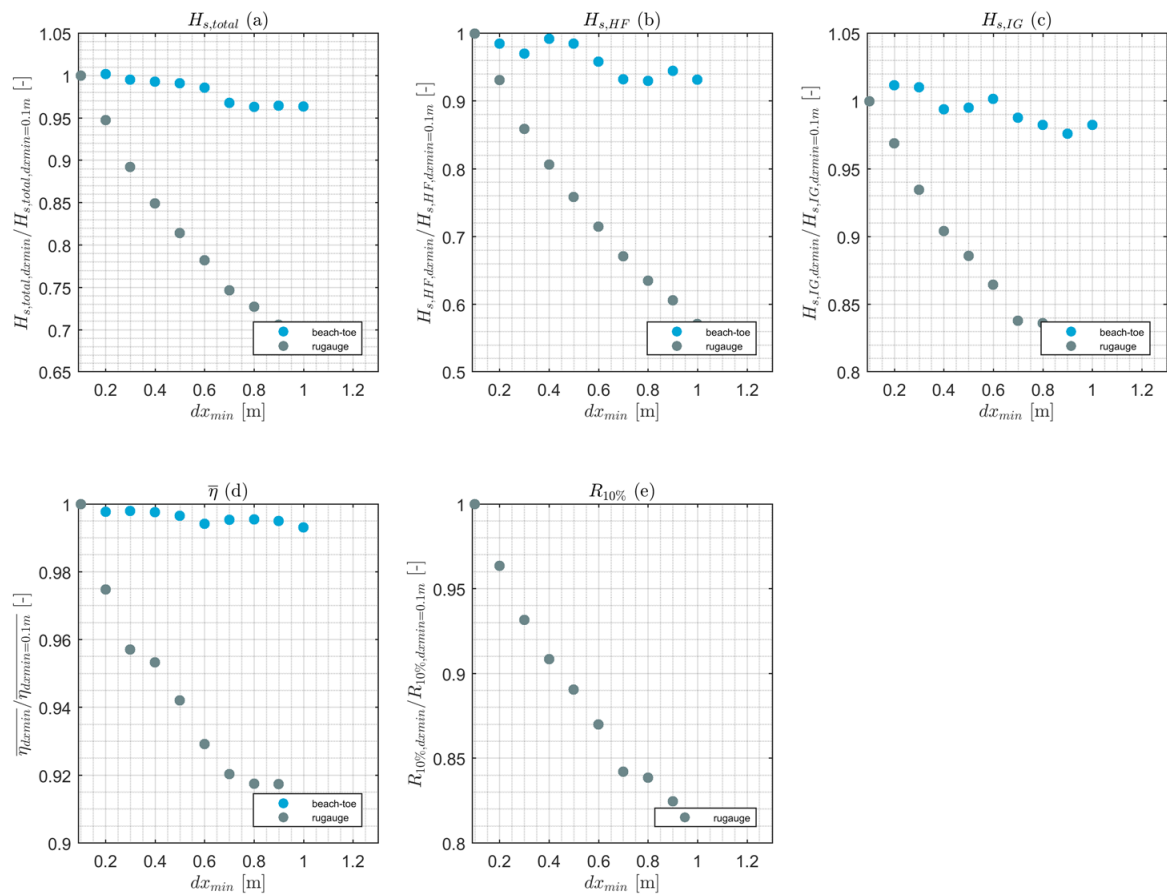


Figure A.5: Normalized wave heights, swash, mean water level and mean shoreline for different grid sizes. The minimum grid size of $dx = 0.1$ m is assumed to be sufficiently small to obtain stable results. The output at the beach-toe shows to be much more stable than the output at the runup gauge. This can be explained partly by Figure A.8.

This does not prove to be valid for the runupgauge which records the moving water line (see the gray dots Figure A.5). These functions do not show asymptotic behavior, which is expected as the grid size approaches $dx = 0$. Figure A.8 (left) shows a sample of the timeseries of the runupgauge, which records the vertical motion of the water line, for different grid sizes. For smaller grid sizes, the peaks continue to increase in height, causing larger runup levels. This is also seen in the right subplot, which shows the variance density spectra for different grid sizes. At $dx = 0.1$ m, the runupgauge does not seem to record a stable signal, as (HF) energy has increased from $dx = 0.3$ m to $dx = 0.1$ m. This could be related to several modelling parameters that affect the flooding/drying scheme that is used in XBNh+. A further analysis to assess the effect of these parameters

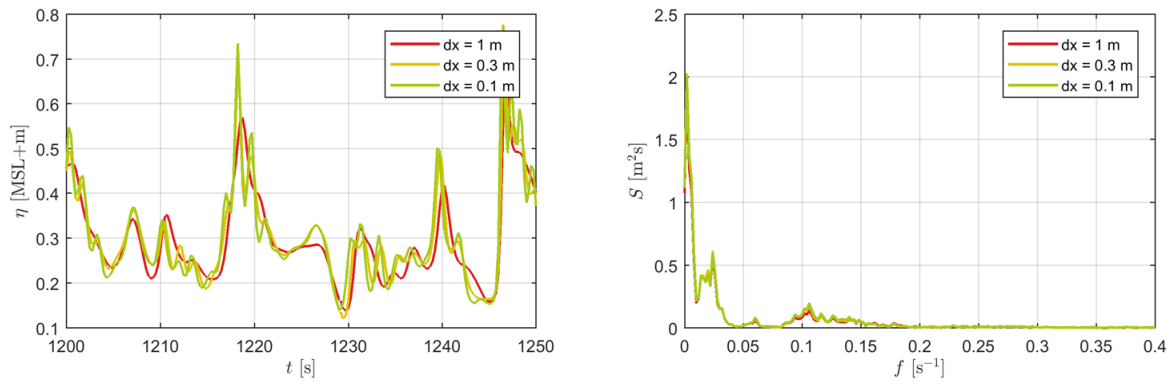


Figure A.6: Left: sample of time series of pointoutput located at the beach-toe, for three different grid sizes. The coarse grid shows less peaks than the two other grid sizes. $\Delta x = 0.3$ m shows to be very consistent with the results of $\Delta x = 0.1$ m. Right: The variance density spectra of the surface elevations computed at the beach-toe, for the same three grid sizes. The largest differences are located in the HF range near $f = 0.1 \text{ s}^{-1}$, though smaller grid sizes are very similar throughout the whole frequency domain.

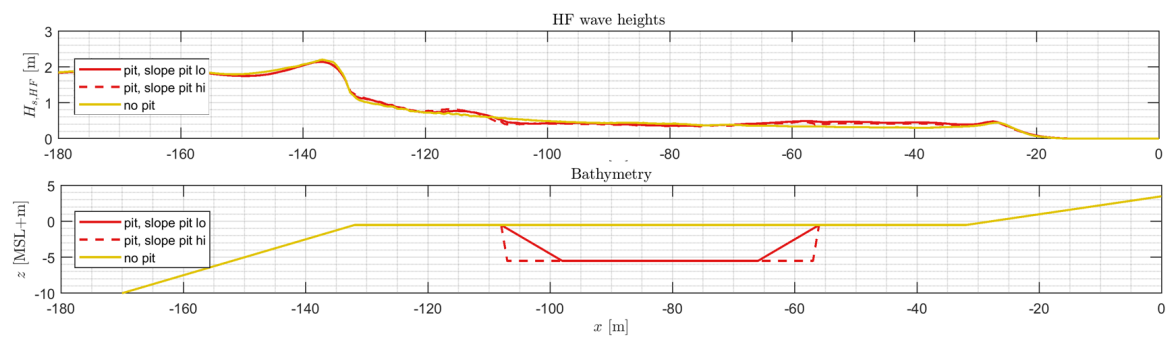


Figure A.7: Comparison of HF wave transformation across two reefs with excavations characterized by different pit wall steepness. The effect of pit slope dampens out over the reef flat towards the beach-toe.

has not been performed. Nonetheless, the shape of the peaks at the left subplot becomes sufficiently smooth at $dx = 0.3$ m, and are assumed to be sufficiently accurate.

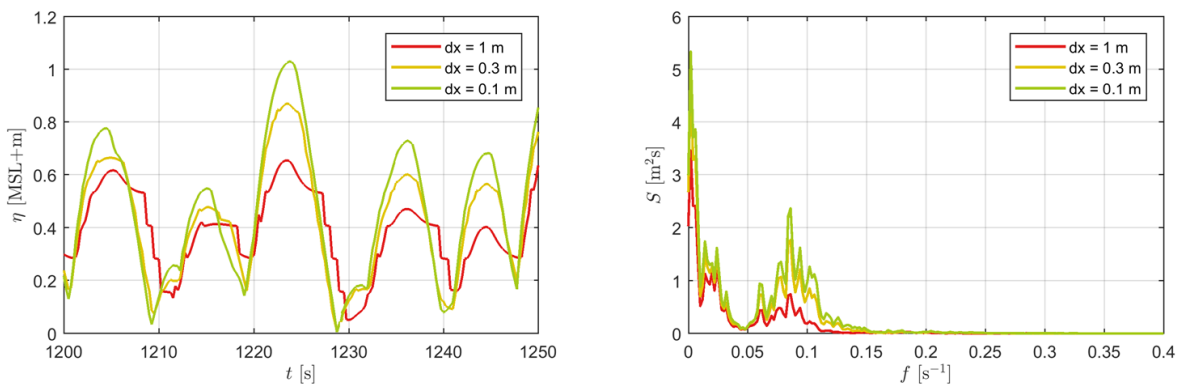


Figure A.8: Left: Sample of time series of vertical surface elevations of the water line, for three different grid sizes. Smaller grid sizes result in higher runup peaks with deeper troughs. Also, the signal becomes significantly smoother, compared to the signal of $\Delta x = 1$ m. Right: The variance density spectra of the vertical motions of the water line, for the same three different grid sizes. Larger grid sizes under predict swash motions in both the IG and HF frequencies, while the errors for the HF frequencies are relatively largest. This under prediction becomes less for smaller grid sizes. Though, as can be seen in A.2, there is no asymptotic behavior of the curve, which suggests that the modelled grid sizes are not entirely stable.

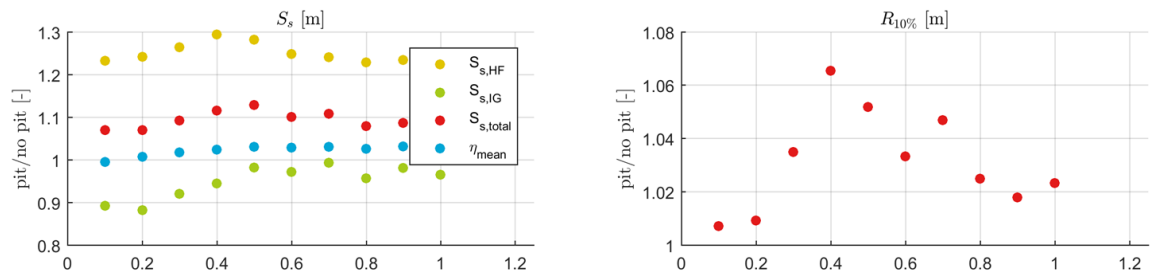


Figure A.9: Variation in swash (left) and normalized runup (right), for different Δx (on x-axis [m]). A distinction is made between HF (yellow), IG (green) and total swash (red). Mean water level (blue) is also presented.

A.3. Results calibration event

This section includes the results from the moderate wave event that was recorded on the 14th of July in 2011, which was used as a calibration event for the XBNh+ model.

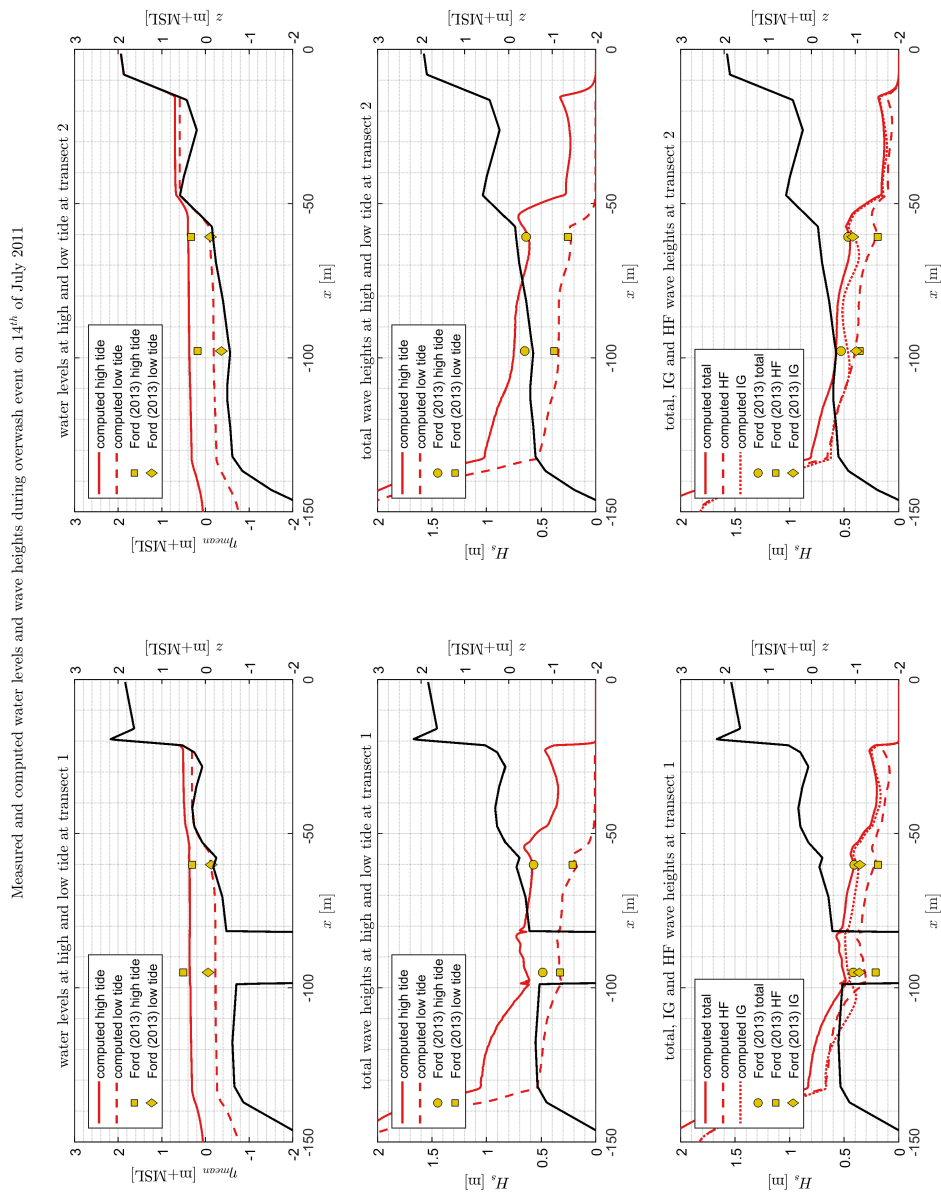


Figure A.10: Measured and computed water levels and wave heights during the mode calibration

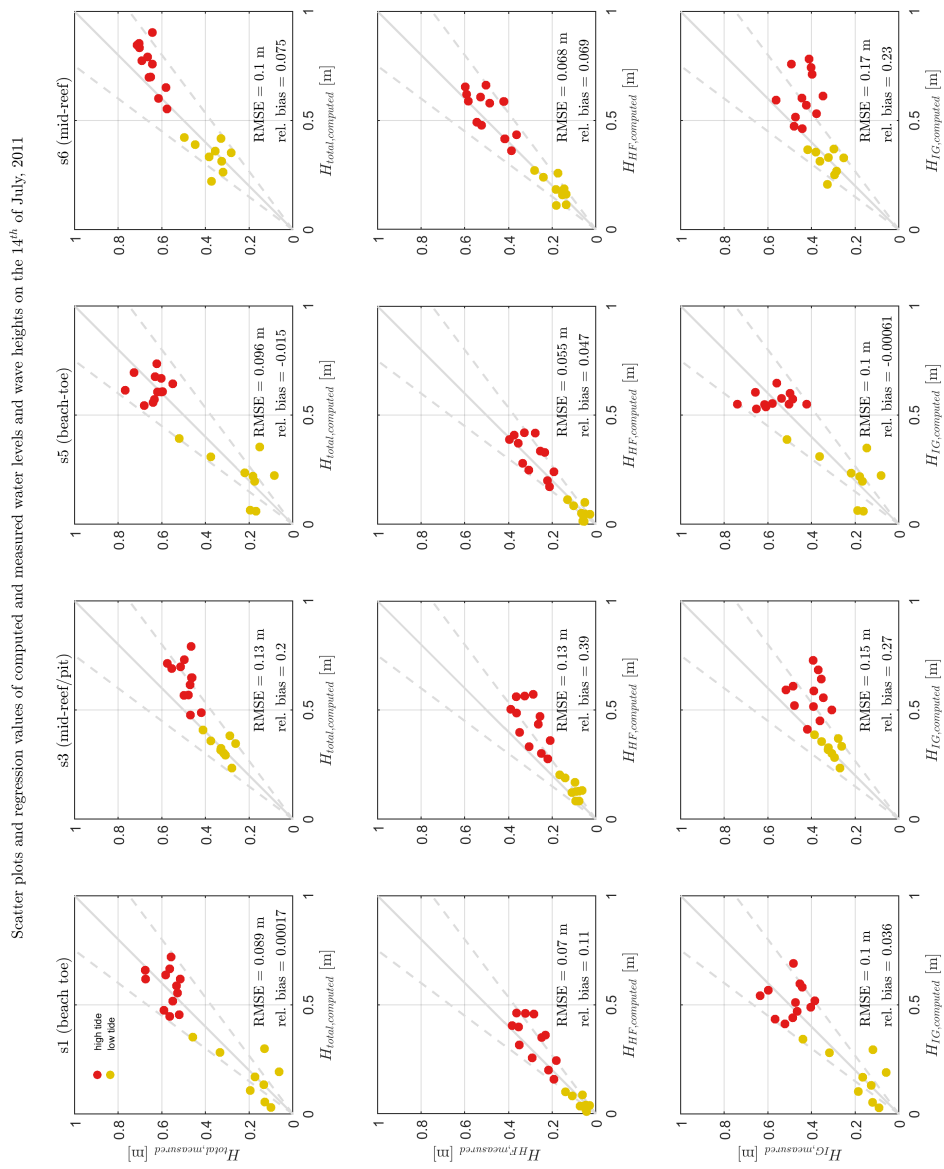


Figure A.11: Scatter plots of measured and computed wave heights during the calibration event at the four locations of the pressure sensors. Model skill is given by RMSE and relative bias

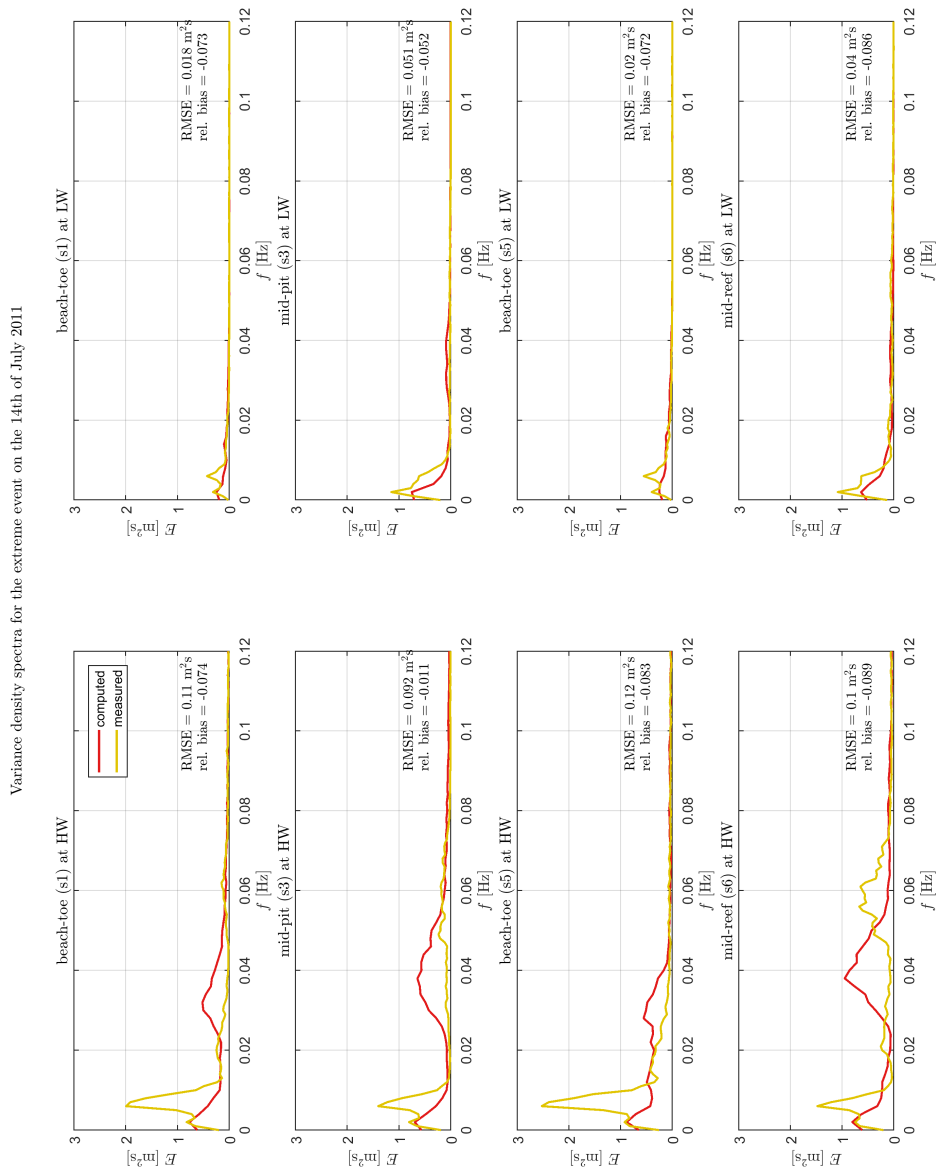


Figure A.12: Measured and computed variance density spectra during the calibration event at the four locations of the pressure sensors. Model skill is given by RMSE and relative bias.

B

1D modelling

B.1. Water level & wave height estimation

This section provides information on the errors that are introduced by sampling a relatively short signal, compared to a run of 24 hours, which is assumed to be of a sufficiently long duration in order to obtain stable results. The errors (confidence intervals, SCI and bias) in this section are related to the estimation of wave heights ($H_{s,total}$, $H_{s,HF}$ & $H_{s,IG}$) and mean water level ($\bar{\eta}$) at the location of the beach-toe. The same methods are applied to the normalized wave heights and water levels (run with pit/run without pit), which isolates the effect of the excavation pits. This is because the time series of the boundary conditions that are used are identical, also leading to lower errors. The former (Figures B.1 & B.2) represent the errors and accuracy of the model to predict relevant hydrodynamic processes, and the latter (Figures B.3 & B.4) represent this for the effect of the excavation pits.

Errors in water level & wave height estimation for random forcing time series

in significant wave heights (total (a), HF (b) & IG (c)) and mean water level ($\bar{\eta}$ (d)), for different simulation times relative

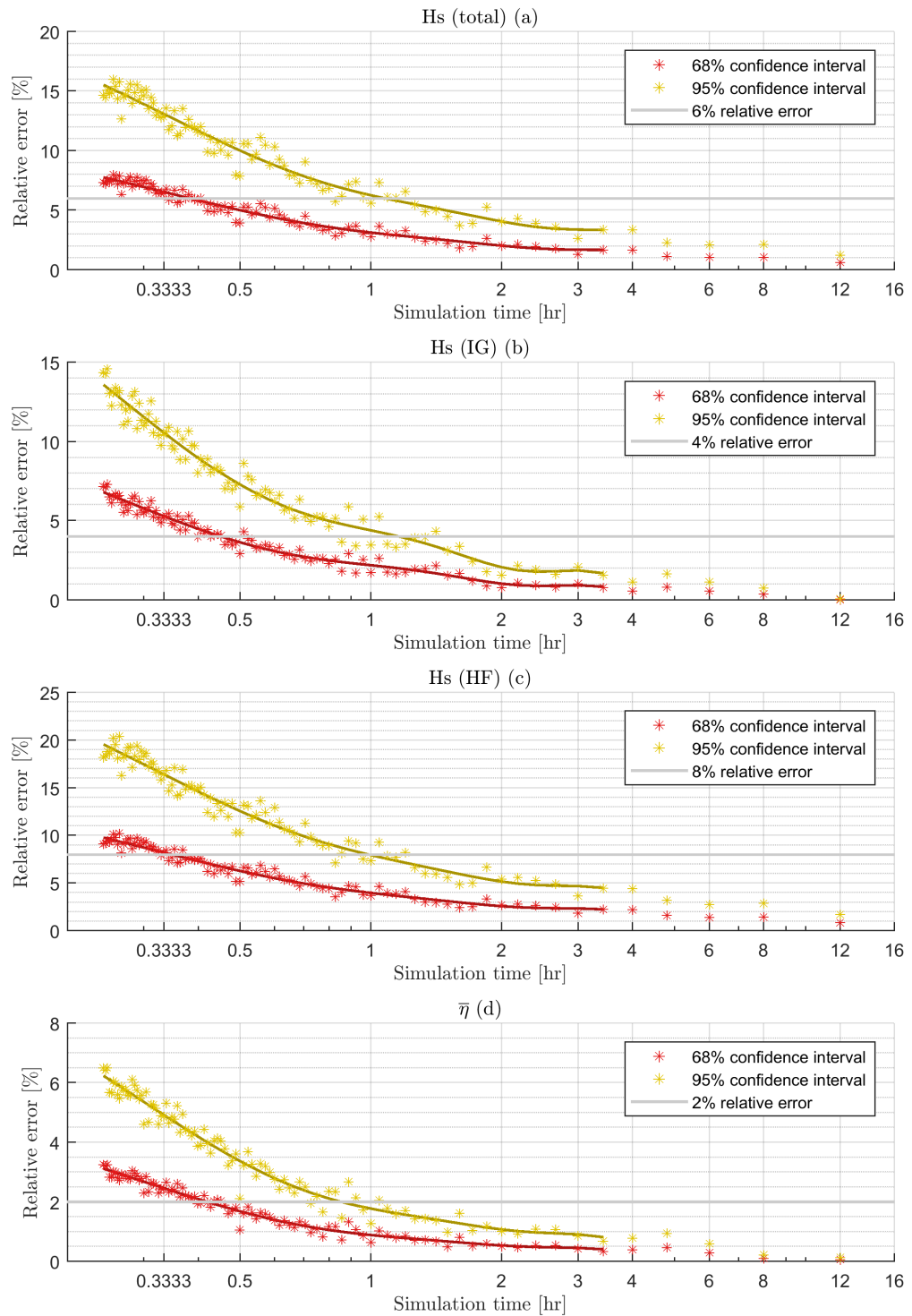


Figure B.1: Relative errors introduced by sampling for 68% and 95% confidence intervals of wave heights and mean water level at beach-toe

errors in significant wave heights (total (a), HF (b) & IG (c)) and mean water level ($\bar{\eta}$ (d)), for different simulation times relative to a 24

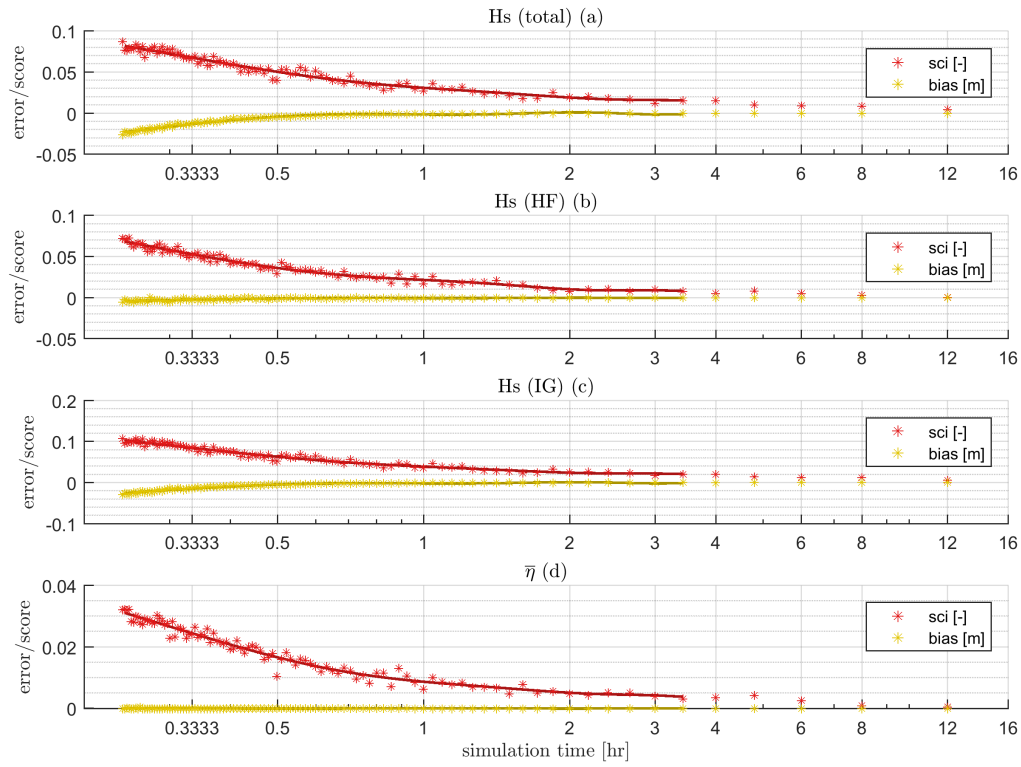


Figure B.2: Model skill errors (SCI & bias) of wave heights and mean water level at beach-toe, introduced by sampling

Errors in relative water level ($\overline{\eta_{pit}/\eta_{nopit}}$) & wave height (H_{pit}/H_{nopit}) estimation for identical forcing time series

and (pit/no pit) significant wave heights (total (a), HF (b) & IG (c)) and mean water level ($\bar{\eta}$ (d)), for different simulation ti

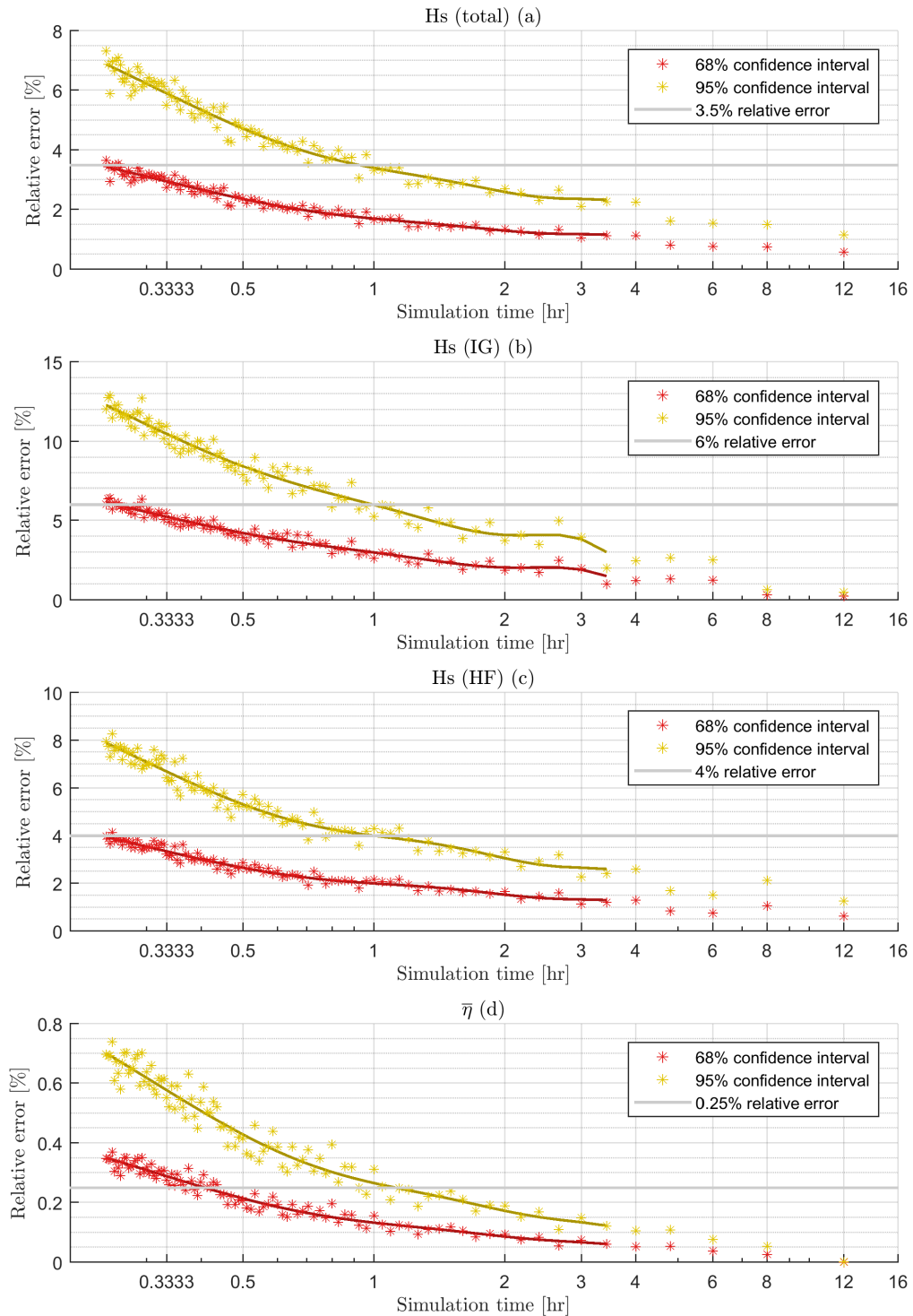


Figure B.3: Relative errors introduced by sampling for 68% and 95% confidence intervals of normalized (pit/no pit) wave heights and mean water level at beach-toe

normalized (pit/no pit) significant wave heights (total (a), HF (b) & IG (c)) and mean water level ($\bar{\eta}$ (d)), for different simulation times rel:

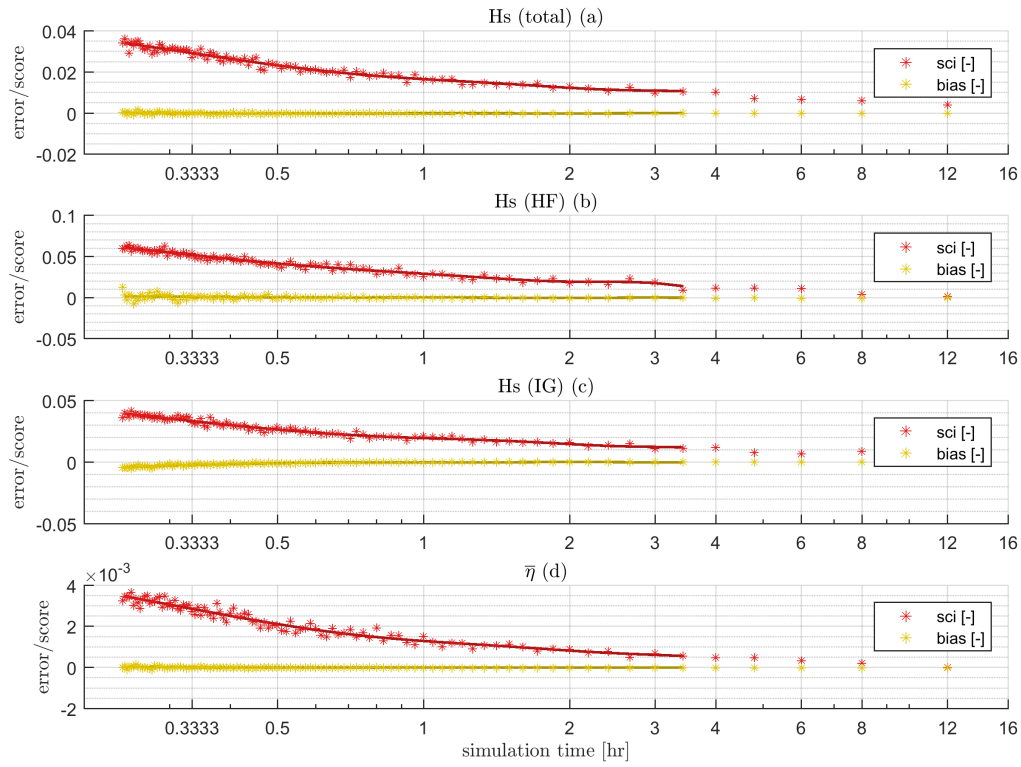


Figure B.4: Model skill errors (SCI & bias) of normalized (pit/no pit) wave heights and mean water level at beach-toe, introduced by sampling

B.2. Runup estimation

Inclusion of extremes for different runup quantiles

Runup can be used as a proxy for beach overtopping, as larger runup will lead to larger volumes of water washing over the beach crest and causing inundation. Not all waves that runup the beach slope will cause overtopping, therefore the extremes should be used in studies that aim to assess coastal hazards. An analysis has been performed that assesses the inclusion of these extremes in the values for different runup quantiles, ranging from $R_{2\%}$ to $R_{20\%}$.

Figure B.5 illustrates in which quantile extreme runup peaks. The function shows a near linear slope up to the $n = 90\%$, from which the runup starts to increase more, leading to a curved function. The extreme peaks are present in the upper quantiles of this function. This is because these peaks have low occurrence probabilities, but are also significantly larger than peaks at lower quantiles.

In most engineering applications, the $R_{2\%}$ is used as a proxy for the "maximum" runup that occurs during a given period. This is because the extreme peaks make up a large fraction of all peaks considered at this quantile. This fraction decreases for lower quantiles. In Figure B.6, the variation in absolute runup (right subplot) and variation in the effect of excavation pits on runup (left subplot), as a function of quantile n is shown using boxplots. These plots show that upper quantiles do have a larger impact on the computed runup, though the mean effect is less than 1 m in absolute sense, and 2% in relative sense.

Adding to this, because lower quantiles also contain the upper fraction of extreme peaks, the correlation between a lower quantile and the upper quantile ($n = 2\%$) is very large (see Figure B.7, left subplot). The center and right subplots show that the errors of runup of fringing reefs with and without pit, in terms of bias and sci, increase significantly for lower quantiles, compared to the upper quantile. However, the errors on the normalized runup (pit/no pit) are sufficiently low and remain (near) constant. These figures imply that a lower quantile than $n = 2\%$ can be used to estimate extreme runup.

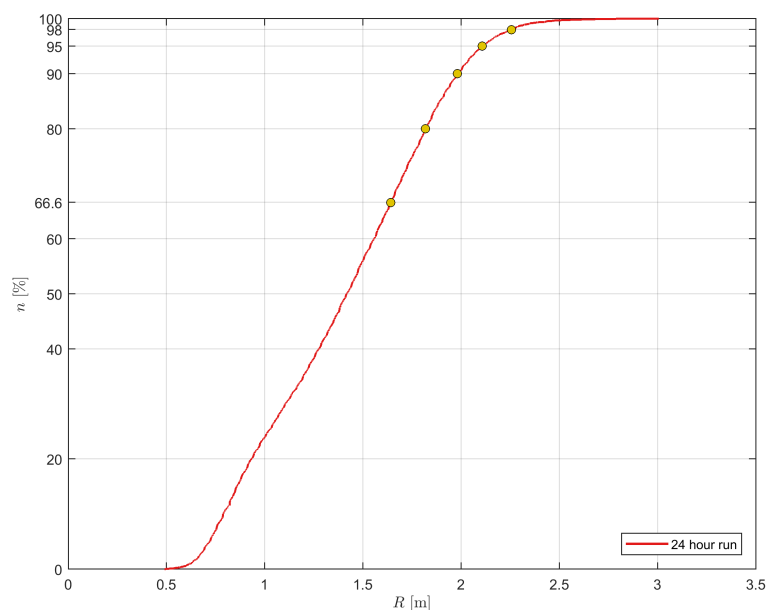


Figure B.5: ECDF of the peaks in a 24 hr runup gauge signal on a fringing reef with pit. The runup values of the 66.6th, 80th, 90th, 95th & 98th quantiles are indicated by the yellow dots. The curve is near linear for $n < 90\%$, and starts to curve for higher values. This curvature is caused by the extreme peaks in the runup signal, which are most likely to cause overtopping.

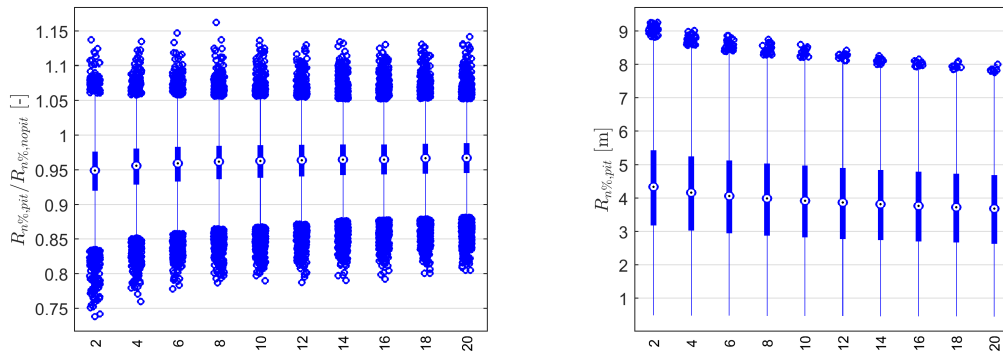


Figure B.6: Boxplots of normalized (pit/no pit) runup (left) and absolute runup (right), for different extreme quantiles, ranging from 2% to 20%. The mean runup increases less than approximately 50 cm, from $R_{10\%}$ to $R_{2\%}$.

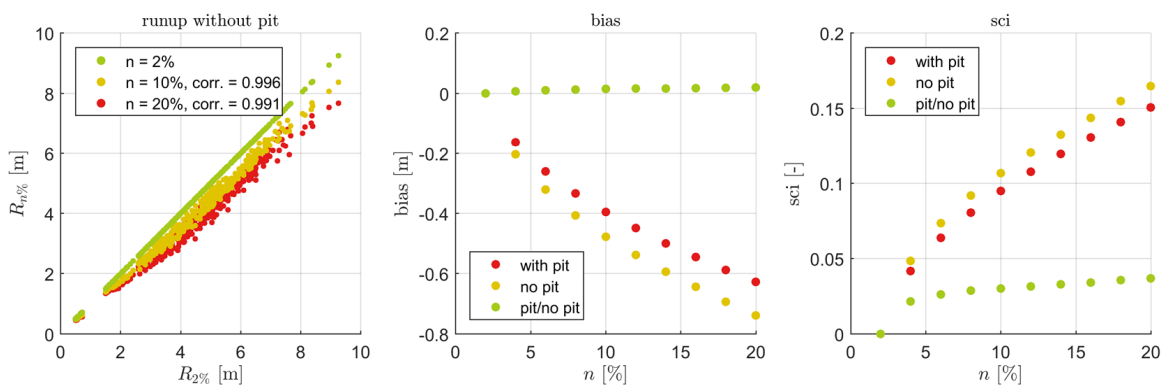


Figure B.7: Correlation (left), bias (center) & sci (right) for different $R_n\%$, compared to a baseline $R_{2\%}$. The runup levels of the modelled reefs are highly correlated to the baseline $R_{2\%}$. Bias and scatter index increase for lower quantiles, but the normalized runup (pit/no pit) remains near constant.

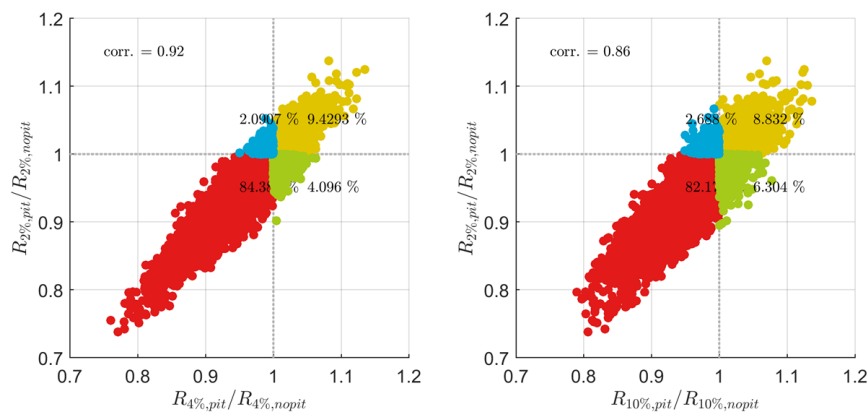


Figure B.8: Correlation of changes in runup for different quantiles. The changes in runup for different quantiles are highly correlated (0.92 for $R_{2\%}$ & $R_{4\%}$ (left subplot), 0.86 for $R_{2\%}$ & $R_{10\%}$ (right subplot)), but there is a chance that reefs experience a different change in extreme runup for different quantiles (blue and green colors). Although these probabilities are significant compared to the combined probability of increase in runup (yellow), the changes in these probabilities is sufficiently small (2.09-2.69% and 4.10-6.30%).

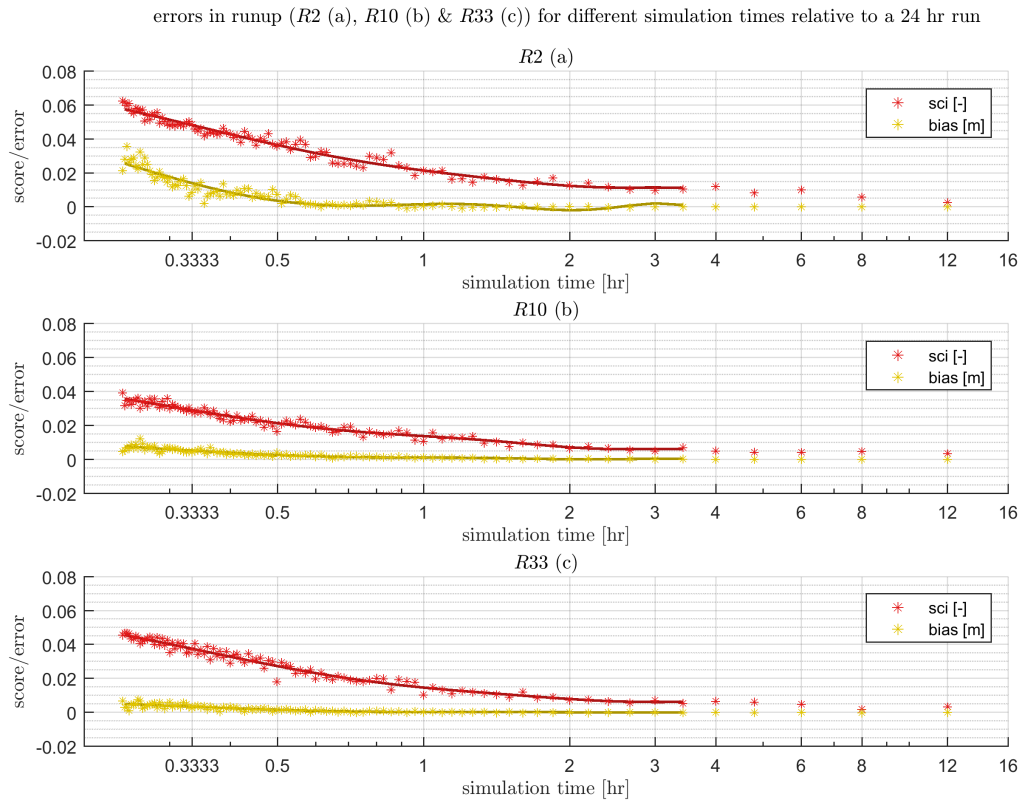
Errors in runup estimation for random forcing time series

Figure B.9: Model skill errors (SCI & bias) of different runup values, introduced by sampling

errors in runup (R_2 (a), R_{10} (b) & R_{33} (c)) for different simulation times relative to a 24 hr run

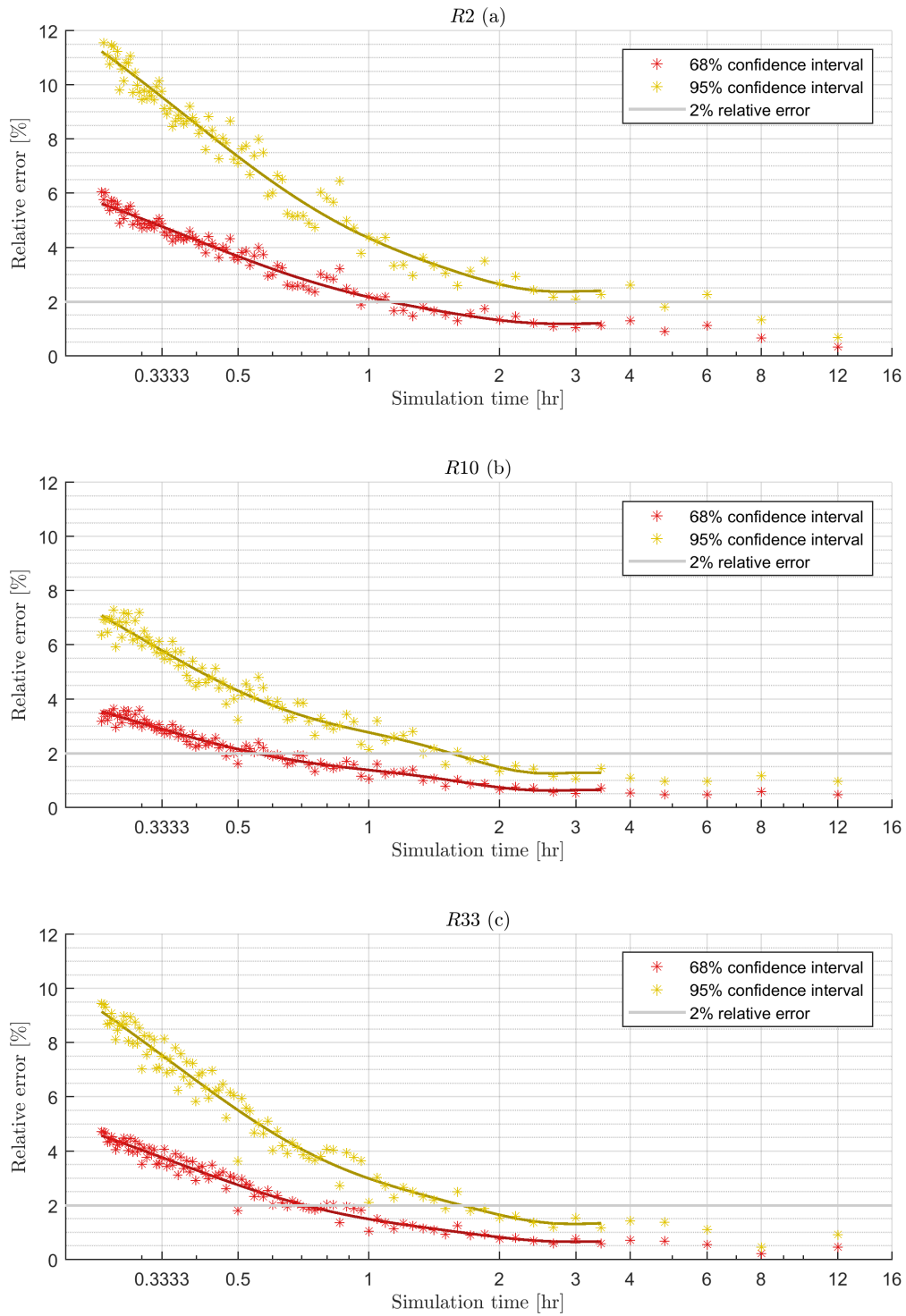


Figure B.10: Relative errors introduced by sampling for 68% and 95% confidence intervals of different runup values

Errors in relative runup (R_{pit}/R_{nopit}) estimation for identical forcing time series

Errors in relative runup (R_{2pit}/R_{2nopit} (a), $R_{10pit}/R_{10nopit}$ (b) & $R_{33pit}/R_{33nopit}$ (c)) for different simulation times relative to

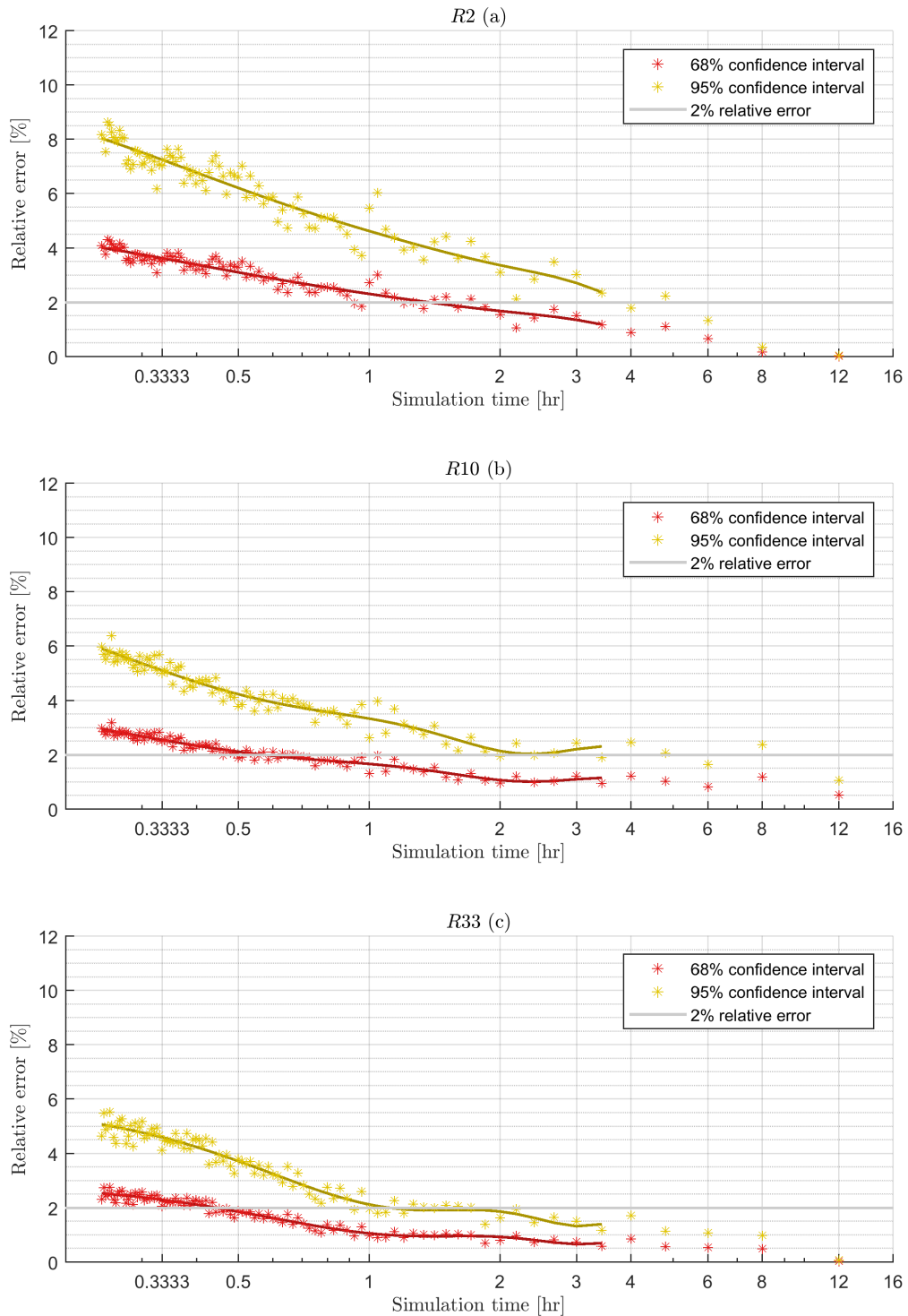


Figure B.11: Relative errors introduced by sampling for 68% and 95% confidence intervals of different (normalized, pit/no pit) runup values

errors in relative runup ($R_{2_{pit}}/R_{2_{nopit}}$ (a), $R_{10_{pit}}/R_{10_{nopit}}$ (b) & $R_{33_{pit}}/R_{33_{nopit}}$ (c)) for different simulation times relative to a 24 hr

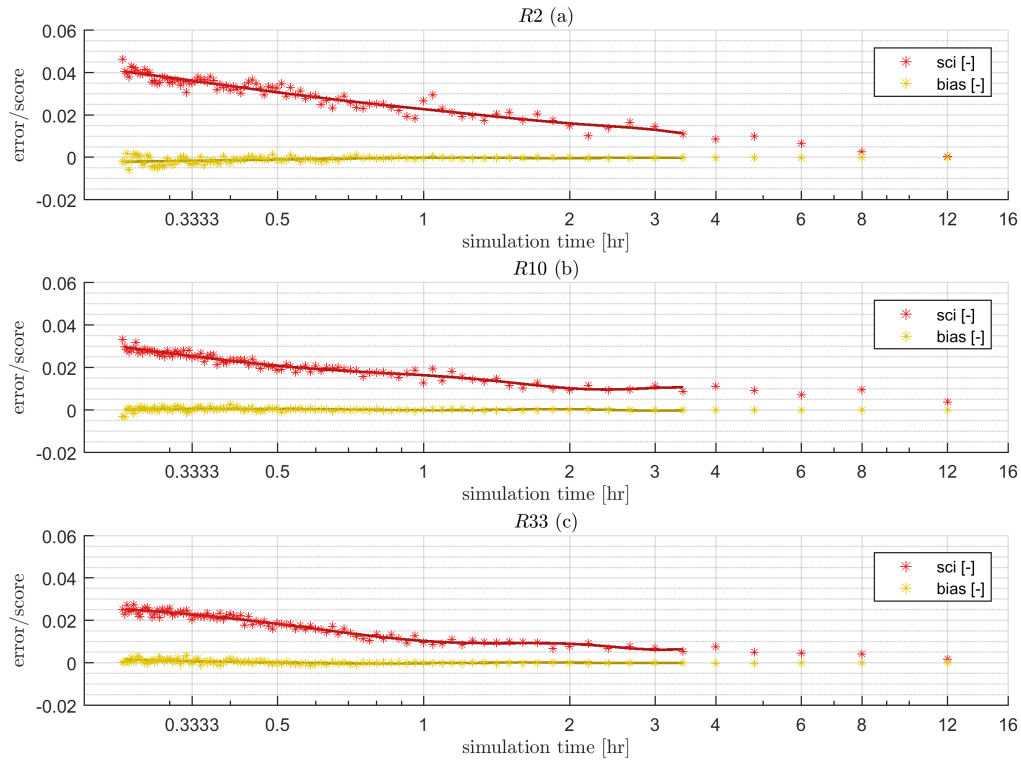


Figure B.12: Model skill errors (SCI & bias) of different (normalized, pit/no pit) runup values, introduced by sampling

B.3. Reef geometry simplification

By simplifying the geometry of an actual reef into a schematic case, some hydrodynamic processes might change (see figure B.13). However, as can be seen in the figure, there are significant similarities between the schematized reef and the "real" reef. The schematized reef is considered to be an appropriate and useful representation of reality, and has been used in previous research as well (Gawehn et al., 2016; Pearson, 2016; Quataert, 2015).

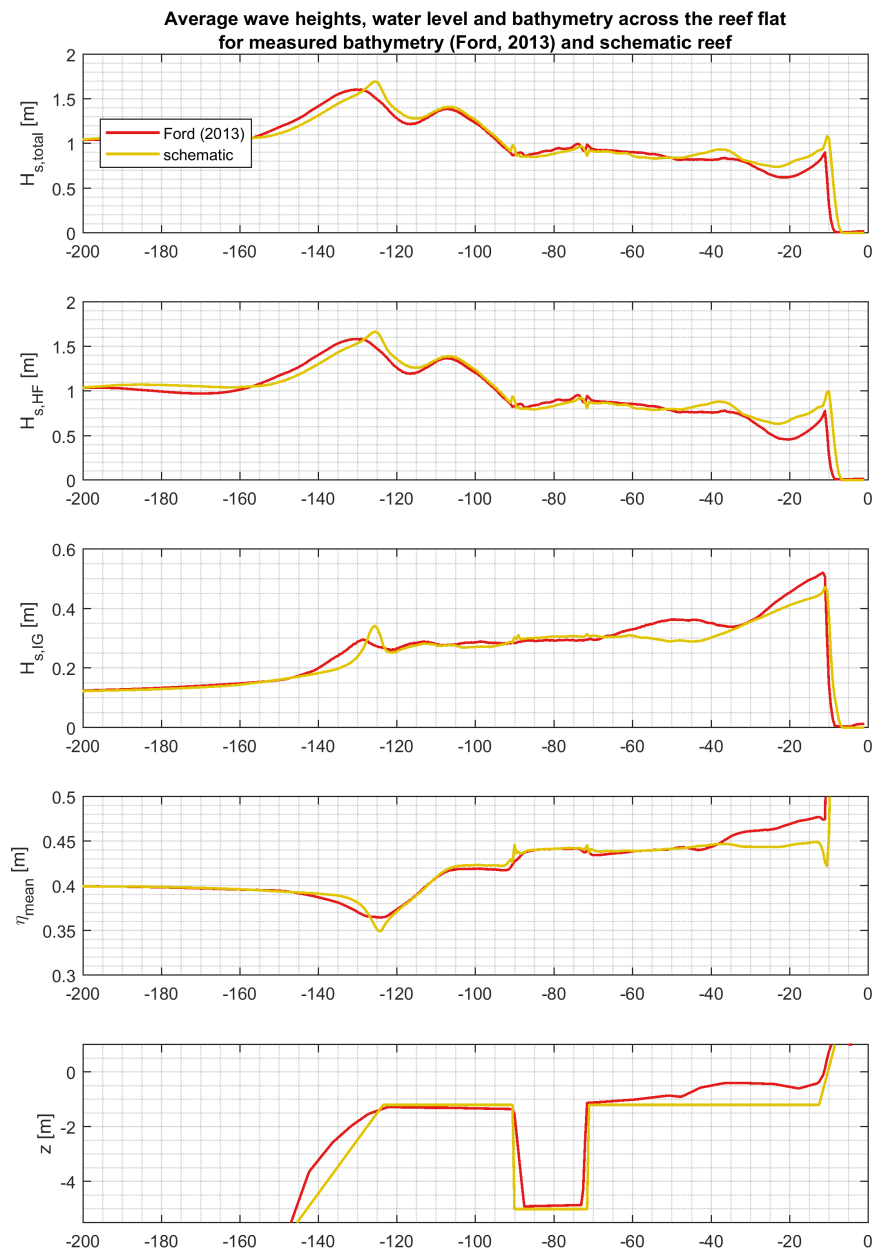


Figure B.13: Wave and water level transformation across the measured reef and a schematized case.

B.4. Single-parameter sensitivity analysis

B.4.1. Influence of hydrodynamic forcing

Reef submergence

Reef (flat) submergence is related to the offshore water levels, such as tidal motions, storm surges and relative sea level rise. Increase of the reef submergence plays a key role in the hydrodynamic processes on the fringing reef. The model outputs show (see Figure B.14) that an increase in reef submergence leads to a decrease in wave-induced setup and an overall increase in wave heights from reef crest to the shoreline. HF wave energy across the reef increase, but IG wave energy increases up to a certain reef submergence, after which the IG wave generation diminishes. Swash and runup both increase for increasing reef submergence. For larger reef submergence, HF swash becomes dominant compared to IG swash.

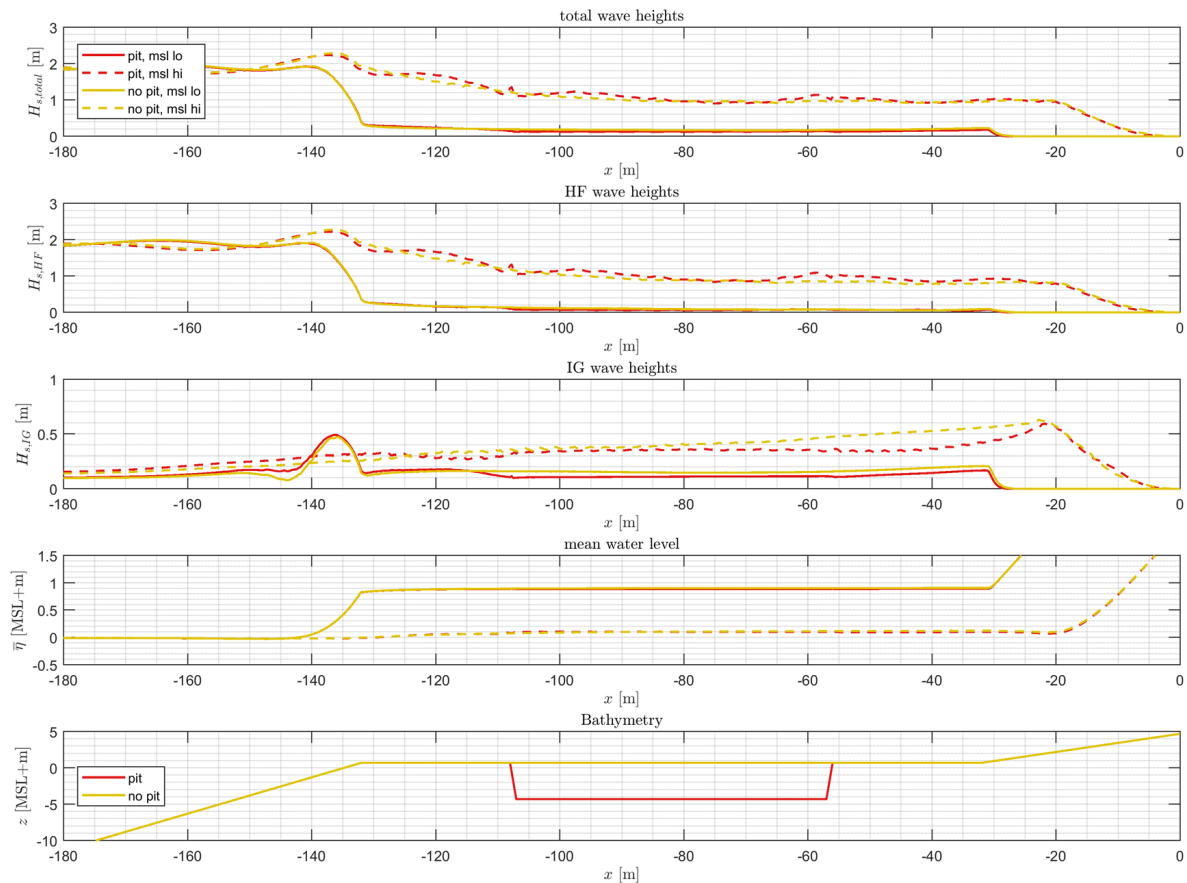


Figure B.14: Global wave (HF & IG) and mean water level transformation for different values of reef submergence. Wave breaking dissipation rates decrease for increasing reef submergence (dotted lines). This leads to a decrease in wave-induced setup.

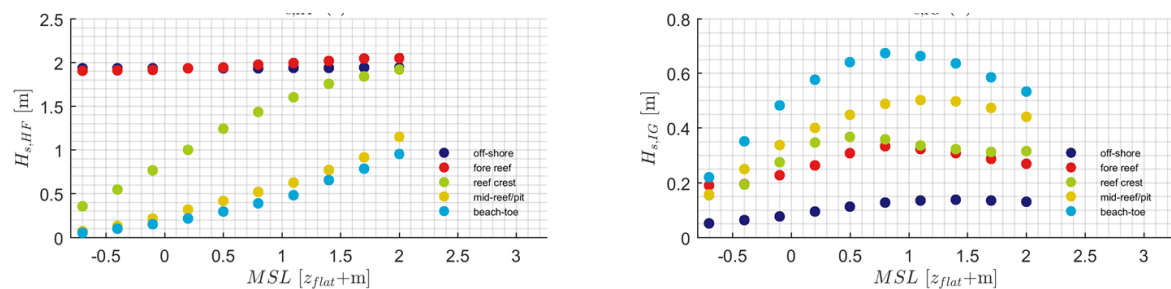


Figure B.15: Variations in HF and IG wave heights at five locations of the reef, for different reef submergence. HF energy at the shoreline increases gradually (see blue dots in left figure). This contrasts with IG wave energy, which reaches an optimum for $0.5\text{ m} < MSL < 1.0\text{ m}$.

The previously described effect of a pit on mean water levels becomes less pronounced for larger water depths over the reef flat. The effect of pits on HF waves (increase) diminishes and the effects on IG waves (decreases) stays similar for larger water depths. Both for emerged and submerged reef flats, pits disrupt the IG waves by approximately 20%.

Both HF and IG swash reach a maximum at water levels of approximately 0.8 m on the reef flat, which results in a maximum runup for the same water depth. For both higher and lower water depths, swash and runup decreases.

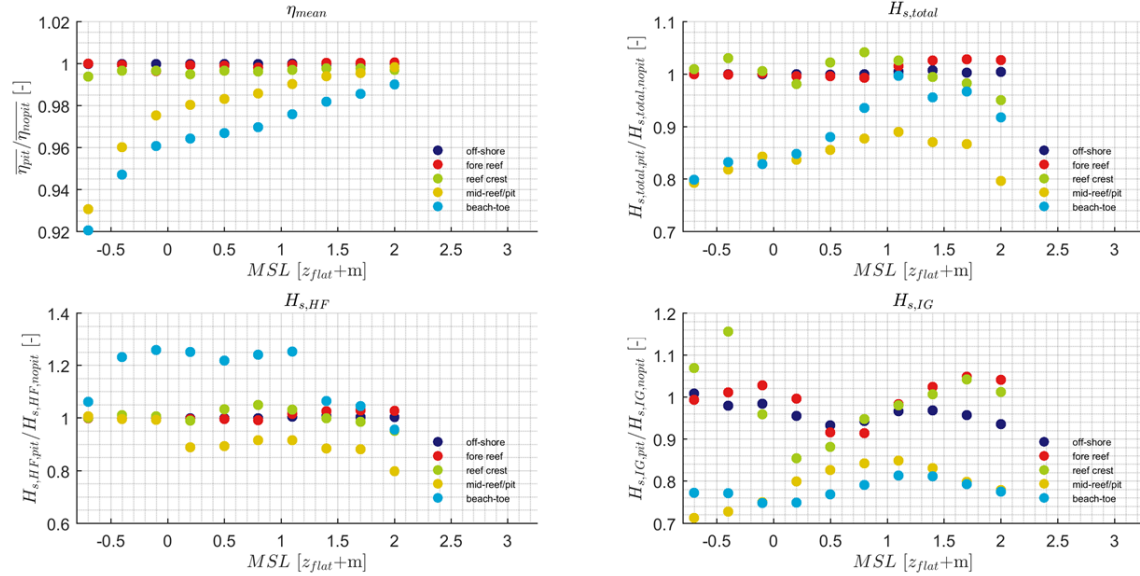


Figure B.16: Normalized water levels and wave heights for different values of reef submergence (MSL).

Offshore wave height

An increase in offshore deep water wave height results in a linear increase in wave-induced setup and wave energy at the shoreline (both HF and IG). Runup and swash are affected similarly.

The effects of pits on wave heights and setup across the reef does not vary significantly. However, increase in runup and swash due to the presence of a pit tends to decrease for larger wave heights, up to a point where the pit decreases the R10% (at $H_{s,0} > 5$ m).

Wave steepness

An increase in wave steepness leads to a decrease in setup across the reef flat, as small decrease in wave energy at the beach toe due to a large decrease in IG wave energy. This probably results from the fact that less IG waves are present in the original spectrum due to a shift of wave frequencies. These result in lower swash and runup.

The effect of pits on wave heights (HF and IG) and water levels decrease for increasing wave steepness. Also, the influence on swash and runup diminishes.

B.4.2. Influence of reef geometry

Fore reef slope

An increase in fore reef slope leads to increase wave heights at the reef crest and an increase in IG wave generation. This results in an increase in setup and higher wave energy. HF wave energy is not affected significantly by a change in fore reef slope, compared to IG waves. Swash and runup increase as well. IG swash increases more than HF swash, which leads to a IG swash dominance for steep slopes ($\alpha_{reef} > 0.2$).

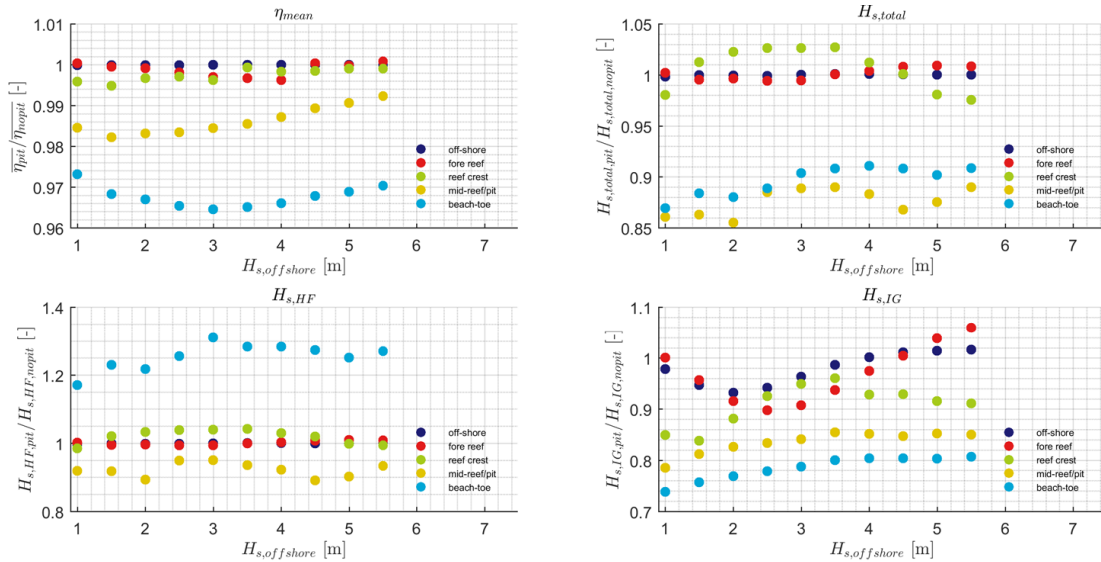


Figure B.17: Normalized water levels and wave heights for different values of reef submergence (MSL).

For gentle slopes ($\alpha_{reef} < 0.15$) HF wave heights at beach toe decrease due to presence of a pit and increase for steeper fore reefs. IG wave heights at beach toe remain similar fore different fore reef slopes. The effect of pits on runup (increase) increases for steeper fore reefs.

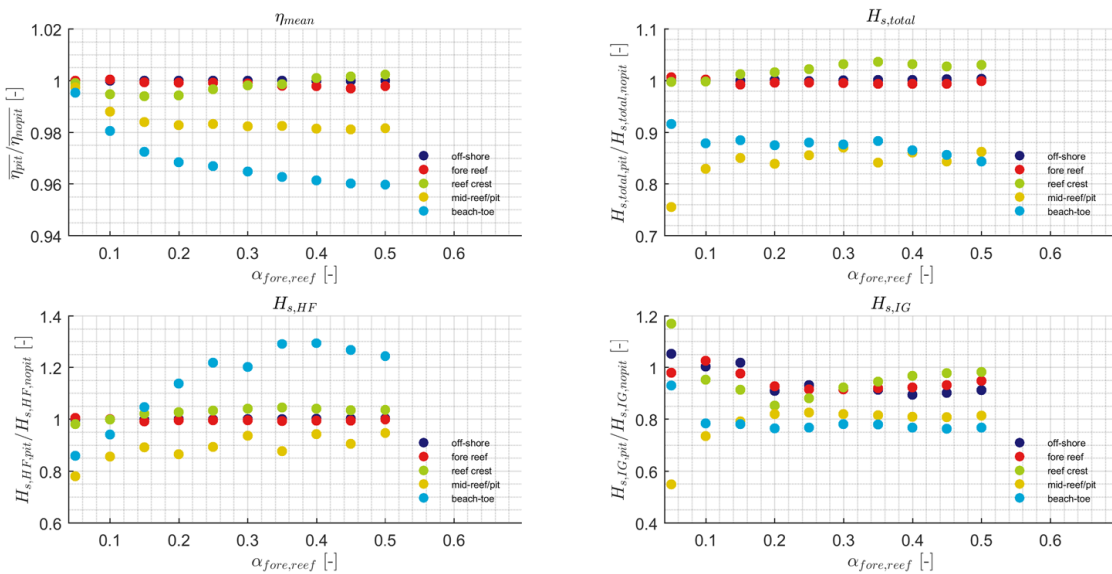


Figure B.18: Normalized water levels and wave heights for different values of fore reef slope.

Reef crest roughness

The modelled effect of reef crest roughness is to slightly decrease water levels on the reef flat and near the shore. An increase in reef crest roughness decreases IG wave heights from the reef crest to the beach-toe. The effect on HF energy is negligible.

A change in reef crest roughness does not significantly influence the effects that excavations have on the fringing reef hydrodynamics.

ect on the maximum runup (which is under debate)

Reef flat roughness

The modelled effect of reef flat roughness is similar to that of reef crest roughness, but differs due to the larger influence on IG waves near the shoreline and negligible influence on water levels over the reef.

The effect of pits on water levels decreases for larger reef flat roughness. The effect on total wave heights decreases up to a point ($C_{f,flat} > 0.06$) where the presence of the pit actually increase wave heights at the beach-toe. This is probably due to a decreased effect of pits on the IG energy at the shoreline for larger roughness values.

Reef flat width

The reef flat width has a large effect on the amount of wave energy that reaches the shoreline, by dissipation of IG waves and HF waves to a lesser extent. For wider reefs this effect decreases.

For a pit with a width of half the reef flat width, water levels at the beach-toe are lowest for narrow reefs. Other visible effects that the effect of pits on HF energy at the beach-toe reverses for reefs wider than 300 m.

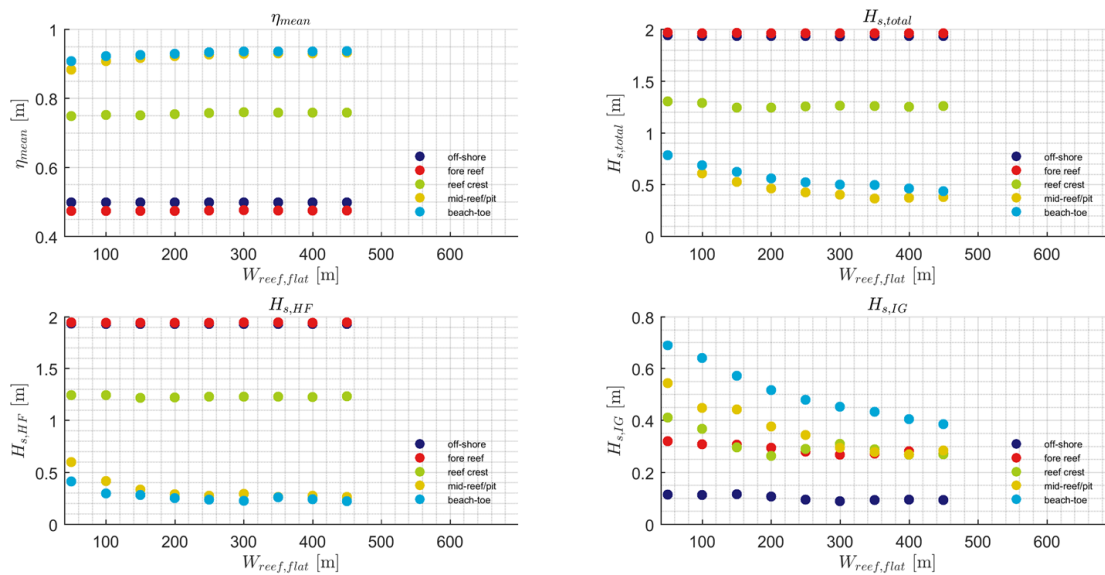


Figure B.19: Water levels and wave heights for different values of reef flat width.

Beach slope

The beach slope has a major impact on the water motions at the shoreline (swash). Gentle slopes are dominated by IG frequencies, as HF waves are dissipated more on gentle slopes. For steeper slopes, the HF and IG components become equal, and reflection at the shoreline increases. The beach slope shows to only have a major effect on the processes near the shoreline.

For gentle slopes ($\alpha_{beac} < 0.075$), swash motions decrease due to presence of a pit. For steeper slopes they HF and total swash increase due to presence of a pit.

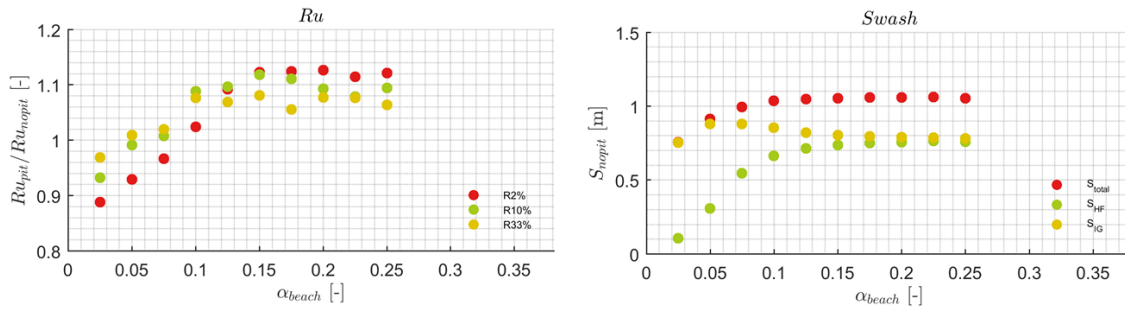


Figure B.20: Normalized runup levels and swash components for different values of beach slope.

B.4.3. Influence of pit geometry

Pit width

The decrease in mean water levels at the beach-toe due to the presence of a pit increase for wider pits. This is probably due to less intense breaking and lower wave forcing due to increased water depth. Additionally, the effect on HF and IG waves at the beach-toe increase for wider pits. Wider pits dissipate HF waves less due to bottom friction and breaking.

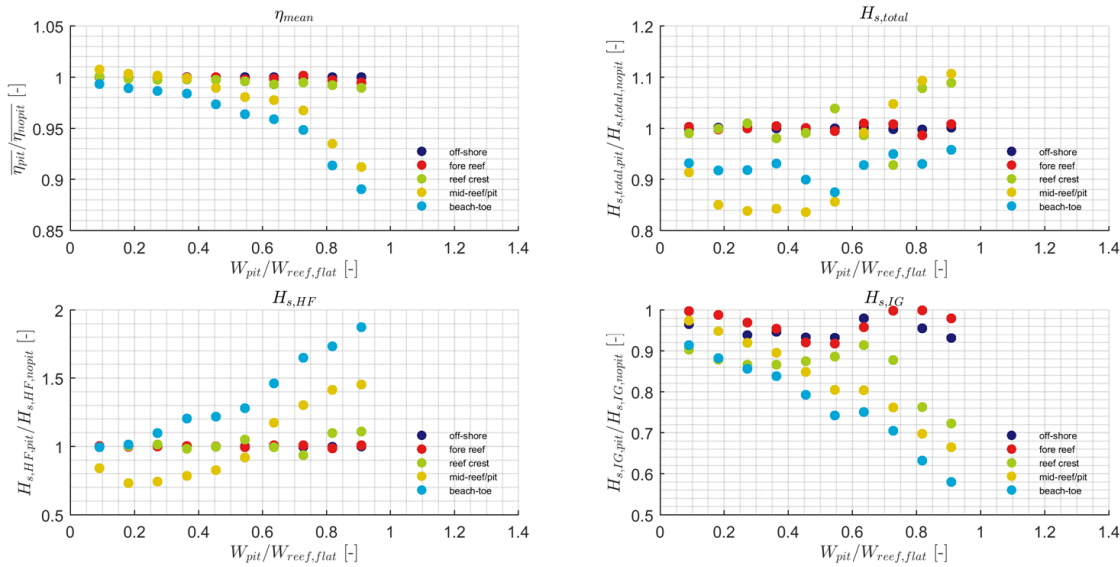


Figure B.21: Normalized water levels and wave heights for different values pit width.

Pit distance from shoreline

The cross-shore location of the pit seems to influence the water levels and HF waves propagation. For pits located closer to the reef crest, changes in mean water level are largest. There is a maximum influence on HF energy for pits located at 60% of the reef flat width from the beach-toe.

Pit depth

Depending on the roughness of the pit bottom, a shallower pit decreases the influence of the pit on the hydrodynamics on the reef. For depths greater than approximately 2 m, depending on pit bottom roughness, the change in effect of pits is negligible.

Pit wall slope

The effect of pit wall slope is negligible (see Figure B.23). From a comparison of model outputs with steep and gentle pit slopes, no significant effects on numerical effects have been found due to steep bathymetry. XBNh+ performs well when modelling pits with steep near-vertical walls. There are numerically induced high

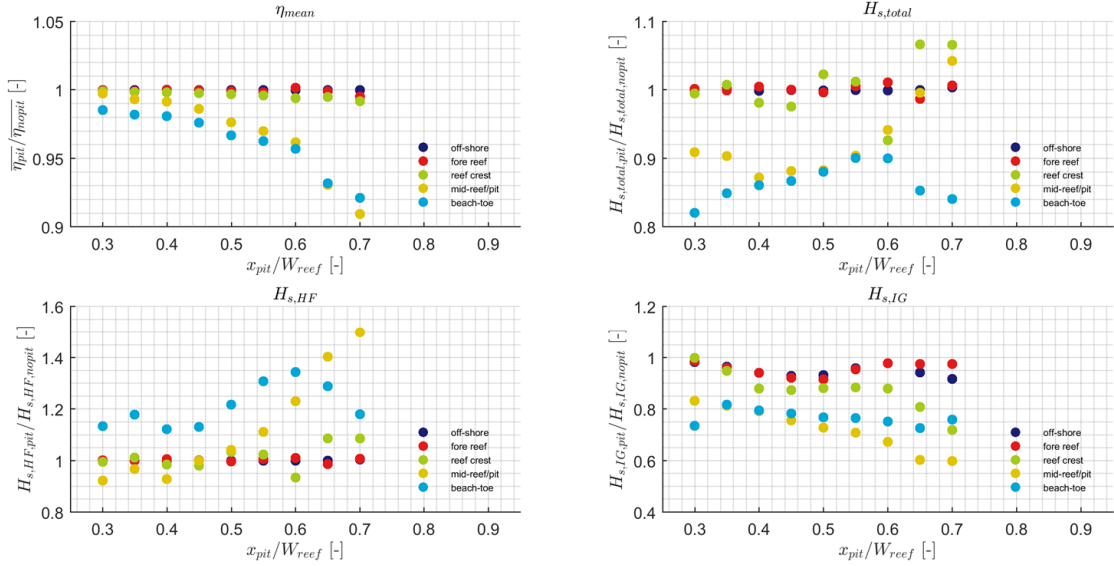


Figure B.22: Normalized water levels and wave heights for different values of cross-shore pit location.

frequency oscillations at the locations of the pit walls, but these dampen out on the reef flat and only produce minor wiggles in the computed wave heights at the pit walls.

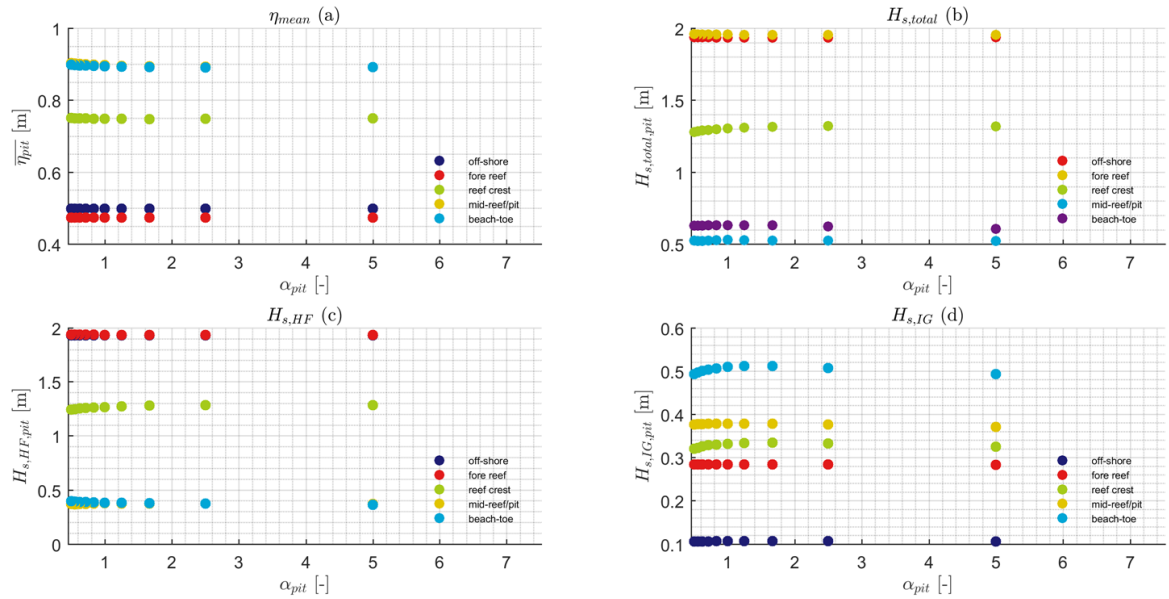
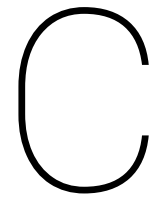


Figure B.23: Variations in mean water levels (a), total wave height (b), HF wave height (c) and IG wave height (d) at five output locations of the model for different values of pit wall slope. These outputs show that there is no significant effect of varying pit wall slope.

Pit bottom roughness

For deep pits ($z_{pit} = -5\text{m}$ below reef flat), bottom roughness is not a factor of influence for reef hydrodynamics. For pits shallower than $z_{pit} = -2\text{m}$ and a high roughness value comparable to the reef crest, IG wave disruption will increase for decreasing pit depth. However, currently pit bottom roughness remains an unknown factor and is likely to depend on excavation methods, the excavation age (which allows for new reef to grow) and pollution.



2D modelling

C.1. Comparison of hydrodynamics in 2D & 1D, without pit

Figure C.1 shows a comparison of wave transformations for a 1D and a 2D XBnh+ model. The 2D effects are similar when comparing the simulation to another with excavation pit. The main observable difference between 1D and 2D is smaller IG wave heights, due to directional spreading of waves, leading to less wave groupiness.

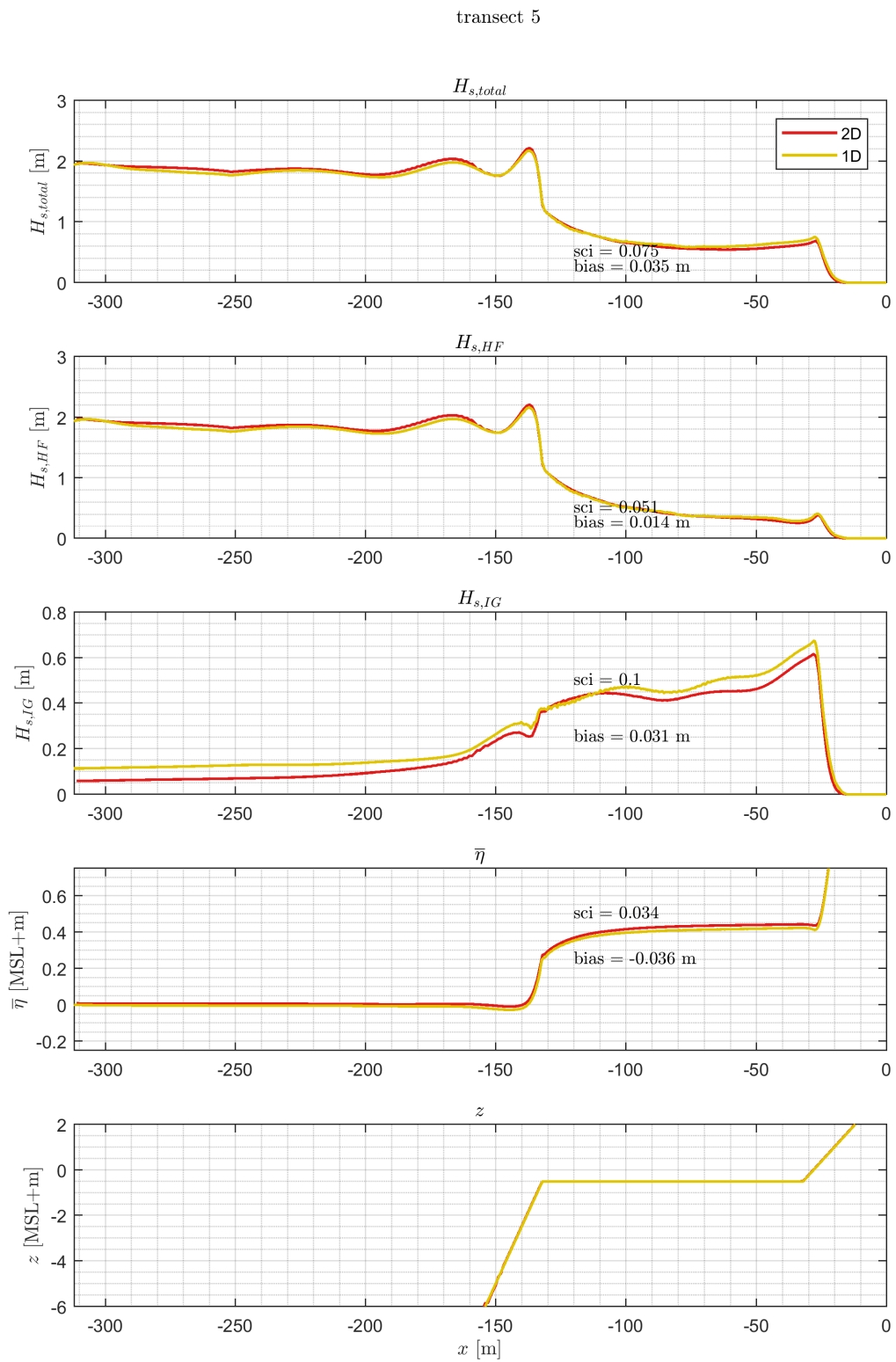


Figure C.1: Comparison of wave heights and mean water levels of a 1D (yellow lines) and 2D (red lines) run without pit.